REPORT DOCUMENTATION PAGE

Form Approved OMB No. 0704-0188

1. REPORT DATE *(DD-MM-YYYY)*	2. REPORT TYPE	3. DATES COVERED *(From – To)*
12-09-2006	Final Report	21 August 2003 - 21-Aug-06

4. TITLE AND SUBTITLE

Polymers Used as Fuel for Laser Plasma Thrusters in Small Satellites

5a. CONTRACT NUMBER
FA8655-03-1-3058

5b. GRANT NUMBER

5c. PROGRAM ELEMENT NUMBER

6. AUTHOR(S)

Dr. Thomas KM Lippert and Lukas Urech

5d. PROJECT NUMBER

5d. TASK NUMBER

5e. WORK UNIT NUMBER

7. PERFORMING ORGANIZATION NAME(S) AND ADDRESS(ES)
Paul Scherrer Institut
OFLB U110
Villigen PSI CH-5232
Switzerland

8. PERFORMING ORGANIZATION REPORT NUMBER

N/A

9. SPONSORING/MONITORING AGENCY NAME(S) AND ADDRESS(ES)

EOARD
PSC 821 BOX 14
FPO 09421-0014

10. SPONSOR/MONITOR'S ACRONYM(S)

11. SPONSOR/MONITOR'S REPORT NUMBER(S)
Grant 03-3058

12. DISTRIBUTION/AVAILABILITY STATEMENT
Approved for public release; distribution is unlimited.

13. SUPPLEMENTARY NOTES

14. ABSTRACT

This report results from a contract tasking Paul Scherrer Institut as follows:
Three different polymers (GAP, PVN and PVC) with two different absorbers (carbon nanoparticles and an IR-dye (Epolite 2057)) have been investigated as fuel for the micro laser plasma thruster. GAP and PVN are energetic polymers with a high decomposition enthalpy of -3829 J/g (PVN) and -2053 J/g (GAP). PVC was used as a less energetic (the decomposition enthalpy of -418 J/g is much lower than for the other two polymers) commercially available reference.
The best overall performance was observed for GAP. In the ms thrust measurements a efficiency of 370% was obtained for GAP+C, which means that chemically stored energy was transferred into thrust. In the fs measurements, higher thrust values were obtained for GAP+IR than for GAP+C. This is also in good correlation with the fs plasma emission measurements. The IR-dye lead to a higher fragmentation in the shadowgraphy measurements, which were performed at low fluences. The metal- and metal-oxidenanoparticles had no positive influence on the plasma and shockwave properties of GAP+IR. In the ns mass spectrometry measurements, GAP showed the highest fragmentation and the fastest C+ ions.
The highest energetic polymer PVN, showed the worst performance in all experiments at high fluences, and only a efficiency of 21% was obtained in the thrust measurements. In the mass spectrometry measurements, strong signals could be assigned to the solvent, which was used to produce the PVN film. Also strong thermal effects, like the formation of fibers and melting were observed. In the shadowgraphy measurements, which were performed in air and at low fluences, the fastest shockwave was observed for PVN+IR. Additional doping with CuO slowed down the shockwave, but also reduced the thermal features. For PVC a efficiency of 50% was determined in the thrust measurements. At high laser fluences, PVC performed worse than GAP, but better than PVN.

15. SUBJECT TERMS
Polymers, laser ablation, micro thruster, LED laser, EOARD

16. SECURITY CLASSIFICATION OF:			17. LIMITATION OF ABSTRACT	18, NUMBER OF PAGES	19a. NAME OF RESPONSIBLE PERSON
a. REPORT	b. ABSTRACT	c. THIS PAGE			BARRETT A. FLAKE
UNCLAS	UNCLAS	UNCLAS	UL	96	19b. TELEPHONE NUMBER *(Include area code)* +44 (0)20 7514 4285

Final Report

Contract FA8655-03-1-3058 for the time period of

October 1, 2003 to August 31, 2006

Lukas Urech and Thomas Lippert

Paul Scherrer Institut

5232 Villigen

Switzerland

Polymers used as Fuel for Laser Plasma Thrusters in Small Satellites

The studies in this project were performed in close cooperation with Claude Phipps (Photonic Associates, Santa Fee, NM), who works on the more applied and testing related aspects of the application of micro laser plasma thrusters (LPT). The main goal of this project was to develop and optimize the performance of polymers as fuel for LPT and to correlate time resolved measurements, such as ns-shadowgraphy and plasma emission spectroscopy experiments, with thrust performance.

Summary

Three different polymers (GAP, PVN and PVC) with two different absorbers (carbon nanoparticles and an IR-dye (Epolite 2057)) have been investigated as fuel for the micro laser plasma thruster. GAP and PVN are energetic polymers with a high decomposition enthalpy of -3829 J/g (PVN) and -2053 J/g (GAP). PVC was used as a less energetic (the decomposition enthalpy of -418 J/g is much lower than for the other two polymers) commercially available reference.

The best overall performance was observed for GAP. In the ms thrust measurements a efficiency of 370% was obtained for GAP+C, which means that chemically stored energy was transferred into thrust. In the fs measurements, higher thrust values were obtained for GAP+IR than for GAP+C. This is also in good correlation with the fs plasma emission measurements. The IR-dye lead to a higher fragmentation in the shadowgraphy measurements, which were performed at low fluences. The metal- and metal-oxide-nanoparticles had no positive influence on the plasma and shockwave properties of GAP+IR. In the ns mass spectrometry measurements, GAP showed the highest fragmentation and the fastest C^+ ions.

The highest energetic polymer PVN, showed the worst performance in all experiments at high fluences, and only a efficiency of 21% was obtained in the thrust measurements. In the mass spectrometry measurements, strong signals could be assigned to the solvent, which was used to produce the PVN film. Also strong thermal effects, like the formation of fibers and melting were observed. In the shadowgraphy measurements, which were performed in air and at low fluences, the fastest shockwave was observed for PVN+IR. Additional doping with CuO slowed down the shockwave, but also reduced the thermal features.

For PVC a efficiency of 50% was determined in the thrust measurements. At high laser fluences, PVC performed worse than GAP, but better than PVN.

1. Materials

The micro-Laser Plasma Thruster (µ-LPT) offers a new option in the field of micro-propulsion for both civilian and military space missions. It meets the requirements of low mass, volume and power consumption, which are critical for these micro satellite platforms.

The µ-LPT is driven by small powerful diode lasers, which emit in the near IR (930-980 nm) with an available power of around 1 to 5 W and a pulse length from 100 µs to the millisecond range [1]. This pulse duration and wavelength require the utilization of materials for the fuel layer with low thermal conductivity, i.e. polymers [1, 2].

The laser beam is focused on a polymer tape consisting of a transparent supporting layer, through which the light passes without perforating it, and an absorbing fuel layer, where the micro-jet is produced by the laser-material interaction. In order to obtain bidirectional thrust on three axes, six single-axis thrust units are needed.

For a 25-kg satellite, a low weight of these propulsion devices (less than one kg) is the most important criterion. Other requirements are at least 75 µN thrust and 300 N-s lifetime impulse [3, 4]. These mission targets can not be reached with commercially available polymers. Therefore, new polymer-absorber systems had to be developed and tested.

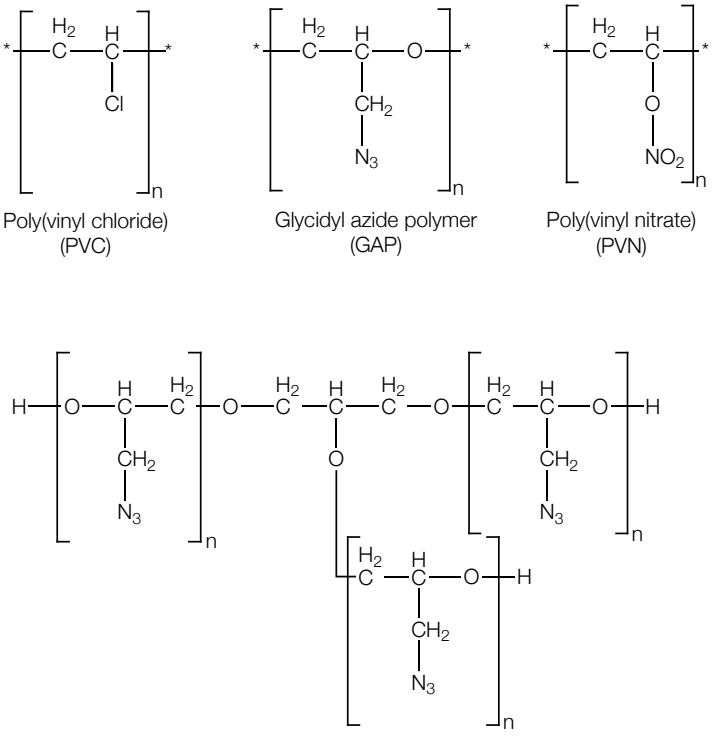

Fig. 1. Structure of the investigated polymers.

One major part of this project consists in the selection and development of suitable polymers for the LPT application. As most polymers do not absorb in the IR range, different dopants, e.g. carbon nanoparticles or IR-dyes (investigated in Report [5]), had to be incorporated in the polymer films. The polymers will be referred to in this report with the abbreviation of the polymer and by indicating the dopant by "+ C" for carbon and "+ IR" for IR-dye.
The investigated polymers were Poly(vinyl chloride) (PVC), a Glycidyl acide Polymer (GAP) and Poly(vinyl nitrate) (PVN) (see Fig. 1).
For GAP a polyole with 2.7 OH groups per chain was used (most probable structure is a mixture of 30 % GAP and 70 % GAP POLYOL). This leads to a more cross-linked polymer compared to a linear polymer like GAP diol.

GAP and PVN are both energetic polymers, which release significant amounts of energy during decomposition. PVC was used as a less energetic and commercially available reference, to compare the influence of the chemically stored energy (properties in Table 1).

Table 1 Decomposition properties of PVC, GAP and PVN

Polymer	**Decomposition Temperature [°C]**	**Decomposition* Enthalpy [J/g]**	**Volume of Detonation Gases [l/kg] [6]**
PVC	241,288,383	-418	
GAP	249	-2053	1052
PVN	204	-3829	1009

*measured by DSC, using carbon doped samples of the polymer.

1.1. PVC

PVC was purchased from Aldrich. A 10 wt-% solution in cyclohexanone was obtained by stirring over night. A 1 wt-% carbon-cyclohexanone solution was added to reach a final carbon concentration in the polymer of 1 wt-%. The polymer-carbon solution was solvent cast on a microscopy slide and dried at 40 °C over night.
Basic, acidic, electrical conductive and carbon nanopearls were investigated as dopants. The aim was to obtain a stable dispersion in the same solvent as the polymer. Only Black Pearls 2000 showed no signs of sedimentation in 24 hours and were therefore used as dopant for PVC.

The carbon suspension was produced by mixing it with a high-speed stirrer (Ultra-Turrax® T25 basic from IKA®) at 30000 rpm for 40 seconds.

1.2. GAP

A 40 % solution of GAP in ethyl acetate was obtained from Nitrochemie Wimmis AG. The GAP solution was mixed with a 1 wt-% dopant-ethyl acetate solution to reach a concentration of 1% carbon or 1.4 % of IR dye. The different concentrations for the two dopants were chosen to achieve an equal linear absorption coefficient at 1064 nm for carbon and IR-dye doped GAP samples.
The solvent was evaporated at 50 °C and 10 mbar, to reduce the solvent content to 30 wt-%, in order reach a viscosity suitable for tape casting.
One drop of the catalyst Dibutyltin Dilaurate and 13 wt-% of Hexamethylen-1,6-diisocyanate were mixed for 5 min with the polymer. The polymer solution was then solvent casted on microscopy glass slides (for ablation, emission and shadowgraphy experiments) or solvent casted with a draw blade on a Kapton film (for thrust and mass spectrometry measurements).
The films were left to polymerize for one day. Then they were stored in a vacuum oven at 50 mbar for 5 hours to remove remaining solvent from the polymer film. The films were then heated to 50 °C at 50 mbar to finish the cross-linking reaction.

Carbon nanoparticles (Black Pearls 2000, Cabot) and Epolite 2057 were used as dopants for GAP. Epolite 2057 was selected because it is stable in ethyl acetate, shows a homogeneous distribution within the polymer film and was stable over time.

Problems

The GAP films reveal a rubber like consistency after drying and tend to be sticky, what would be a problem for the tape applied as fuel for LPT. Probably not all of the solvent could be removed, even after drying the films at a pressure of $2 \cdot 10^{-5}$ mbar for 24 hours (Fig. 2).
The weight of the polymer films was measured after casting, after drying under air and in vacuum, and after cross- linking at 50 °C. After 96 hours of drying in vacuum, 2.8 % (GAP with 16.6 % cross-linker), 3.1 % (GAP with 14.9 % cross-linker), 3.7 % (GAP with 16.6 % cross-linker) of the solvent remain in the polymer film.

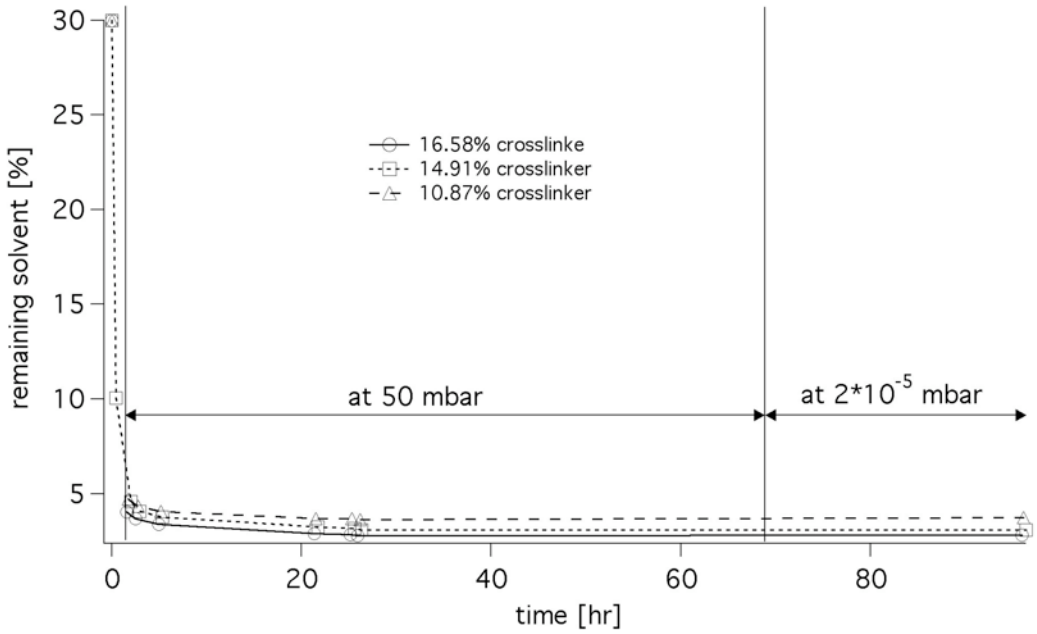

Fig. 2. Amount of solvent left in GAP films after drying, cross-linking and storage at 100 mbar and $2 \cdot 10^{-5}$ mbar.

Different cross-linker concentrations (from 8 % to 25 %) were also tested, but the consistency did not change.

A easy solution to this problem was to apply a layer of chalk powder on the film surface. This efficiently prevented the tapes from sticking to the support-layer of the next layer when they were spooled up.

1.3. PVN

PVN was synthesized according to a procedure described by Stecker et al [7] and Diepold [8].

A 25 wt-% solution of PVN in acetone was mixed with a 1 wt-% basic carbon-acetone solution. The polymer was cast on a glass slide and dried under a saturated acetone atmosphere (Fig. 3). Drying in air results in the formation of a solid PVN membrane on top of the solvent, which leads to the formation of bubbles by trapping the evaporating acetone. Allowing the solvent to evaporate in a saturated solvent atmosphere inhibits the formation of this membrane.

The PVN films were very soft, but not as sticky as the GAP films. Longer drying under elevated temperature (40 °C) did not harden the polymers. This may also be a problem for the LPT application.

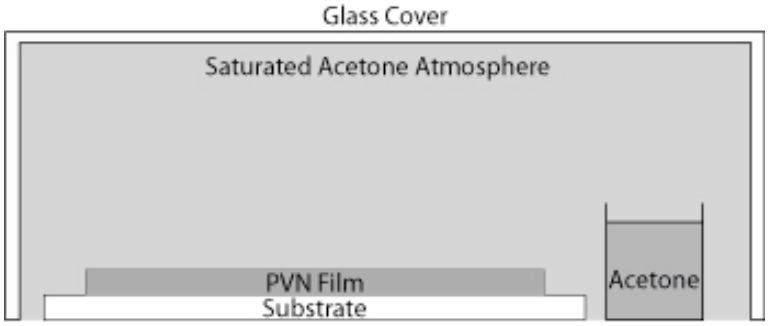

Fig. 3. Setup for the slow drying of PVN, to avoid bubble formation.

1.4. Additional doping with metal- and metal oxide-nano-particles

Metal (Al (for GAP)) and metal-oxide (CuO (for GAP and PVN)) nano-particles have been added to the IR-dye doped energetic polymers to further improve and control the energy release.

The metal particles can react with nitrogen, C, CO or O_2 produced by the decomposition of the polymer (e.g. AlN) [9]. Additional energy would be gained by the formation of such stable compounds. It has been reported that the addition of metal particles increases the decomposition energy of GAP [10] and that the addition of metal-oxides to PVC influences the onset of the thermal decomposition [11, 12].

1.5. Particle size distribution in the carbon doped polymers

The exact particle distribution within the polymer films could not yet be determined, as the applied carbon is amorphous and can therefore not be analyzed by conventional methods such as X-ray diffractometry. For the X-ray diffraction experiment a cubic sample exhibiting a volume of about 0.3 mm^3 was cut from the bulk material. The cube was glued (highly diluted Araldite®) to a glass fiber and mounted on a goniometer for sample alignment in the beam. The experiments were performed with a rotating anode X-ray source (Molybdenum Kα1, 0.70926 Å) and a beam size of about 0.3 mm. The data was collected for 5 minutes using an Mar345 image plate detector at a sample to detector distance of 150 mm.

In Fig. 4 the X-ray diffraction pattern of GAP+C is shown. The dark ring corresponds to the glass capillary which was used as support. No signal from the polymer or the carbon nanoparticles is visible.

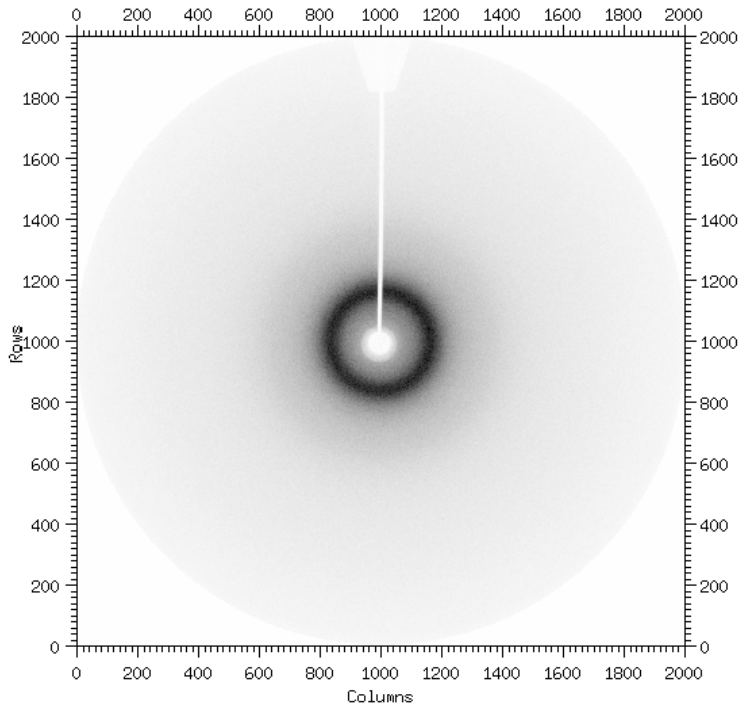

Fig. 4. X-ray diffraction measurement of GAP+C to determine the particle size distribution. Only background is detected.

A measurement at the Material Science X-Ray tomographic microscopy (XTM) Beamline at the Swiss light source (SLS) [13] was performed on GAP+C to determine the agglomeration rate and particle size distribution of the carbon nanoparticles in the polymer. The motivation for this experiments was the possibility to use the difference in the phase contrast for GAP and the carbon nanoparticles [14]. A few cross-sections of a GAP+C film on a Kapton™ film are shown in Fig. 5. The two letters give the orientation of the slice.

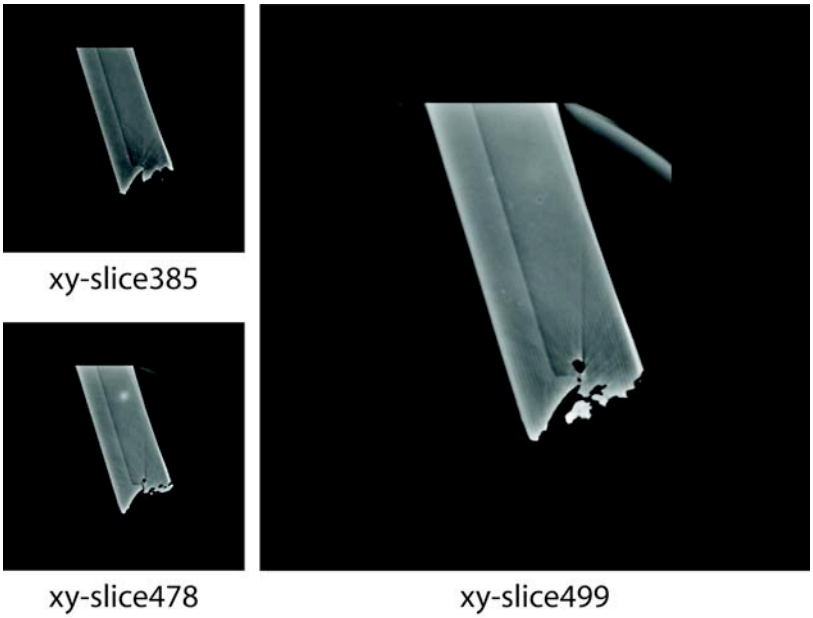

Fig. 5. Cross-sections of a GAP+C film on Kapton recorded at the XTM Beamline at the SLS.

In all images, two phases can be distinguished. The larger phase corresponds to GAP+C, the thinner layer is the Kapton substrate. Within the GAP+C-layer no carbon clusters can be distinguished from the polymer. The resolution of the XTM Beamline is around 1 µm, and should therefore be sufficient to observe carbon clusters in the expected size range of 15 µm. The most reasonable explanation for the lack of a second phase in the GAP+C film is the similar phase contrast of the amorphous carbon sooth used as absorber and the polymer, which also consists to major part of carbon (36 wt-%).

The dopant particle distribution seems to have a significant influence on the ablation behavior. A more homogeneous distribution of smaller particles would most probably result in a better performance of the carbon doped polymers.

2. ns Experiments in Air

2.1. Ablation Experiments

All ablation experiments were performed with the fundamental (λ = 1064 nm) wavelength of a Nd:YAG laser (Brilliant BW Nd:YAG, Quantel, τ = 6 ns) with a Gaussian beam profile that contains some hotspots (from burn-marks on our laser rod), which complicate the analysis.
The ablation rates for PVC, GAP and PVN were studied as a function of the laser fluence. The depth of the ablation craters were measured with a surface profilometer (Sloan Dektak 8000). The ablation parameters, α_{eff} (effective absorption coefficient) and F_{th} (threshold fluence) were calculated according to equation 1 [15, 16]:

$$d(F) = \frac{1}{\alpha_{eff}} \ln\left(\frac{F}{F_{Th}}\right) \qquad (1)$$

The plasma threshold fluence (F_{plasma}) was determined by visually detecting the onset of plasma formation with increasing laser fluence.

Ablation rates

The ablation rate of PVN+C could not be obtained with a surface profilometer, as the polymer is too soft. The threshold fluence ($F_{th\ PVN+C}$ =860 mJ/cm^2) was therefore determined by using an optical microscope.

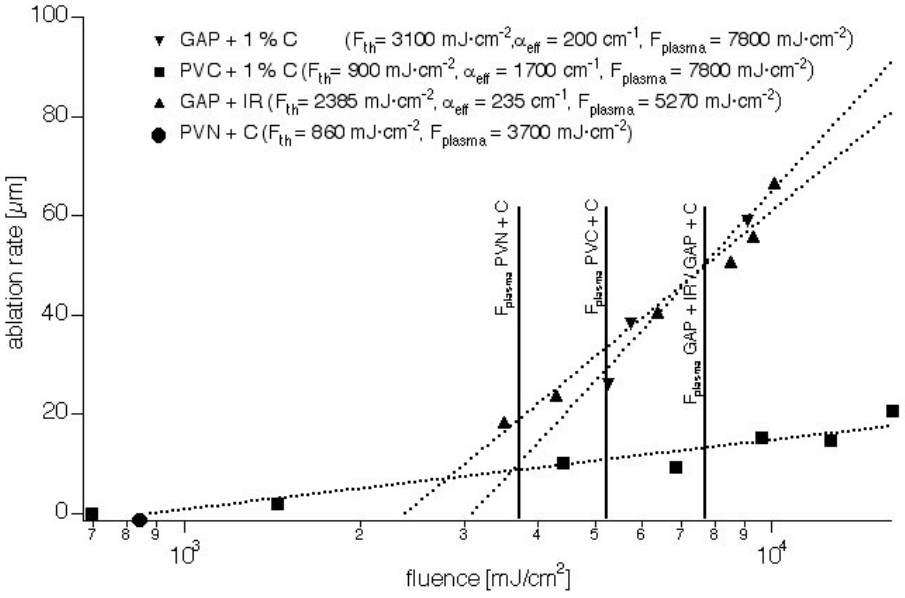

Fig. 6. Ablation rates of PVC+C, GAP+C, GAP+IR and PVN+C at 1064 nm. The ablation rates for PVC+C, GAP+C are adapted from Report [5] to allow a direct comparison of the results.

The threshold fluence was similar for GAP with both dopants ($F_{th\ GAP+C}$ = 3100 mJ/cm^2 and $F_{th\ GAP+IR}$ = 2385 mJ/cm^2). PVC+C reveals a significantly lower ablation rate and threshold fluence ($F_{th\ PVN+C}$ =900 mJ/cm^2) than the GAP films.

Only small differences in the ablation rate between the two dopants were found for GAP. At very high fluences (above 40 J/cm^2) a constant ablation rate is observed for GAP (not shown in Fig. 6). This is most probably due to plasma shielding [17] and the breakdown of air, that is also observed at this fluence.

Ablation spot morphology

All four polymers were irradiated with one pulse at a fluence of 33 J/cm^2 to analyze the different ablation spot morphology. The ablation spots were analyzed with a Scanning Electron Microscope (SEM) (Fig. 7) and an optical microscope.

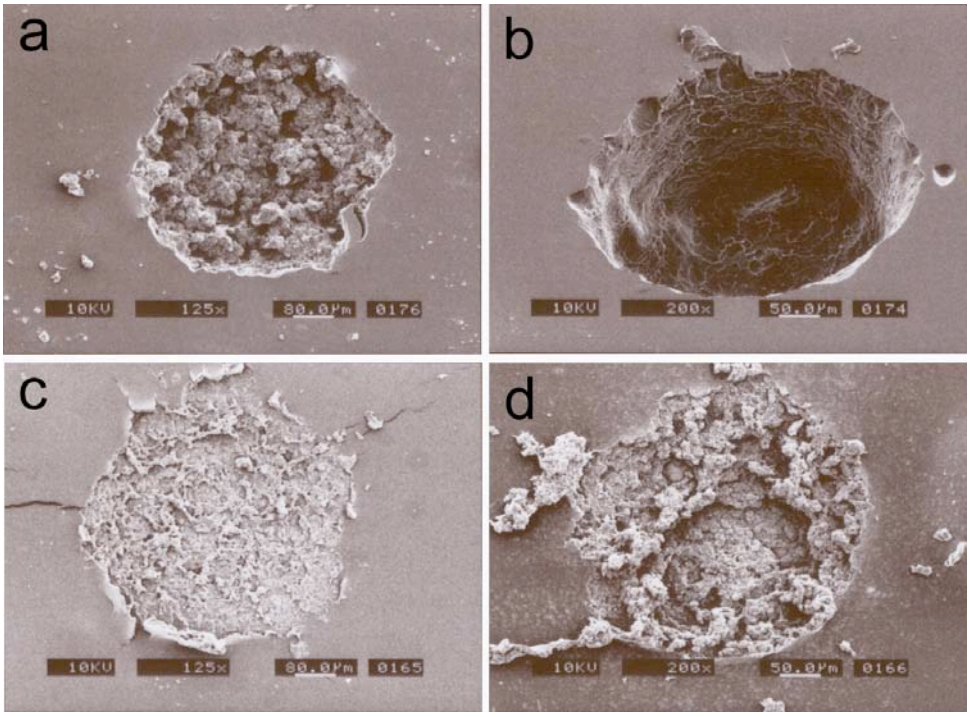

Fig. 7. SEM images, showing the different ablation spot morphologies of (a) GAP+C, (b) GAP+IR, (c) PVN+C and (d) PVC+C after irradiation for one pulse with 33 J/cm^2 at 1064 nm with a 125 times magnification.

GAP+IR (Fig. 7b) reveals an ablation crater with a sharp edge and smooth walls. This is most probably due to the molecular distribution of the IR-dye in the polymer, which leads to a homogeneous absorption of the light in the polymer layer.

The morphologies of the ablation craters of all carbon doped polymers are much rougher compared to GAP+IR.

The carbon nanopearls used in GAP and PVC with a nominal size of 15 nm tend to agglomerate into larger clusters with sizes in the range of 10 to 20 µm [18]. This agglomeration can result in the formation of local hotspots, which decompose the material in their vicinity. This local decomposition results in formation of gaseous products and the ejection of the carbon nanoparticles and polymer fragments between the hotspots [19]. The difference between the carbon doped materials may be explained by the application of different carbons. In the case of PVN basic carbon sooth was used instead of carbon nanopearls, because no stable suspension of carbon nanopearls could be produced in acetone. The basic carbon sooth shows a different agglomeration behavior and also the particle size distribution might differ from carbon nanopearls.

In the case of the energetic polymers, additional energy is produced by the decomposition of the material. This energy may cause a further decomposition of the surrounding material and an additional production of gaseous products. This could be the reason that ejected material is not as pronounced redeposited on the surface as observed for PVC+C (Fig. 7d).

The bottom of the ablation crater of GAP+C (Fig. 8a) reveals a very rough texture with holes in the range of 10 to 20 µm, which is in the same order of magnitude as the "expected" agglomerated carbon nanoparticles. The ablation of GAP+IR (Fig. 8b) reveal a much smoother surface at the bottom of the ablation crater, with structures that resemble filaments

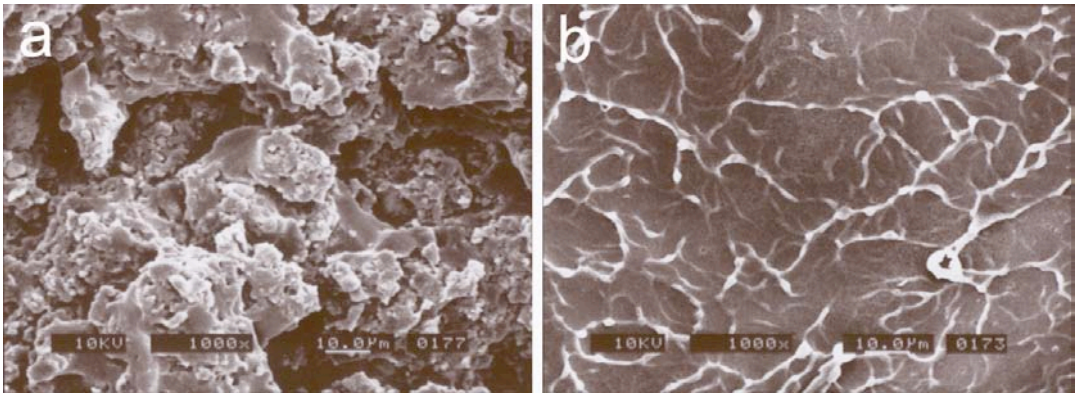

Fig. 8. SEM image of the bottom of the ablation crater of (a) GAP+C and (b) GAP+IR after irradiation for one pulse with 33 J/cm^2 at 1064 nm with a magnification of 1000 times.

2.2. Shadowgraphy

Shadowgraphy is a fast measurement that can be performed under ambient conditions. From the recorded images, it is possible to determine the shockwave and particle velocity. Also the shape of the shockwave and the particle plume can be used to study the ablation behavior of the different polymers. The shadowgraphy measurements are performed at a fluence below

the plasma formation threshold fluence, and the observed properties may therefore be difficult to compare to other experiments, that are performed at much higher fluences.

A pump probe setup was used for the shadowgraphy measurements. A 400 µm ablation spot was produced with the pump laser (λ = 1064 nm). As probe source, a XeCl excimer laser (λ = 308 nm, Compex 205 from Lambda Physics, τ = 30 ns) was used to excite a laser dye (Rhodamine 950, from Exiton). The experimental setup is shown in Fig. 9.
All shadowgraphy experiments were performed under ambient conditions using the fundamental wavelength (λ = 1064 nm) of a Nd:YAG laser (Brilliant BW Nd:YAG, Quantel, τ = 6 ns) with a Gaussian beam profile that contains some hotspots.

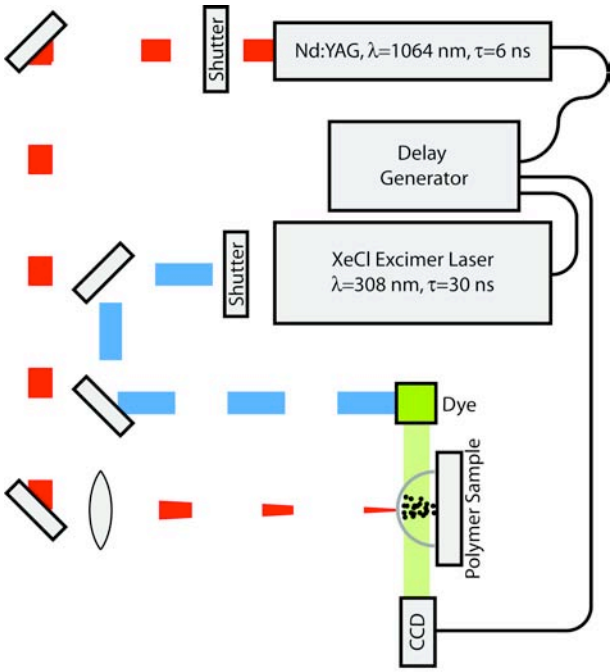

Fig. 9. Scheme of the pump probe setup used to record the shadowgraphy images.

The recorded images were digital enhanced to improve the visibility of the relevant details, e.g. the shockwave and particles ejected from the polymer.

Results

GAP+IR

In the shadowgraphy images of GAP+IR no ejected particles are visible (Fig. 10). This indicates a high conversion rate of ablated material into to the gaseous state.

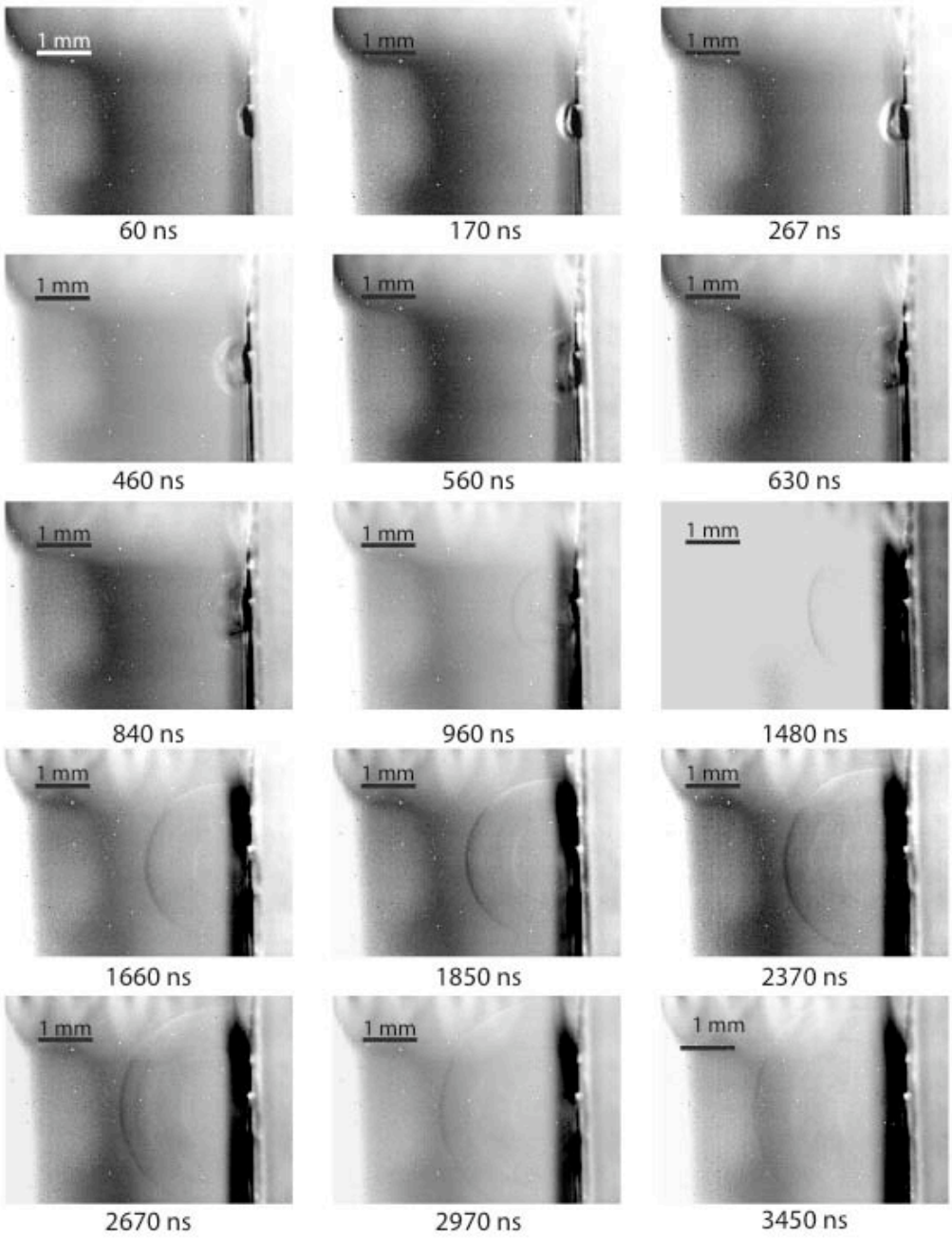

Fig. 10. Shadowgraphy images of GAP+IR. The times indicate the delay of the picture to the pump laser beam. The polymer was irradiated with a fluence of 2.87 J/cm^2 at 1064 nm.

At later times, e.g. 1500 ns, the shockwave can be divided into two different domains. The front domain looks very smooth, whereas the following domain displays a disturbed appearance (Fig. 11). The rear of the shockwave is traveling much slower, which leads to an increase in size of this disturbed area. The shockwave in air is visible as a layer of compressed air. This compression changes the density and thereby the index of refraction. In the second domain, the compressed air relaxes and expands not uniformly and slower than the shockwave front. This leads to an increase in size of the second domain with time.

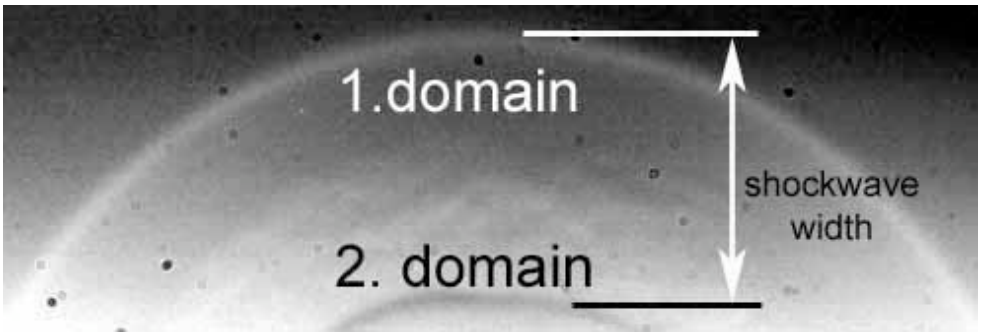

Fig. 11. Shadowgraphy image of the shockwave of GAP+IR after irradiation with a fluence of 2.87 J/cm^2 at 1064 nm. The shockwave can be separated into two parts, a smooth domain (1. domain) and a disturbed domain (2. domain).

The shockwave velocity of GAP+IR decreases with decreasing fluence (Fig. 12). At higher fluences more material is decomposed, and more energy is set free in addition to the higher laser energy. The shockwave speed decreases exponentially over time, what can be explained by the "drag" of air, in which the shockwave propagates. The shockwave propagation perpendicular to the surface is two times faster than the propagation parallel to the surface, due to the drag (in this case also from the polymer surface).

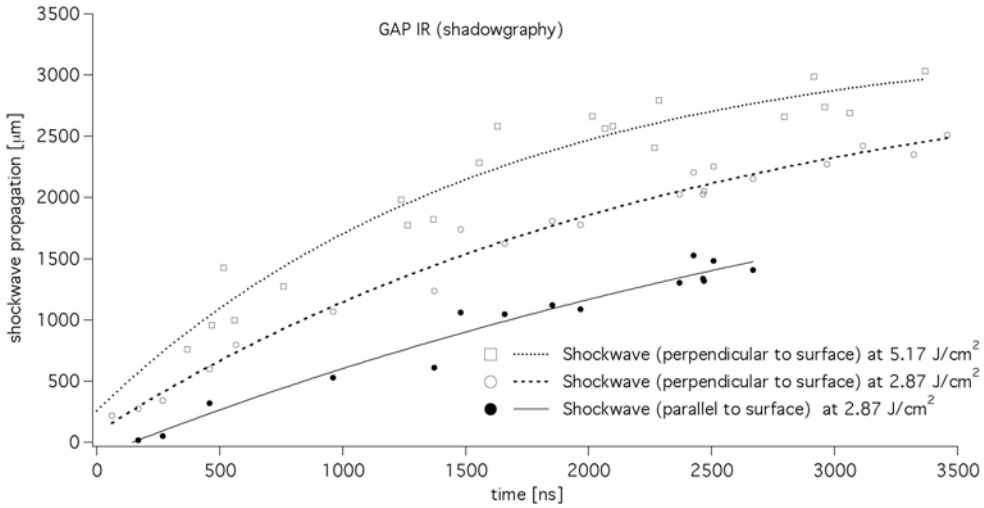

Fig. 12. Analysis of the shockwave front propagation of GAP+IR after irradiation at 1064 nm with a fluence of 5.17 J/cm^2 and 2.87 J/cm^2.

PVN+C

A shockwave is visible for PVN+C after 90 ns, followed by the ejection of particles (Fig. 13). After 500 ns the particle cloud can be separated in two parts. A fast traveling part that overtakes the shockwave after 600 ns and a slower bigger part that is expanding mainly perpendicular to the surface and is closing up to the shockwave front after 2300 ns. The fast traveling particles have to break through the dense shockwave front and bulk it out (Fig. 14).

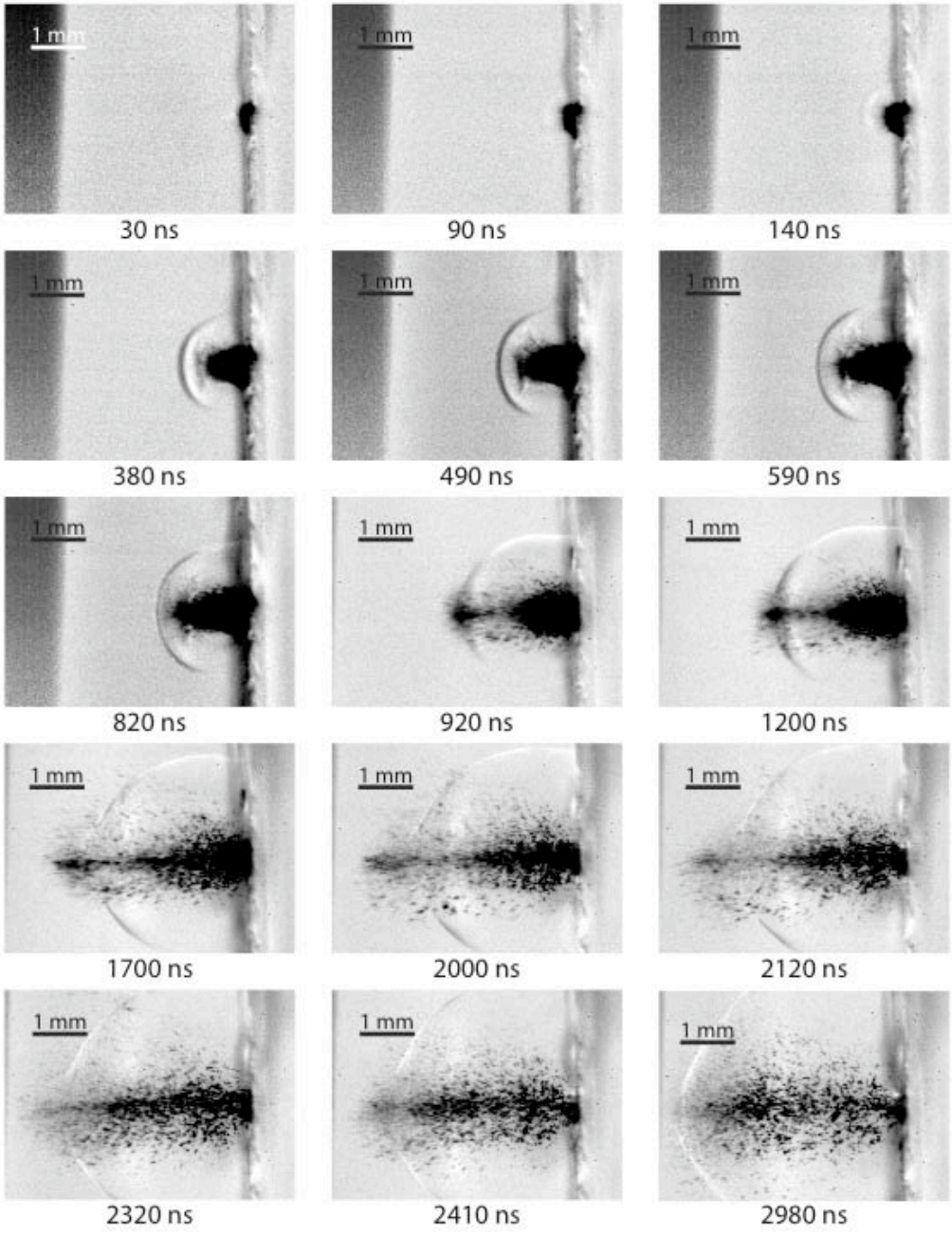

Fig. 13. Shadowgraphy images of PVN+C. The times indicate the delay of the picture to the pump laser beam. The polymer was irradiated with a fluence of 2.78 J/cm^2 at 1064 nm.

The shockwave velocity perpendicular and parallel to the surface decay both exponentially (Fig. 15). This is caused by the "drag" of the air in which the shockwaves travel. The shockwave propagation perpendicular to the surface is traveling two times faster than parallel to the surface.

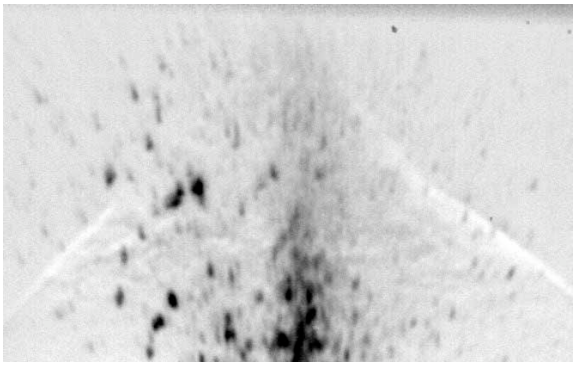

Fig. 14. The particles ejected by PVN+C overtake the shockwave front and thereby bulk it out.

The particle front is slowed down from 2580 m/s to 1700 m/s in the process of breaking through the shockwave front. This may is most probably due to the higher density of the air at the front of the shockwave. The change of velocity of the particles is clearly visible in the change of the slope of linear fits in Fig. 15 (-----) after the particles pass through the shockwave.

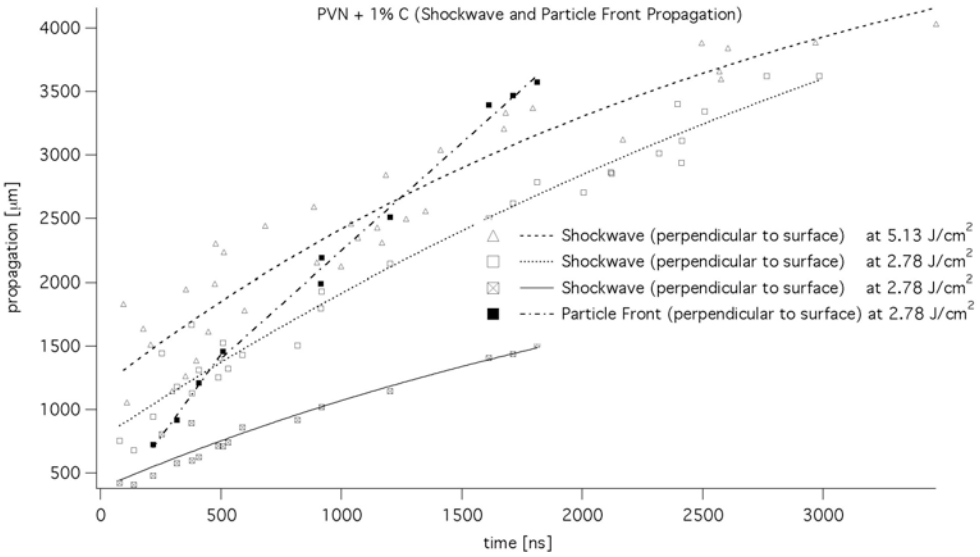

Fig. 15. Analysis of the shockwave and particle front propagation of PVN+C after irradiation at 1064 nm with a fluence of 5.13 J/cm^2 and 2.78 J/cm^2.

A comparison with data for GAP+C and PVC+C from [5] reveal that the influence of the IR dye in GAP is visible, but not very pronounced (Fig. 16). PVN+C is traveling much faster, and the decay of the propagation velocity is slower compared to GAP and PVC, while PVC+C reveals the slowest propagation velocity.

During the decomposition of the more energetic polymers GAP and PVN more energy is released compared to PVC (Table 1). This additional energy leads to a faster propagation of the shockwave. This effect can also be observed for GAP+C and GAP+IR. In the shadowgraphy images for GAP+IR no particles are visible, suggesting that more of the

removed polymer has been transformed into the gaseous state than in the case of GAP+C, where a large amount of solid particles is observed in the products. The shockwave of PVN+C, which shows the most exothermic decomposition properties, reveals the fastest propagation, even for the not complete decomposition into gaseous products.

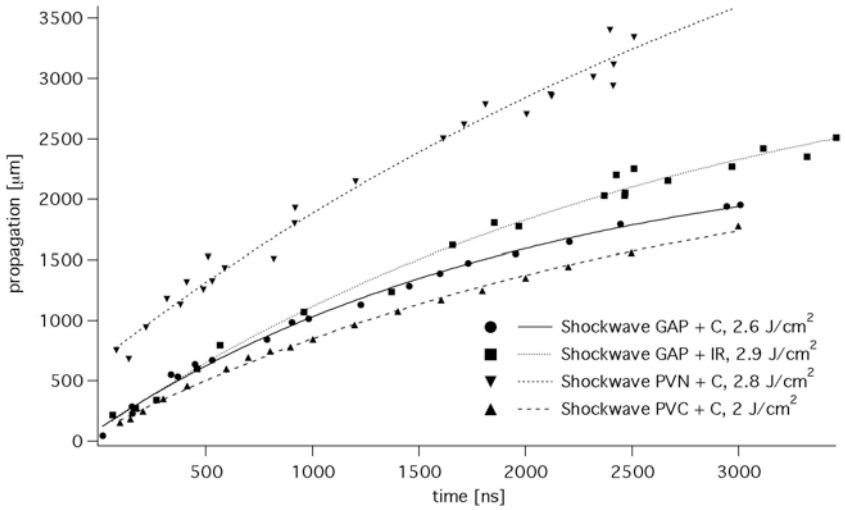

Fig. 16. Shockwave propagation of GAP+IR, GAP+C, PVN +C and PVC+C.

GAP doped with IR-dye and Al- or CuO-Nanoparticles

GAP doped with the IR-dye will be used as a reference to study the influence of Al- and CuO-nanoparticles as additional dopant. A hemispherical shockwave with no solid fragments has been observed for GAP+IR. This lack of solid fragments indicates a high conversion rate of the polymer into gaseous products. In the case of the energetic polymers, this means, that decomposing the polymer more completely produces more energy.
The metal and metal-oxide nanoparticles were added prior to evaporating the solvent. In both cases 1% of metal or metal-oxide was added to the polymer.

A hemispherical shockwave is observed for GAP+IR+CuO (see Fig. 17). During the first 2 µs no fragments are visible in the ablation plume. This indicates a high conversion rate of the polymer into gaseous products. The copper oxide particles have a nominal size of 10 nm and are not visible in the shadowgraphy images as long as they do not agglomerate.

After about 1 µs (see arrow in Fig. 17), gaseous products that are formed by the decomposition of the polymer are visible as a second, very disturbed front, which expands slower than the shockwave.

The CuO seems to have only a minor influence on the ablation properties. The main differences between GAP+IR with copper oxide and GAP+IR, is the expansion of gaseous products, which formed a sharper front in the case of GAP+IR.

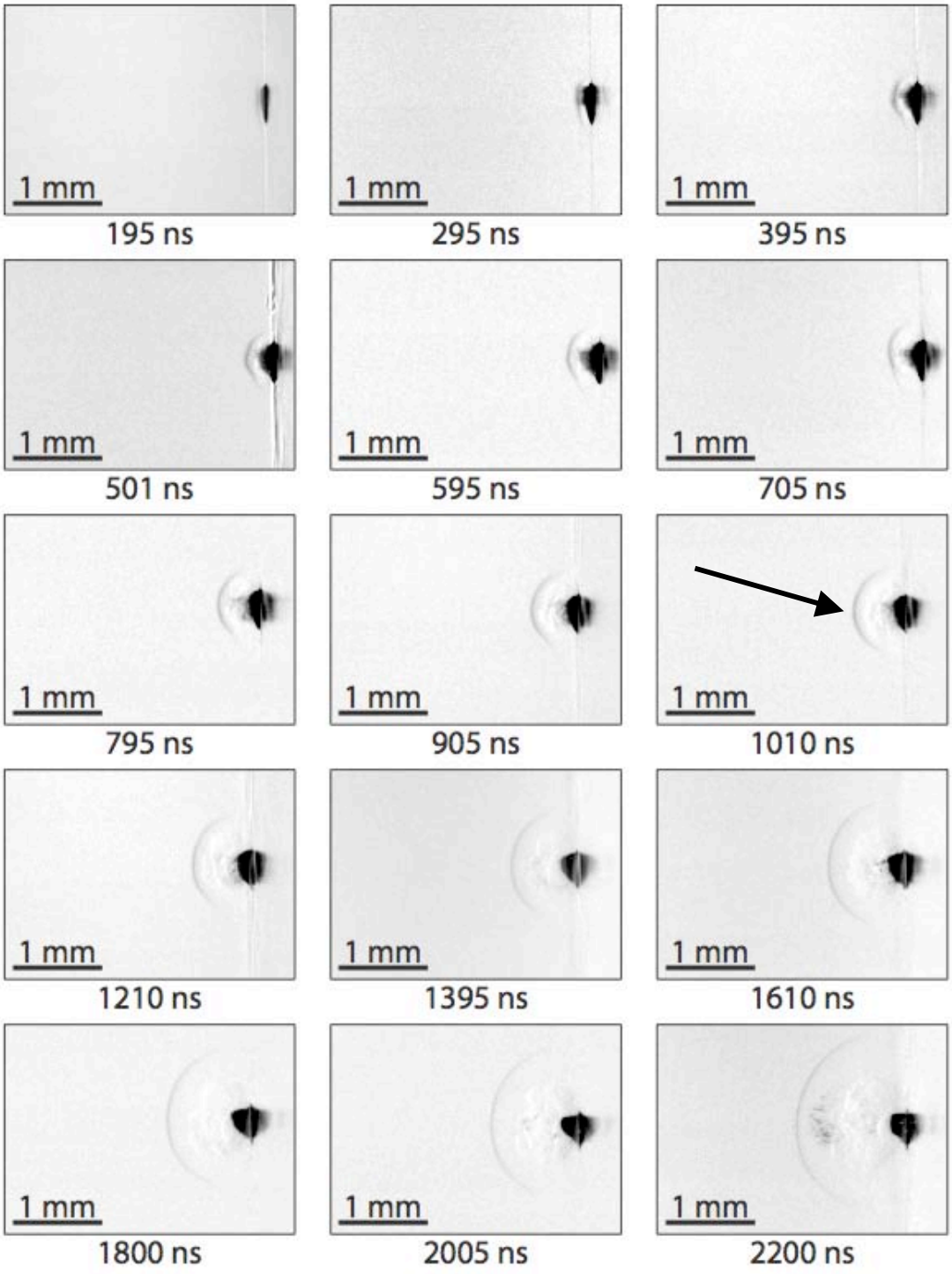

Fig. 17. Shadowgraphy images of GAP+IR+CuO after irradiation with 1064 nm laser light at a fluence of 5.1 J/cm^2.

For GAP+IR+Al a hemispherical shockwave can be observed (shown in Fig. 18). Solid products with a size of 20 to 50 µm are ejected from the polymer 500 ns after the laser pulse

and travel behind the shockwave. A distinct front from expanding gaseous products cannot be distinguished (as seen in the case of GAP+IR+CuO).

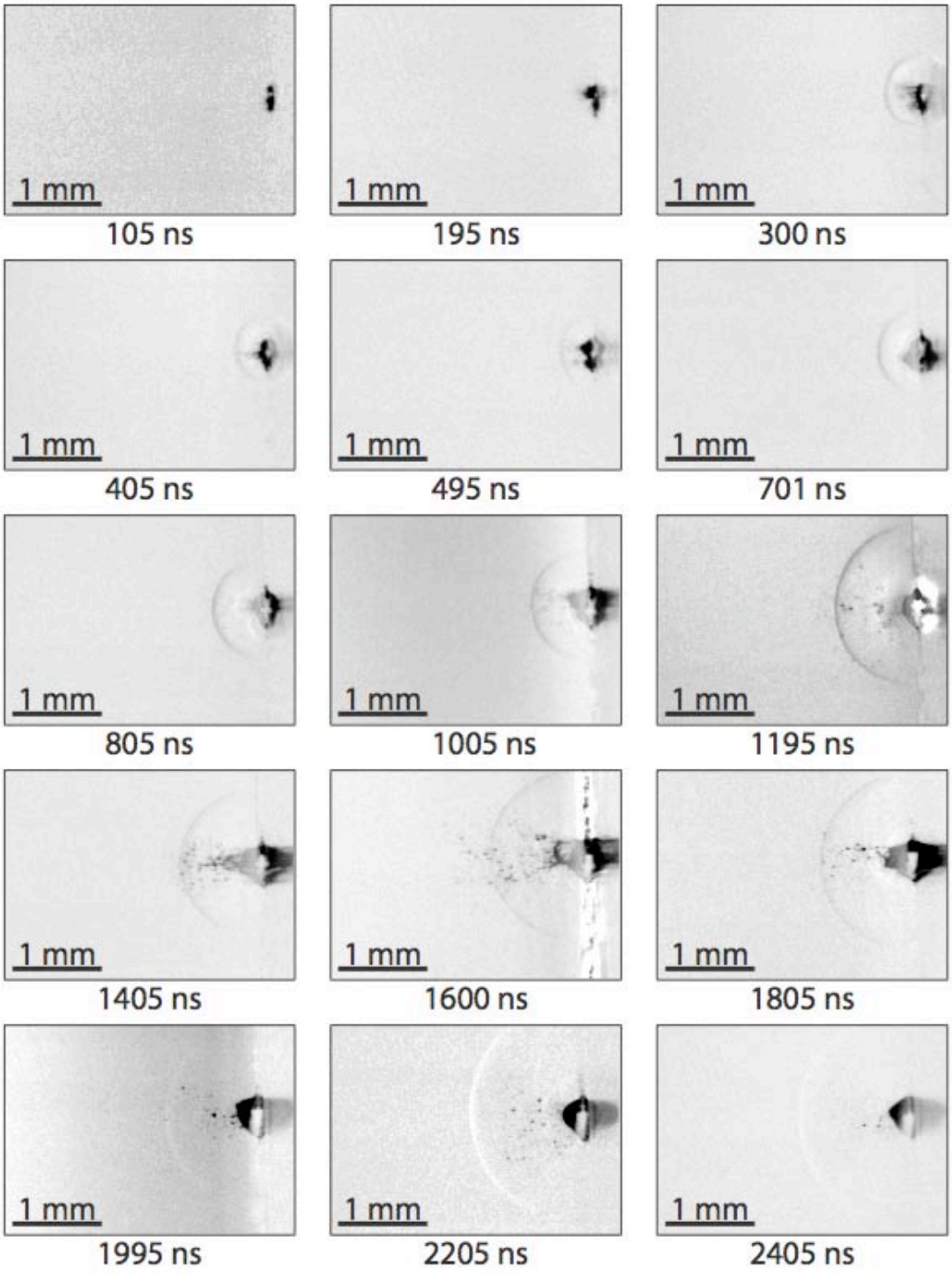

Fig. 18. Shadowgraphy images of GAP+IR+Al after irradiation with 1064 nm laser light at a fluence of 5.1 J/cm^2.

The main difference of Al-doped GAP+IR to GAP+IR with and without copper oxide is the presence of big particles in the ablation plume. This has previously only been observed for carbon doped polymers [5, 20] and resulted in a lower momentum coupling coefficient.

A similar shockwave velocity has been determined for GAP+IR with Al- or CuO-nanoparticles (Fig. 19). In both cases the shockwave speed is lower than for GAP+IR and reveals also a faster decay over time. A reason for the lower shockwave velocities might be that the CuO and Al particles absorb energy without reacting with the polymer or polymer fragments and act therefore just as inert material or even additional "energy sink". This influence might only be observed at the low fluences used for the shadowgraphy measurements where for the thrust measurements much higher fluences are used.

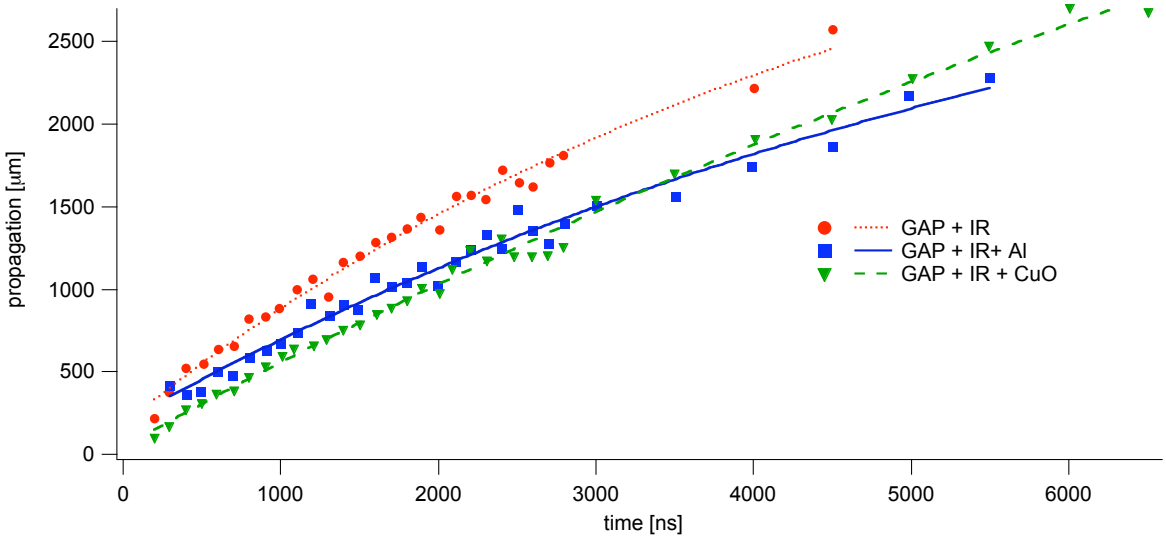

Fig. 19. The shockwave velocity for GAP+IR (●) and GAP+IR doped with Al-(■) or CuO-nanoparticles (▼).

The ablation craters for GAP+IR and GAP+IR+CuO have a similar appearance (shown Fig. 20). Sharp edges are visible in both cases. The uneven structure on the crater bottoms is an image of the inhomogeneous beam profile of our Nd:YAG laser. Also no re-deposited material and no large agglomerates are detected on the films in the vicinity of the crater. This indicates that the CuO nanoparticles do not influence the absorption process in IR-dye doped GAP and only slow down the shockwave as they use energy that could otherwise be used to decompose the polymer.

For GAP+IR+Al a very uneven ablation crater can be observed. Material is re-deposited on the polymer surface. Around the ablation crater clusters of Al-nanoparticles and polymer in the range of 20 to 40 µm are visible. This is similar to the size of the particles observed in the ablation plume with the shadowgraphy measurements. This indicates, that the Al-agglomerates are not broken up and are merely inert material that is ejected. The agglomeration of aluminum has already been observed during the sample preparation. The stability of the Al-dispersion must be improved to produce films with a more homogeneous

distribution of Al-nanoparticles. In Fig. 20(right) the agglomerates of the Al nanoparticles are clearly visible as dark spots around the ablation crater with diameters of up to 30 µm.

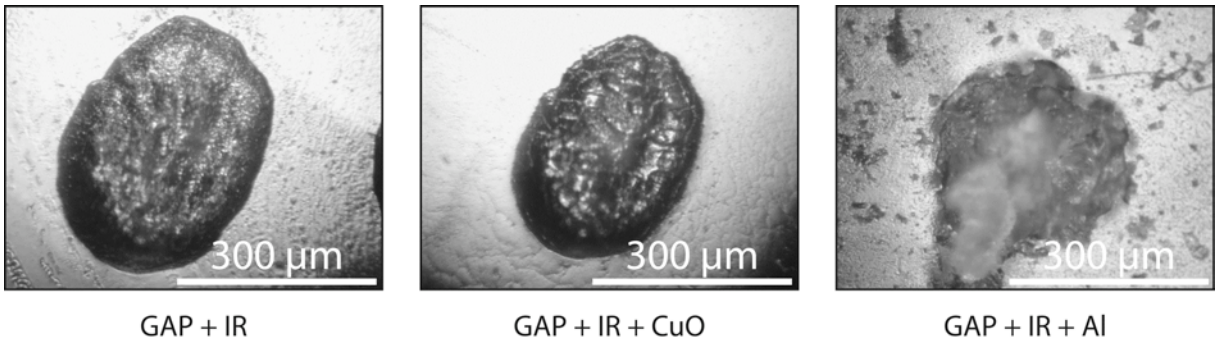

Fig. 20. Microscopy images of the ablation spots of GAP+IR (left), GAP+IR+CuO (middle) and GAP+IR+Al (right) after irradiation with one pulse at 5.1 J/cm^2

The doping with Al- or CuO-nanoparticles does not improve the shockwave properties of IR-doped GAP. In the case of Al, the formation of clusters in the polymer film leads to a less homogeneous ablation crater and the ejection of small fragments. A slower shockwave is also shown for GAP+IR+Al and GAP+IR+CuO compared to GAP+IR. A reason for this may be again the low fluence used in the shadowgraphy measurements. The metal particles act as inert mass and are ejected without reacting with the polymer. This would lower to energy to available for the decomposition of the exothermic polymer. To confirm this, thrust measurements with high fluences have to be performed on GAP+IR+CuO and GAP+IR+Al.

PVN doped with IR-dye and CuO-Nanoparticles

PVN doped with carbon had shown good results in the shadowgraphy measurements. A large amount of fast traveling solid fragments are observed. Is has been shown that the utilization of a IR-dye as absorber improved the ablation properties of GAP (a sharper ablation crater and no solid fragments in the ablation plume). Therefore the same IR-dye has been used for PVN, and the influence of 1% CuO-nanoparticles was also tested. PVN+IR films doped with Al-nanoparticles were also produced, but the agglomeration was even more pronounced than in the case of GAP+IR+Al.

The polymer films were produced as described earlier. The metal-oxide nanoparticles were added prior to solvent casting the polymer solution.

An “egg-shaped” shockwave is observed for PVN+IR up to 500 ns after the laser pulse (shown in Fig. 21), followed by gaseous products that are generated from the decomposition of the polymer.

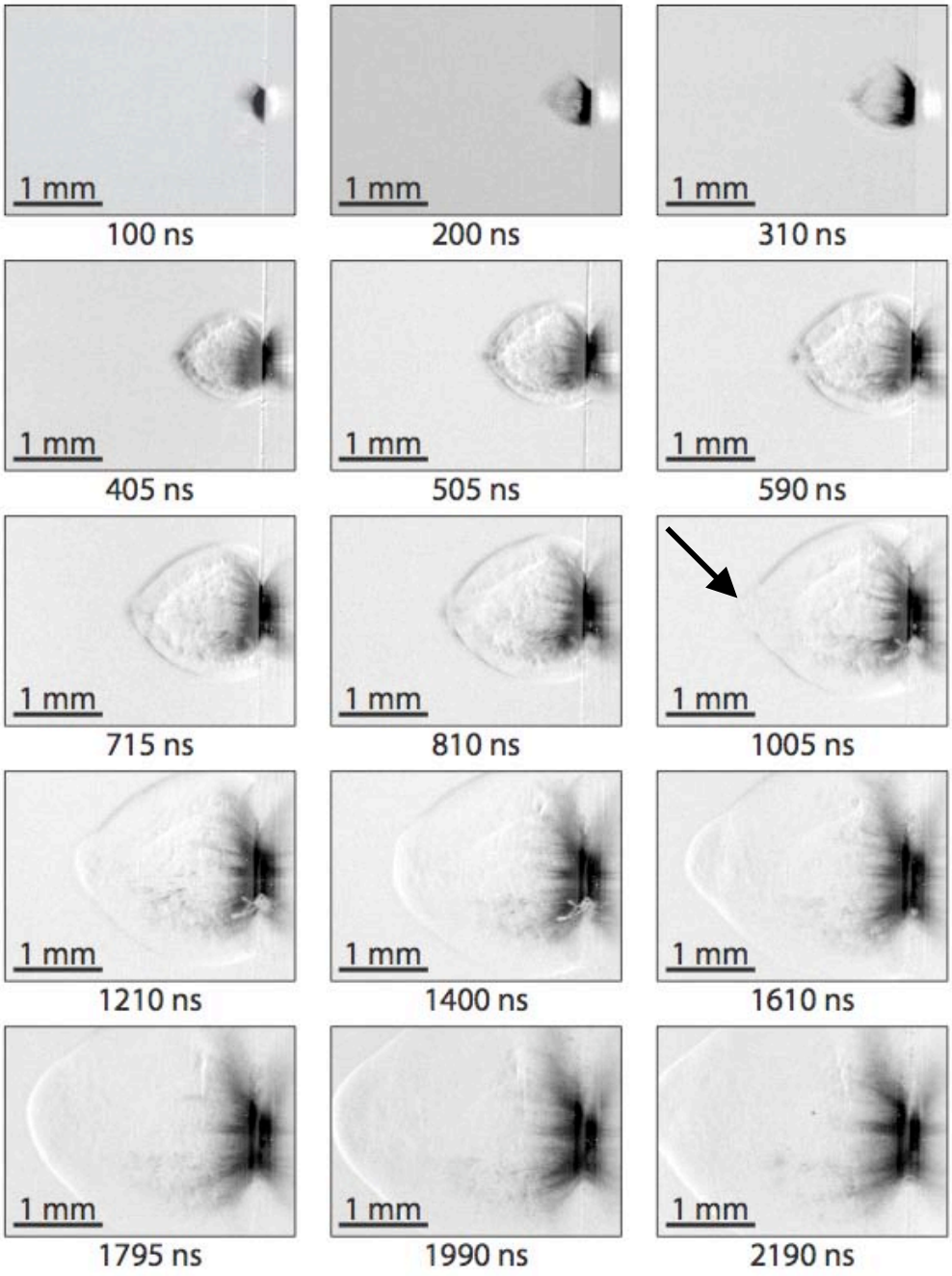

Fig. 21. Shadowgraphy images of the shockwave expansion of PVN+IR after irradiation with 1064 nm laser light at a fluence of 5.1 J/cm^2 during the first 2 µs.

The expansion of the shockwave is more directional for PVN+IR than for any other investigated polymer. After 1 µs an expanding gas front overtakes the shockwave and forms a bump. Solid fragments can only be observed close to the polymer surface in the form of "strings" or "fibers" [21, 22] that are visible until 2 µs after the laser pulse. 3 µs after the laser pulse the "fibers" disappear and small particles are visible that form a dense cloud in front of the polymer (shown in Fig. 22) for several microseconds.

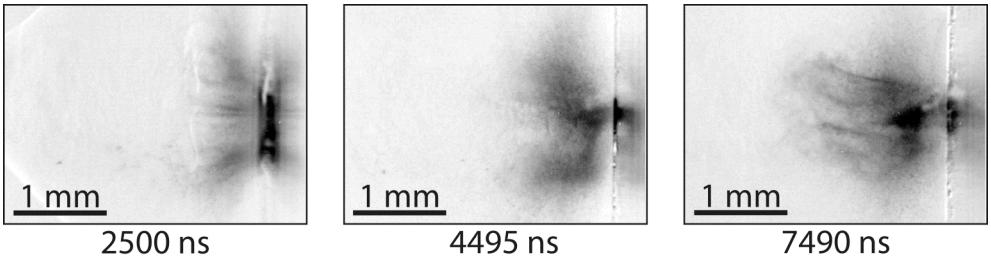

Fig. 22. Shadowgraphy images of the particle ejection of PVN+IR after irradiation with 1064 nm laser light at a fluence of 5.1 J/cm^2.

In the case of PVN+C, more and larger particles were observed. These particles showed a similar behavior like the gaseous products in PVN+IR+CuO. They were also very directional and overtook the shockwave within the first microsecond. The fast shockwave and reduction of solid ejection product are promising signs for PVN+IR, but this assumption has to be tested by thrust measurements.

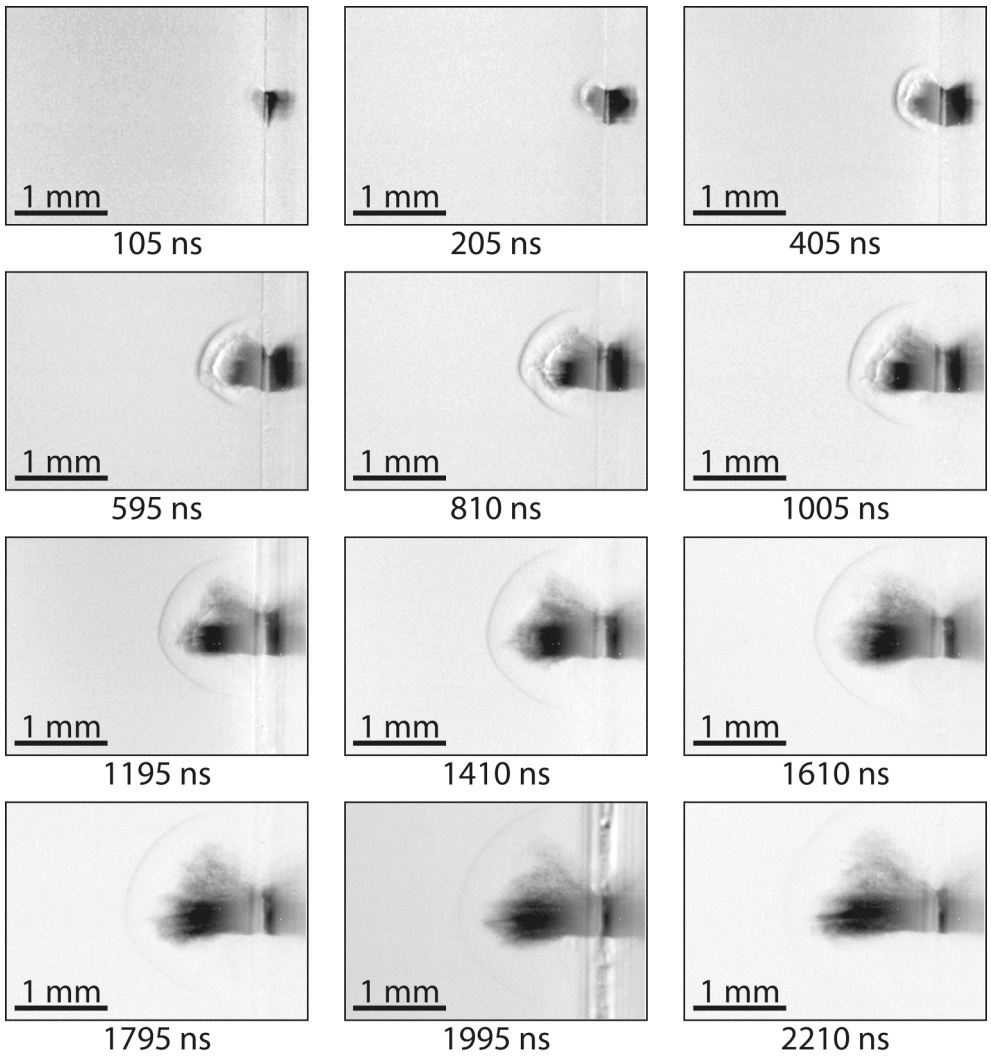

Fig. 23. Shadowgraphy images of PVN+IR+CuO after irradiation with 1064 nm laser light at a fluence of 5.1 J/cm^2.

For PVN+IR with 1% CuO an almost hemispherical shockwave is observed (shown in Fig. 23)

During the first microsecond a second front that can be attributed to the expanding gaseous products is visible behind the shockwave. Solid particles are visible from 200 ns after the laser pulse. The asymmetric expansion of the particle plume is due to the inhomogeneous laser beam profile. The ejected particles travel slower, but more directional, perpendicular to the surface than the shockwave. The compact particle plume starts to break up after 4 µs and larger particles, with a diameter of up to 30 µm are visible. For GAP+IR+CuO no fragments were detected in the ablation plume. This is an indication that the copper suspension is stable enough to inhibit the formation of agglomerates. The particles observed in the ablation plume of PVN+IR are therefore polymer fragments and not CuO particles.

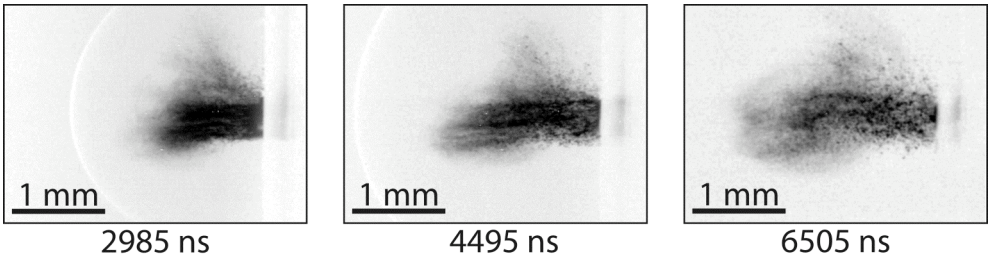

Fig. 24. Shadowgraphy images of PVN+IR+CuO after irradiation with 1064 nm laser light at a fluence of 5.1 J/cm^2.

The shadowgraphy images show a close resemblance to GAP+C. The main difference is the directionality and the size of the fragments and the disappearance of the gaseous front.

The shockwave velocities of PVN+IR is about 1.8 times higher than for PVN+IR with 1% CuO (see Fig. 25). In both cases an exponential decay of the propagation velocity was observed.

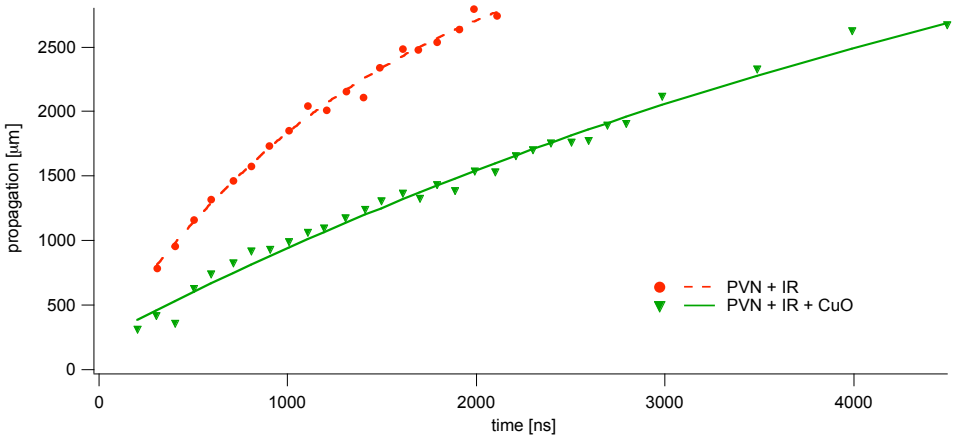

Fig. 25. The shockwave velocity for PVN+IR (●) and PVN+IR doped CuO-nanoparticles (▼).

The effect of CuO on the shockwave velocity is more pronounced for PVN than for GAP. The energy that is removed from the ablation site by the ejected CuO could be used to decompose more polymer. As PVN is a more energetic material than GAP and therefore more energy is "lost", if the same amount of copper is ejected.

The ablation craters for PVN+IR and PVN+IR+CuO have a similar appearance. In both cases sharp edges are visible. Around the ablation crater "fibers" are visible that reach a length of 300 µm for PVN+IR and 100 µm for PVN+IR+CuO. Structures like these have been reported for PMMA and have been attributed to molten polymer that are ejected during the laser pulse [21, 22]. The bottom of the ablation crater for both dopants has a molten and re-solidified appearance. The CuO particles "carry" away some energy from the ablation crater and thereby reduce the thermal features in the ablation plume and in the remaining polymer.

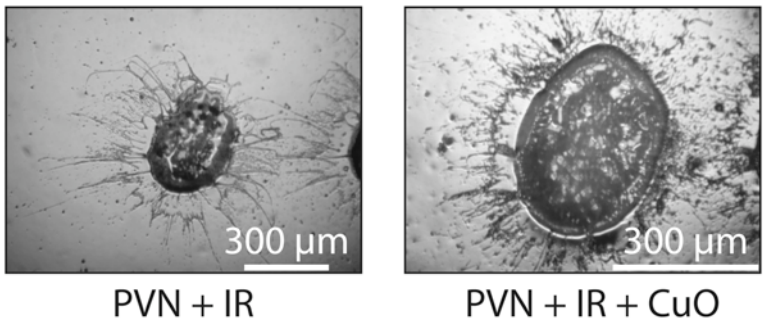

Fig. 26. Microscopy image of the ablation spot of PVN+IR (left) and PVN+IR+CuO (right) after irradiation with one pulse at 5.1 J/cm^2. The ablation crater has the same diameter in both cases, but the images were taken at different magnification.

Strong thermal effects were observed for PVN doped with IR-dye. The ablation crater appeared molten and re-solidified "fibers" remained on the surface around the ablation crater. Particles were also observed in the ablation plume, contrary to GAP+IR, where no fragments could be detected. PVN is a thermoplast with a softening temperature of 30 to 45 °C [6] and is therefore very sensitive to temperature increases. GAP on the other hand is a cross-linked polymer that shows no signs of melting or softening.

An additional doping of PVN+IR with CuO nanoparticles result in the reduction of these thermal effects, but yields also a lower shockwave velocity and the ejection of more and larger fragments. Thrust measurements on both polymer/dopant systems have to be performed to quantify the energy release and to investigate the influence of Al and CuO at fluences that are high enough to initiate a reaction with the polymer.

Shadowgraphy summary

Shadowgraphy was applied as fast, non-vacuum method to test the different polymers, where the shockwave velocity is used as indicator for the thrust performance of the polymer.

The expansion velocity of the shockwave has been calculated 1 µs after the laser pulse (vertical line in Fig. 6).

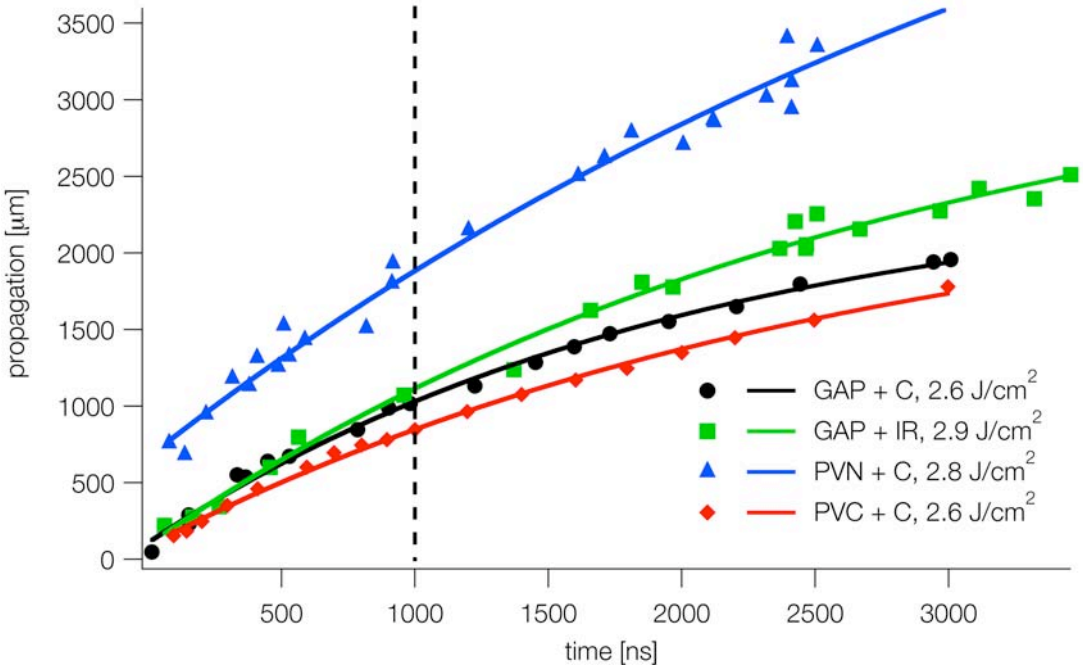

Fig. 27. The shockwave velocity obtained from shadowgraphy measurements. The vertical line indicates the 1 µs time delay, for which the velocities are listed in Table 2 .

The highest expansion velocity has been observed for PVN+IR, followed by PVN+C, GAP+IR, GAP+C and PVC+C (see Table 2).

Table 2 Expansion velocities for the shockwave.

Polymer	**Shadowgraphy [m/s]**
GAP+C	710 (at 2.6 J/cm^2)
GAP+IR	850 (at 2.9 J/cm^2)
GAP+IR+Al	695 (at 5.1 J/cm^2)
GAP+IR+CuO	600 (at 5.1 J/cm^2)
PVN+C	1080 (at 2.8 J/cm^2)
PVN+IR	1835 (at 5.1 J/cm^2)
PVN+IR+CuO	940 (at 5.1 J/cm^2)
PVC+C	630 (at 2.6 J/cm^2)

This result corresponds well to the decomposition enthalpies of the polymers. PVN, the polymer with the highest decomposition enthalpy, has the fastest shockwave, while for PVC the lowest shockwave velocity and decomposition enthalpy was measured. The metal- and metal-oxide-nanoparticles have a negative influence on the propagation velocities of the shockwave of both energetic polymers in this low fluence range. It is noteworthy to emphasize that the shadowgraphy measurements are performed in air and at much lower fluences than the spectroscopic and thrust measurements.

2.3. Plasma Emission spectroscopy in air

The next step after the shadowgraphy measurements and a possible link to the thrust measurements are plasma emission spectroscopy measurements in air. They are also performed under ambient conditions (as the shadowgraphy measurements), but at much higher fluences (in the same region as the thrust experiments).

All emission spectroscopy experiments in air were performed under ambient conditions with the fundamental (λ = 1064 nm) of a Nd:YAG laser (Brilliant BW Nd:YAG, Quantel, τ = 6 ns) with a Gaussian beam profile that contains some hotspots.

The plasma temperatures were determined by comparing the time resolved measurements of the CN Violet peaks around 389 nm and simulated rotational-vibrational spectra calculated by LIFBASE [23] as described in [5].

The plasma temperature of GAP+C and PVC+C were investigated and described in the previous report [5]. The electron densities of the plasma created by the ablation of GAP and PVC was also determined in this project, to complete these measurements and to allow the comparison of all the results.

The electron density in the plasma was calculated from the Stark broadening of the H Balmer α peak at 656 nm. The analysis of Stark-broadened spectral-line profiles is one of the most widely applied methods of plasma diagnosis. The physics behind this method is the broadening of the atomic emissions by the electric fields produced by nearby ions and electrons [24, 25]. The full width at half maximum (FWHM) of the H Balmer α was measured and compared to the data published by Gigosos and Cardeneso [25], who listed the electron densities as a function of the temperature, the ion-emitter reduced mass, and the FWHM.

Results

GAP+C, GAP+IR, PVN+C and PVC+C

All spectra have been recorded at fluences above F_{plasma} and below the fluence, where the breakdown of air (40 J/cm^2) is observed.

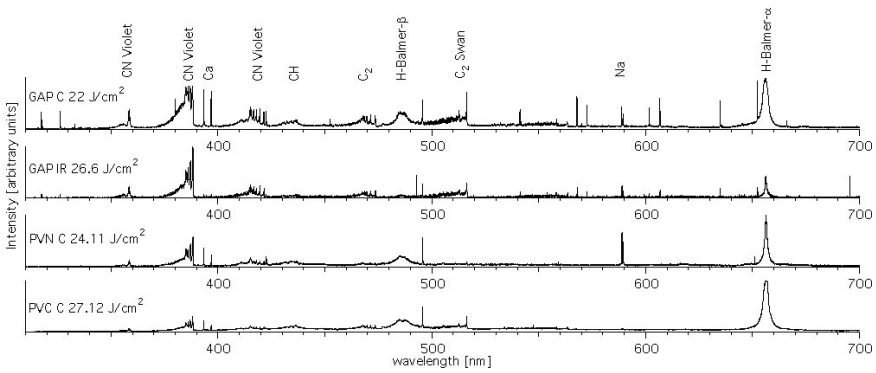

Fig. 28. Plasma emission overview spectra for GAP+C, GAP+IR, PVN+C and PVC+C at similar fluences.

The overview spectra for all four polymers are shown for fluences between 22 and 27 J/cm^2 and a delay time of one µs after the laser pulse in Fig. 28.

In all spectra of Fig. 28, peaks of diatomic (CN Violet, C_2 and CH) [26] and atomic (H, Ca and Na) species are visible. Ca is only observed in the spectra of the carbon doped polymers and seems to be a common impurity in carbon, whereas the hydrogen is created during the fragmentation of the polymers.

The peaks of the emission spectra recorded for IR-dye doped GAP are generally less intense compared to the peaks detected for carbon doped GAP. Only the CN Violet and the C_2 Swan systems are clearly visible, while from the atomic peaks only the H Balmer α at 656 nm is observed. The H-Balmer β peak at 486 nm can only be barely distinguished from the background.

The intensity of the atomic peaks (Fig. 29(right)) decreases much faster than the peaks of the diatomic species (Fig. 29(left)). The H Balmer α peak has almost disappeared after 2 µs, whereas the CN violet system can be distinguished from the background for up to 10 µs after the laser pulse.

The influence of the air is not yet quantified, but measurements in vacuum allow a better comparison of the influence of the polymer properties (see chapter 3).

The decrease of the plasma temperature with time is shown for GAP+IR and PVN+C in Fig. 30. GAP reveals a higher initial temperature than PVN, but also a faster decrease. For both polymers, an increase of the plasma temperature can be observed in the first µs.

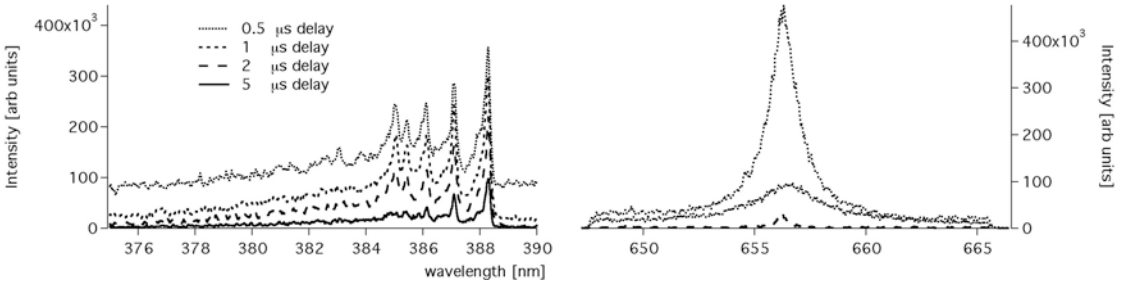

Fig. 29. Plasma emission spectra of PVN+C at a fluence of 24.1 J/cm^2 with different delay times after irradiation. The CN Violet system at 389 nm is shown on the left, while H Balmer α at 656 nm is shown on the right

The influence of the fluences was the same for both polymers. With decreasing laser fluence, the maximum temperature increases followed by a faster decrease (Fig. 31). A faster expanding plasma (analog to the shockwave velocity) and also a higher maximum temperature (more energy is released into the plasma) was in principle expected for higher fluences, but the obtained results show the opposite. A possible origin for this results the influence of the air, which will be tested by performing the experiments in vacuum.

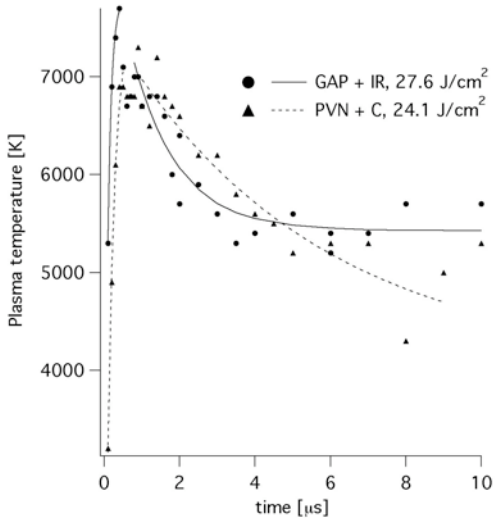

Fig. 30. Plasma temperatures vs. delay time for GAP+IR and PVN+C at similar fluences.

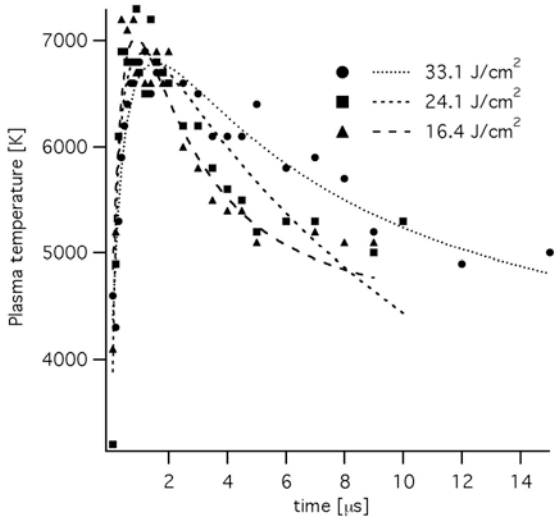

Fig. 31. Plasma temperatures vs. delay time of PVN+C for different fluences.

The electron density in the plasma is similar for all polymers at short times (Fig. 32). GAP with both dopants reveals a faster decrease of the electron density than PVN+C and PVC+C.

The maximum electron density is not influenced by the irradiation fluence, whereas for lower fluences a faster decay is observed (shown in the case of PVN+C in Fig. 33). The decrease of the electron density could be accelerated by the atmosphere (air) in which the experiments are performed. Measurements in vacuum show results with only the influence of the polymer (chapter 3.1).

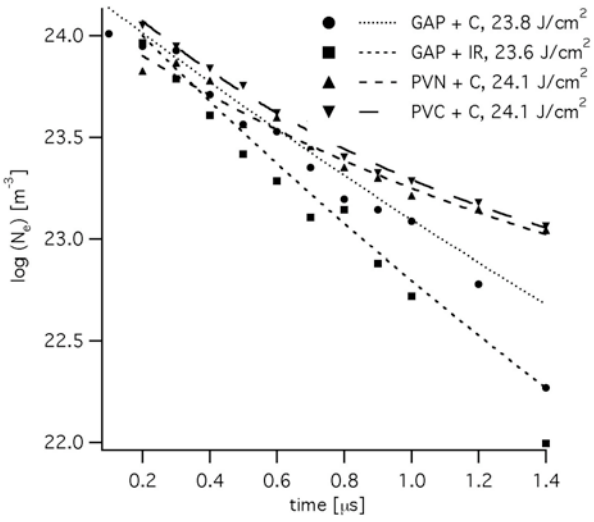

Fig. 32. Electron density delay time for GAP+C, GAP+IR, PVN+C and PVC+C

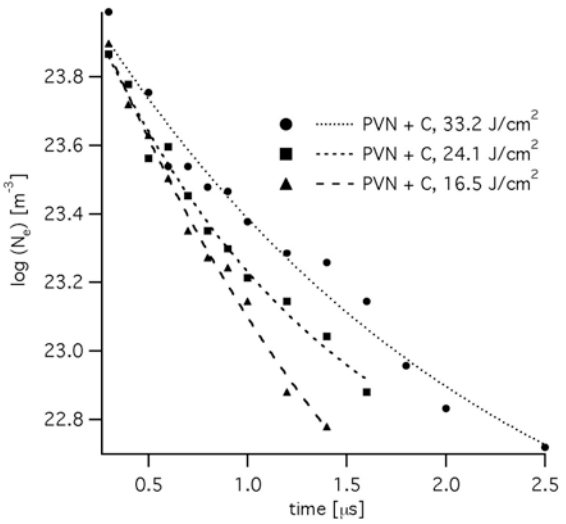

Fig. 33. Electron density delay time for PVN+C at different fluences

The decay of the electron density is observed in the same time range than the observed increase in the plasma temperature (Fig. 34). This increase could therefore be caused by a combination of CN radicals ejected from the polymer with electrons in the plasma, which could result in to highly excited molecules.

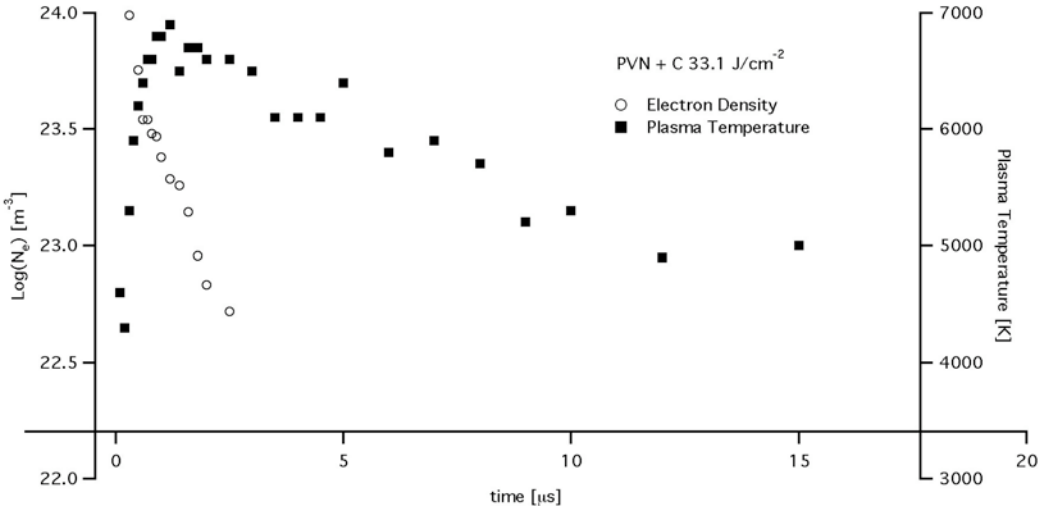

Fig. 34. The change of plasma temperature and electron density over time for PVN+C at a fluence of 33.2 J/cm^2

GAP doped with IR-dye and Al- or CuO-Nanoparticles

All spectra were recorded at a fluence of 24 J/cm^2 under ambient conditions. In Fig. 35 the emission spectra 1 µs after the laser pulse of GAP+IR without and with Al- or CuO-nanoparticles are shown. The most prominent feature are the CN Violet peak systems around 389 nm (0. Order) and around 778 nm (1. Order), but also other atomic (Na, Ca, O, Cl and H) and diatomic (C_2 and CH) species are visible. Peaks that can be assigned to Al and Cu dopant were also detected. C_2 and CH are products from the fragmentation of the polymer backbone, whereas Na, Ca and Cl are impurities in the polymer film (or on the polymer surface).

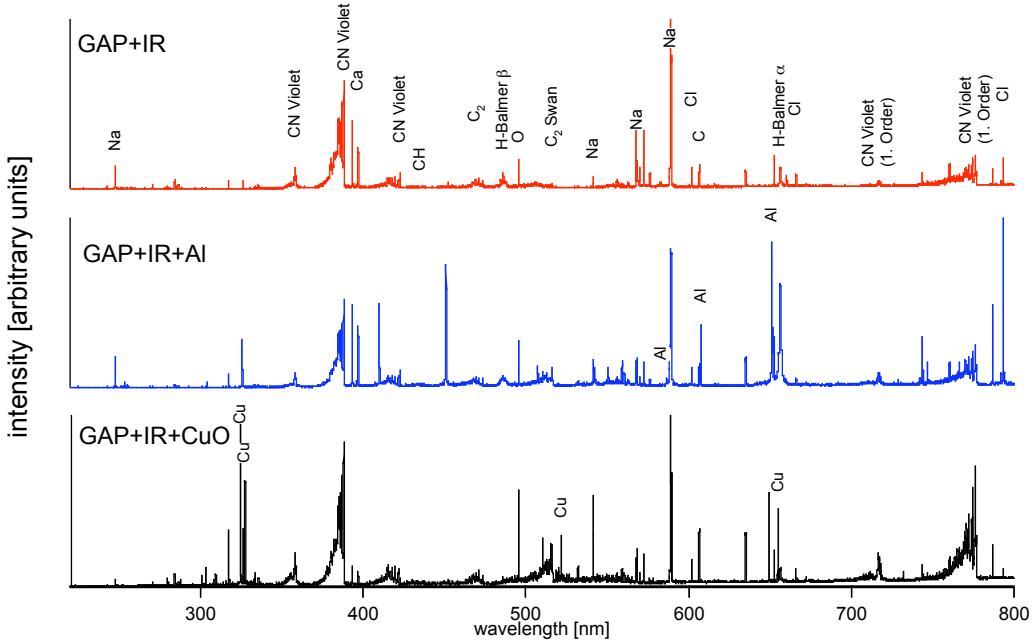

Fig. 35. Plasma emission spectra for GAP+IR (red) with Al- (blue) and CuO-nanoparticles recorded 1 µs after irradiation with 1064 nm at 24 J/cm^2.

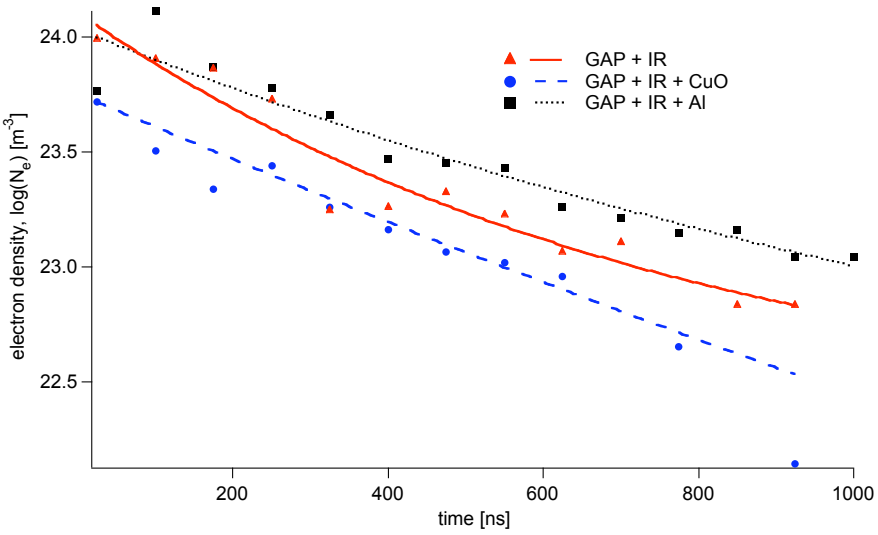

Fig. 36. Electron density for GAP+IR with Al- and CuO-nanoparticles 1 µs after irradiation with 1064 nm at 24 J/cm^2.

The electron density calculated from the Stark broadening of the H Balmer α line at 656 nm is similar for all polymer-dopant systems. The lowest initial values and the fastest decay were measured for CuO doped GAP+IR.

The change of the plasma temperature with time is shown in 0. An increase of the plasma temperature can be observed during the 500 nanoseconds. After a fast decrease, the plasma temperature seems to stay constant until the CN Violet peaks are too weak to be fitted.

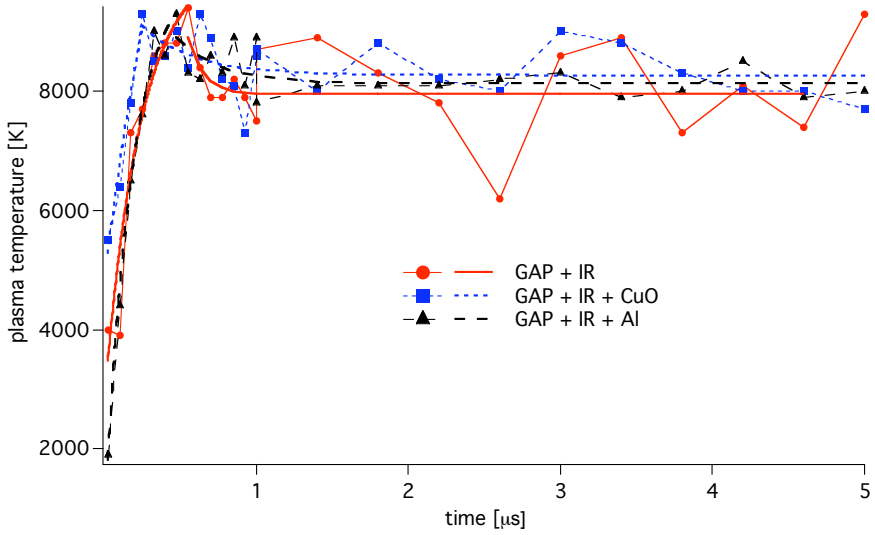

Fig. 37. Plasma temperature for GAP+IR with Al- and CuO-nanoparticles 1 µs after irradiation with 1064 nm at 24 J/cm^2 calculated from the CN Violet peaks around 389 nm.

No pronounced influence of the metal- and metal oxide-nanoparticles could be observed with the time resolved plasma emission measurement in air. The measurements have to be performed in vacuum the remove the influence of the air and to have a more intense and larger plasma plume.

3. ns Experiments in Vacuum

3.1. Experimental Setup for ns experiments in vacuum

Plasma Emission Spectroscopy in Vacuum

The plasma emission spectroscopy measurements in air give a good idea of what species are present in the plasma plume. But the influence of the air, which has been demonstrated by measuring the CN Violet emission for PVC might have a much higher influence than originally expected. The plasma plume in air is also too much confined to perform spatial resolved measurements.

Therefore a new plasma emission setup that allows time and space resolve plasma emission spectroscopy had to be designed and set up.

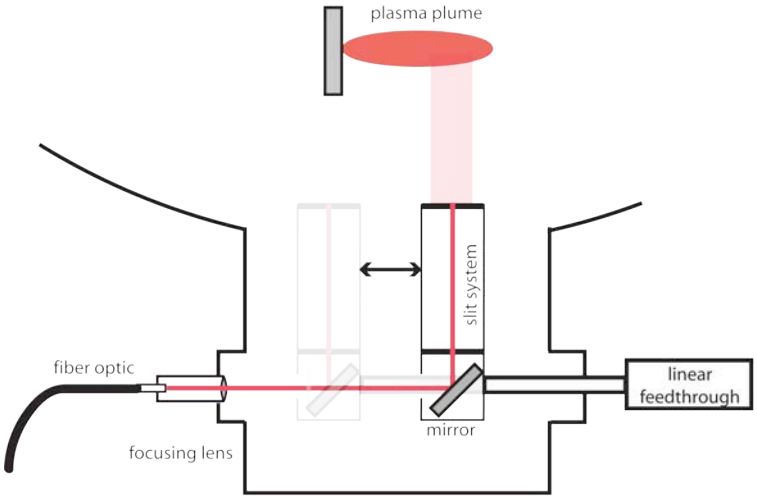

Fig. 38. Experimental setup used for the plasma emission experiments. By moving the slit system and the mirror with linear feedthrough, the whole plasma can be mapped.

The spatial resolution of the new plasma emission spectroscopy was achieved by moving a double slit system parallel to the symmetry axis of the expanding plasma. Two slits arranged at 90° with a width of 1 mm were used in a distance of 15 cm to the plasma. The light passes through the slit system, is reflected by a mirror and focused on a fiber optic. The slit-system and mirror can be moved parallel to the expanding plasma with a linear feedtrough with a precision of 50 µm.

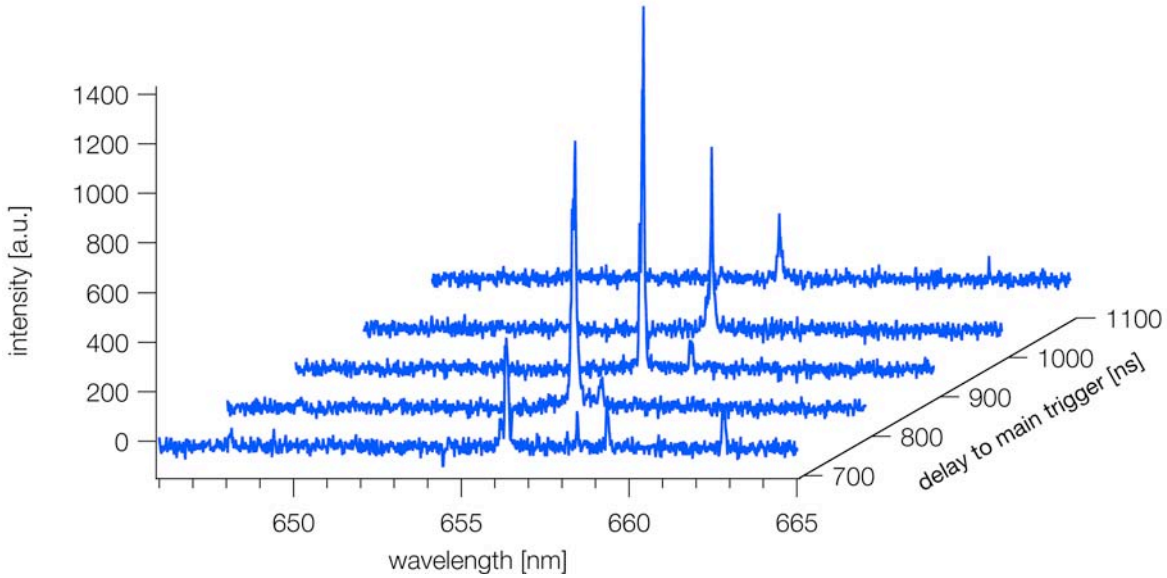

Fig. 39. Time resolved plasma emission spectra of GAP+IR in a distance of ~3 mm from the sample surface. Each spectrum represents a different delay time to the main trigger signal.

The fiber optic is coupled to the spectrometer (Acton 500) and a gated ICCD camera (Princeton Instruments). The time resolution was achieved by delaying the trigger signal between the external trigger of the laser and the trigger signal to the ICCD-camera (example given in Fig. 39).

For the plasma emission spectroscopy experiments the fundamental wavelength (λ = 1064 nm, τ = 6 ns) of a Nd:YAG laser (Brillant B from Quantel) with a supergaussian beamprofile with some hotspots was utilized. The plasma emission spectroscopy was performed in a UHV (ultra high vacuum) chamber at a pressure of $8 \cdot 10^{-8}$ mbar. The sample was mounted on a xyz – manipulator (see Fig. 40), with the sample surface perpendicular to the emission spectrometry setup. The manipulator was used to create a matrix of measurements spots in the polymer with 2 laser pulses per position on the sample.

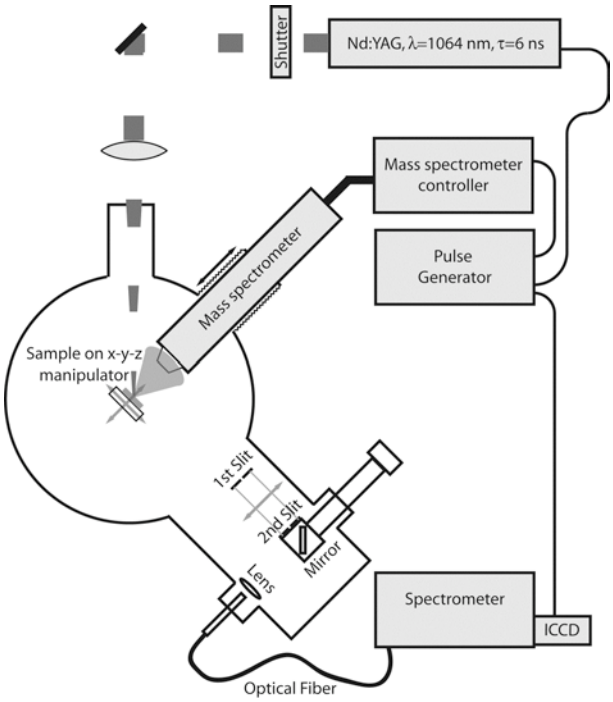

Fig. 40. Experimental setup for UHV system used for the plasma emission experiments.

ns Mass Spectrometry in Vacuum

All mass spectrometric measurements have been performed in a UHV chamber with a Electrostatic Quadrupole Plasma (EPQ) Analyzer (Series 1000) from Hiden Analytical. A specialty of this QMS is the possibility to measure masses and kinetic energies in the plasma, which is very dense compared to vacuum. The measurement chamber is equipped with a double load-lock, which ensures a high vacuum and short pumping times after the sample transfer, but as a drawback, also a relatively long transfer time. A high sample usage is therefore important to minimize the time losses from the sample transfer.

The sample was mounted on a x-y-z translation stage and placed in the chamber with its surface normal pointing at the mass spectrometer (MS). The distance between the sample and the nozzle of the MS can be varied by moving the MS. The pulsed laser beam is aimed at the surface in a 45° angle. The resulting plasma expands perpendicular to the sample surface towards the MS. Due to the limited space on a single polymer sample and the relatively high fluences used to produce a plasma only a limited number of ablation spots per sample were available. A special experimental setup (Fig. 41) had to be used, to optimize the usage of the sample and to optimize the measurement signal.

A pulse generator sends a trigger signal (①) to the MS, but is blocked when the laser-shutter is closed to inhibit a triggering of the MS while the sample is moving. After a set delay to the MS trigger, a second signal (②) is sent to the Flashlamp of the Nd:YAG laser. A photodiode is then used to record the timing of the laser pulse (③) with an oscilloscope. The time span between the trigger signal for the MS and the laser pulse is referred to as "pulse delay", the length of the MS trigger signal is the "pulse width". The pulse delay is necessary to ensure that all species have been recorded. Normally a 10 µs pulse delay has been used with a 10 ms gate width.

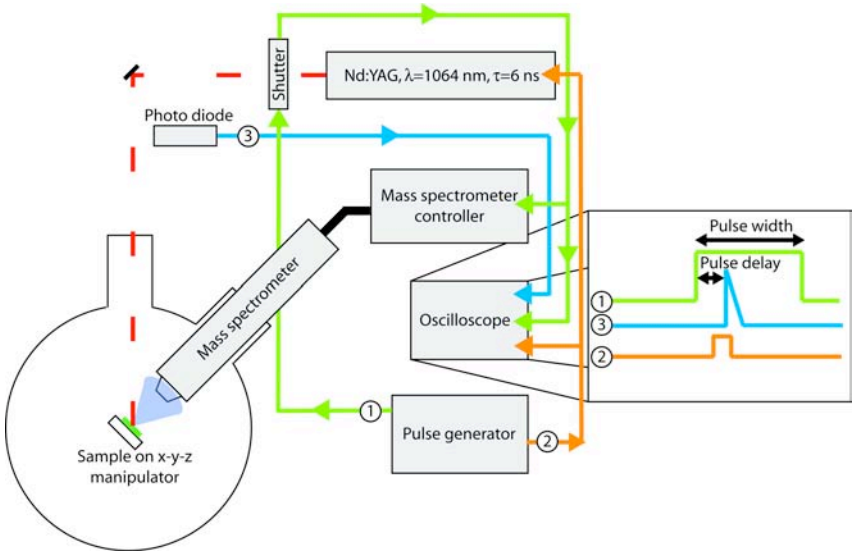

Fig. 41. Scheme of the Mass spectrometry setup.

For all polymers, the produced uncharged fragments, the positively charged ions (+ions) and the kinetic energy of the +ions for selected masses have been recorded.

All mass spectrometry measurements have been performed at room temperature and a pressure $1 \cdot 10^{-7}$ mbar.

New features implemented in the experimental setup

- The substrate holder in the UHV (ultra high vacuum) chamber can be heated to 800° C. It can therefore be used to study the thermal decomposition of the polymers. Additionally it can be cooled to -200°C with liquid nitrogen. This could feature could be used to reduce thermal influences during the ablation process.
- A ion gun is build in the chamber and can be used for SIMS (Secondary Ion Mass Spectrometry) experiments in combination with the MS, allowing surface analysis and depth profiles.
- A new measurement card allows to measure energy and mass selective TOF (Time of Flight) signals. This measurements gives insight to the exact time of formation of specific fragments.
- A Langmuir probe has been implemented to measure the ion flux in the plasma and can be used to quantify the ions measured with the QMS.
- The UHV system is designed to allow a fast exchange of the entrance window without destroying the UHV. This is important, as the irradiation sources ranges from 193 nm to 10 µm, which require different optical windows.

3.2. Plasma emission spectroscopy in vacuum

Time and space resolved plasma emission spectra of H-Balmer α line at 656.6 nm have been recorded for an irradiation fluence of 25 Jcm^{-2}. The temporal position of the maximum intensity for each distance from the sample surface was used to calculate the propagation velocity of the excited hydrogen along the central axis of the plasma plume (see Fig. 42).

The fastest hydrogen was observed for GAP+C and PVC+C, followed by GAP+IR and PVN+C. The expansion velocities are compared in Table 3 .

Table 3 Expansion velocities hydrogen from the H-Balmer α line.

Polymer	Plasma emission [m/s]
GAP+C	46000
GAP+IR	36700
PVN+C	31100
PVC+C	48300

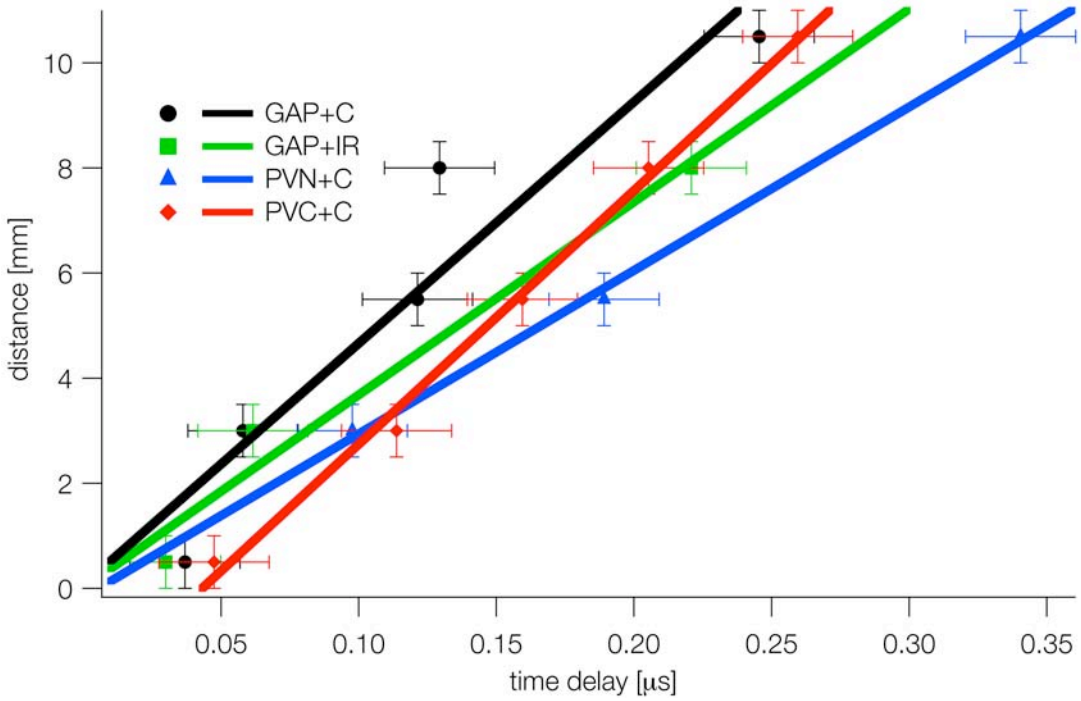

Fig. 42. The distance versus time delay for the detection of the maximum intensity of the H-Balmer α peak at 656.6 nm. The irradiation was performed with a fluence of 25 Jcm^{-2} at 1064 nm.

3.3. Mass Spectrometry measurements on GAP, PVN and PVC

In the mass spectrometry measurements the polymer/dopant composites can be investigated at the same conditions as in the thrust measurements, i.e. under vacuum and at fluences above the plasma threshold fluence. A quantification of various features like type, distribution and kinetic energy of fragments and conversion rates of the polymer into gaseous products are possible.

PVC doped with carbon nanoparticles

In Fig. 43, the mass spectrum of neutral fragments of PVC+C after irradiation at 1064 nm with a fluence of 10 J/cm^2 is shown. This fluence is well above the plasma threshold fluence of ~6 J/cm^2. The main decomposition fragments can be assigned to Cl and HCl and to fragments from the polymer backbone that have also been observed for thermal degradation of PVC [27-29].

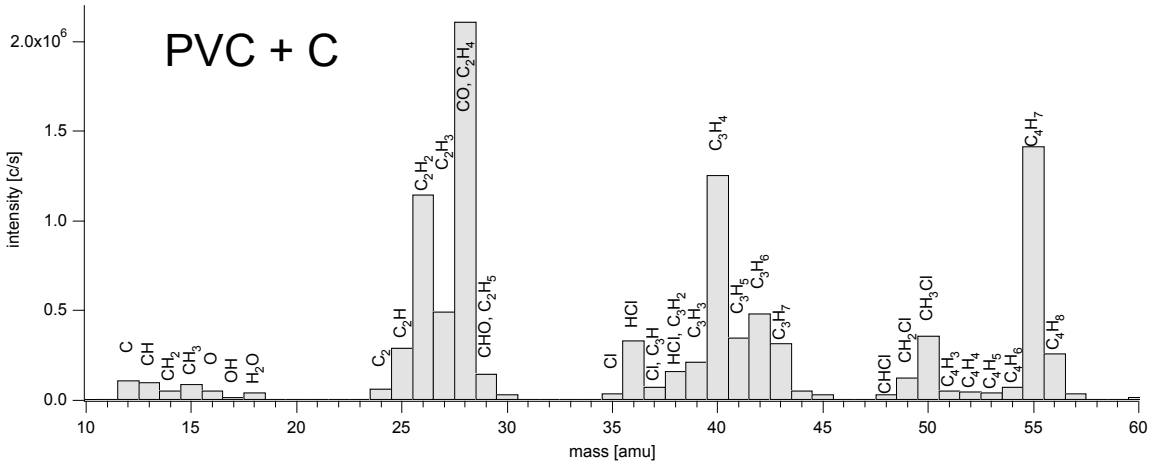

Fig. 43. Mass spectrum of the neutral fragments from PVC+C after irradiation with 10 J/cm^2 at 1064 nm.

All major peaks above 50 amu can be assigned to cyclohexanone [30], that was used as solvent for PVC.

The most intense +ion signal at mass 12 can be assigned to C^+ from the dopant (carbon), the solvent, and the polymer backbone. The main decomposition products of the polymer, i.e. Cl and HCl and small fragments from the polymer backbone are also present.

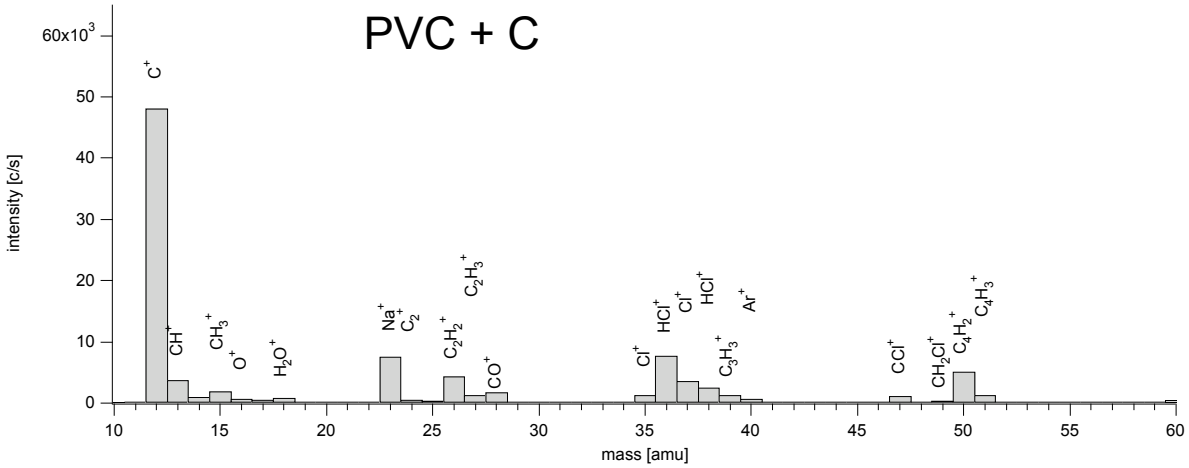

Fig. 44. Mass spectrum of the positive charged ion fragments from PVC+C after irradiation with 22.6 J/cm^2 at 1064 nm

The energy distribution of HCl^+ for different fluences is shown in Fig. 45. At a fluence of 6.5 J/cm^2 most ions have a kinetic energy of 10 to 20 eV. With increasing energy the total amount of HCl^+ increases and ions with higher kinetic energies (30 to 80 eV) are detected.

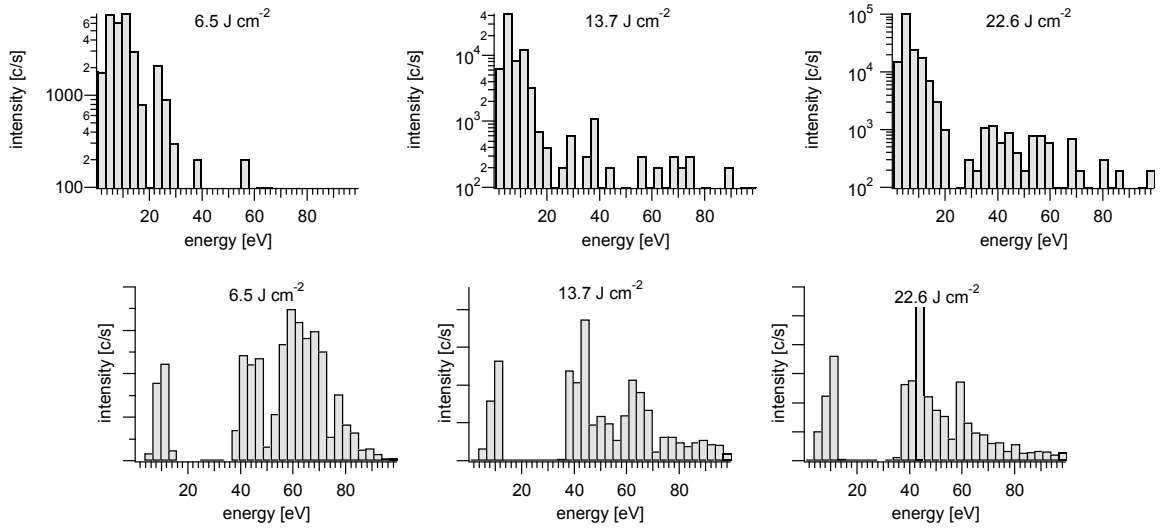

Fig. 45. Kinetic energy distribution for HCl^+ (top) and C^+ of PVC+C for different irradiation fluences with 1064 nm.

The same measurements were also performed for C^+, but no change in the distribution of the kinetic energy could be observed. Only the signal intensity increased with the fluences.

GAP doped with carbon nanoparticles and IR-dye

The neutral mass spectra for GAP+C and GAP+IR are shown in Fig. 46.

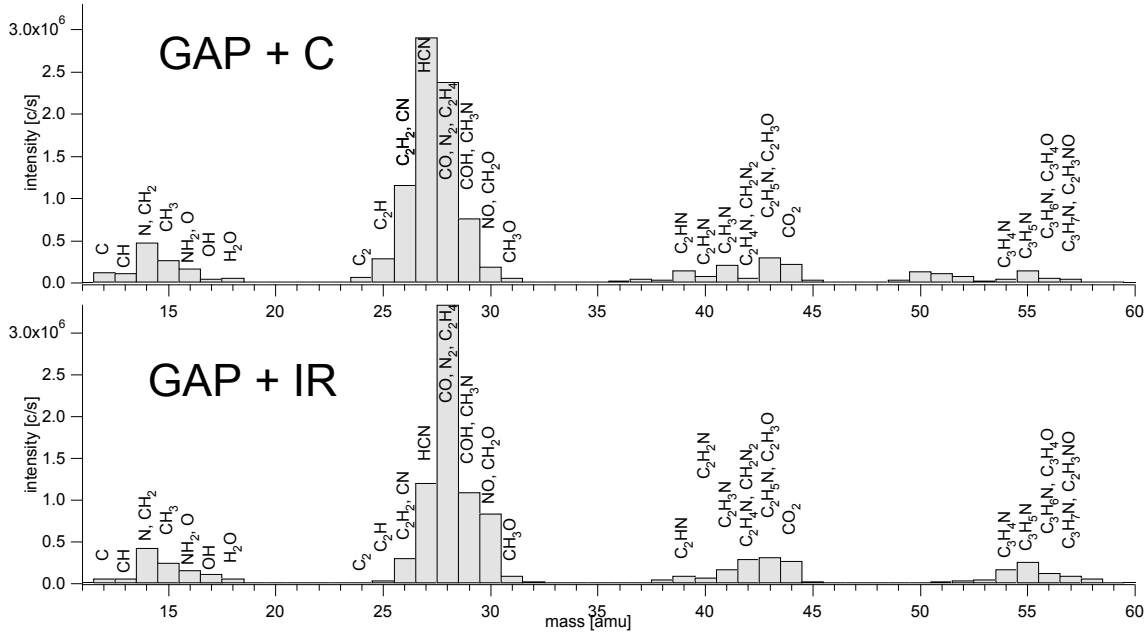

Fig. 46. Mass spectrum of the neutral fragments from GAP+C (top) and GAP+IR (bottom) after irradiation with 10 J/cm^2 at 1064 nm.

For both dopants the same fragments were detected, but with different intensities. The strongest peak in the spectra of carbon doped GAP can be assigned to HCN, whereas the IR-dye doped GAP seems to decompose mainly into N_2. A weak C_2 signal can only be detected

for GAP+C, which indicates that it originates from the dopant. No fragments with a mass above 60 amu are detected. Also no traces from ethylacetate [30], which was used as solvent for GAP, was detected. This is different to PVN and PVC where strong signals were assigned to the solvent. One possible reason is the production process of the films, i.e. GAP is cross-linked from a 70 wt-% polymer solution, whereas PVN and PVC are solvent cast from 10 to 20 wt-% solutions. This results in less trapped in the polymer after the production process in the case of GAP films.

The same signals for GAP with both dopants have been detected in the positive ion spectra. The strongest signal in the case of the carbon doped GAP could be assigned to Na^+. Also Cl has been detected which indicates a contamination of either the polymer or the dopant by NaCl. A much stronger signal for Na^+ has been detected for all carbon doped polymers compared to the IR-doped GAP. For the carbon doped polymers a surface contamination by careless handling can be excluded, as such a strong signal for Na^+ would not be caused by a small deposition on the surface, suggesting that the Na is a contamination in the carbon sooth. The strongest peak for GAP+IR can be assigned to C^+. This indicates a higher fragmentation of the polymer backbone for the IR-dye doped GAP, which is consistent with the shadowgraphy measurements. In the ablation plume of the IR-dye doped GAP no fragments were visible, whereas for GAP+C a large amount of heavy fragments were detected.

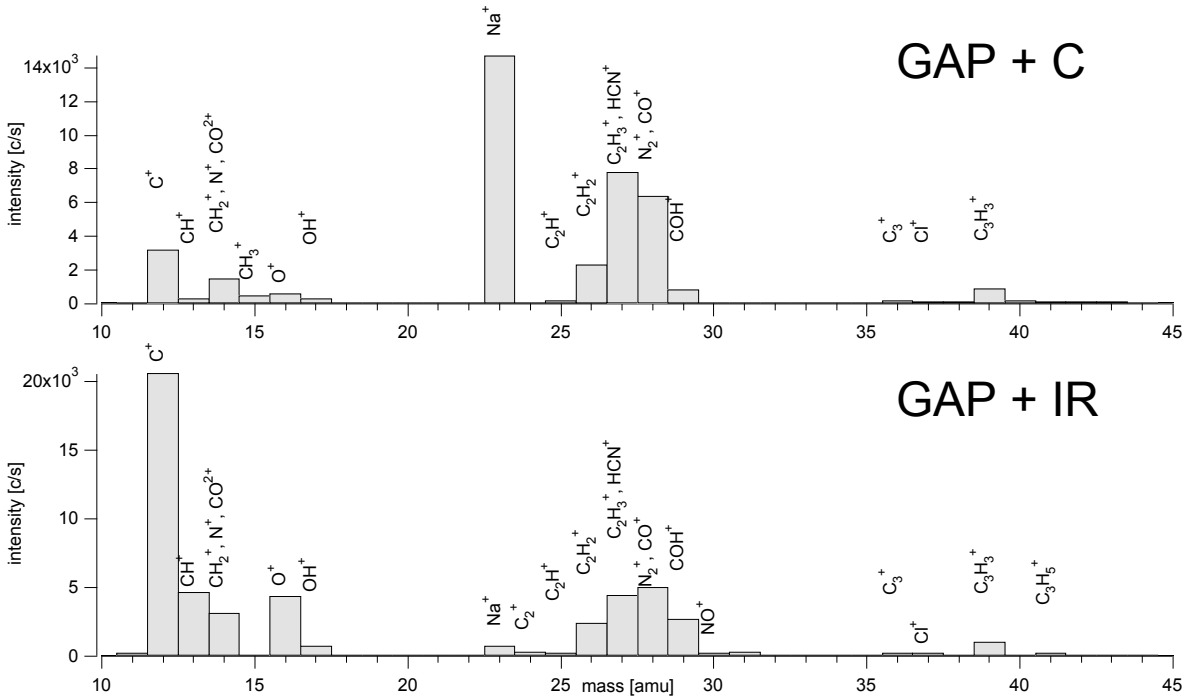

Fig. 47. Mass spectrum of the positive charged ion fragments from GAP+C (top) and GAP+IR (bottom) after irradiation with 13.7 J/cm^2 at 1064 nm

Other fragments from the polymer are again N_2^+ and HCN^+ and fragments from the polymer backbone. As observed in the neutral spectra, the intensities between N_2^+ and HCN^+ are switched for the two dopants, suggesting differences in the secondary decomposition.

A possible decomposition pathway for GAP with both dopants is shown in Fig. 48. In a first step N_2 is released from the azide group. In a second step either NH_2 or HCN are removed, before the decomposition of the polymer backbone starts [31-33].

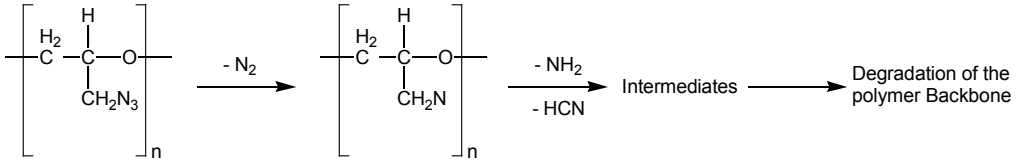

Fig. 48. Proposed decomposition pathway for GAP+C and GAP+IR for irradiation with 1064 nm.

The kinetic energies of C^+ for GAP+C and GAP+IR for different irradiation fluences are shown in Fig. 49.

For GAP+C (top) two distributions can be distinguished. A first maxima is observed around 10 eV, the second much stronger and broader distribution is located at ~55 eV. With increasing fluence, more ions are detected, but the ratio between the two peaks and the distribution is not changed as observed for PVC+C. Also the maximal intensity is of the second peak is similar for both polymers.

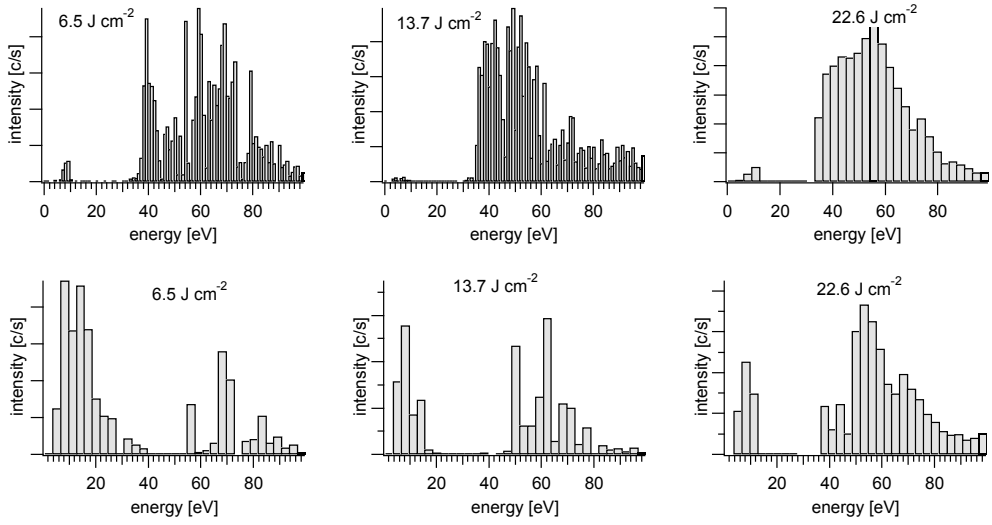

Fig. 49. Kinetic energy distribution for C^+ from GAP+C (top) and GAP+IR (bottom) for different irradiation fluences with 1064 nm.

In the case of GAP+IR (bottom) a strong signal at ~10 eV is observed at the lowest fluence of 6.5 J/cm^2. The intensity of this peak remains constant for all fluences. A second peak around 55 eV shows a strong dependence on the irradiation fluence. At 6.5 J/cm^2, the maximum is

lower than for the first peak, at 13.7 J/cm^2 the same intensity for both peaks is observed and at 22.6 J/cm2, the second peak is stronger than the first peak. The maximal intensity of the peak at 55 eV is similar for GAP with both dopants at the highest fluence.

For GAP with both dopants the same fragments were observed, but with different intensities. The backbone of the IR-doped GAP decomposes into smaller fragments. The kinetic energy is also influenced more by the irradiation fluence. This might be caused by the different distribution of the two dopants in the polymer. The IR-dye is distributed on a molecular level and the energy is therefore absorbed more uniformly than in the case of the carbon doped GAP, where carbon agglomerates of up 20 µm may be present [18]. These agglomerates absorb the laser light and form local hotspots. Polymer in the close surrounding of these hotspots then is exposed too much higher temperatures than the IR doped GAP at the same fluence. In the case of the carbon doped polymer, less polymer is therefore decomposed, but the ionic fragments have a already higher energy at lower fluences than in the case of IR-dye doped GAP. Only at the highest irradiation fluence, the same intensity could be observed for ions from both GAP/dopant-systems.

PVN doped with carbon nanoparticles

The most intense peak in the neutral mass spectra for PVN+C is 28, which can be assigned to CO, as the formation of N_2 in the plasma plume is not very likely. No fragments at higher masses, such as 89 amu (monomer mass) or O_2 were detected.

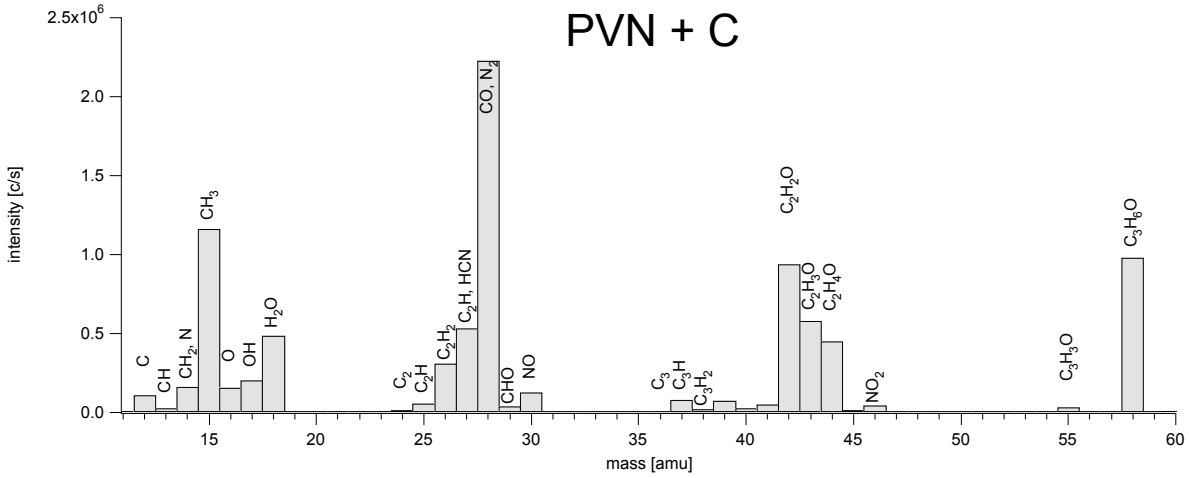

Fig. 50. Mass spectrum of the neutral fragments from PVN+C after irradiation with 10 J/cm^2 at 1064 nm.

The strong signals at mass 58 and 43 can be assigned to acetone [30], which is the solvent used to cast the films from a 10 to 20 wt-% polymer solution. The solvent evaporates fast and

forms a dense surface layer. Solvent below this layer is then trapped in the polymer film and cannot be removed in the normal vacuum drying procedure.

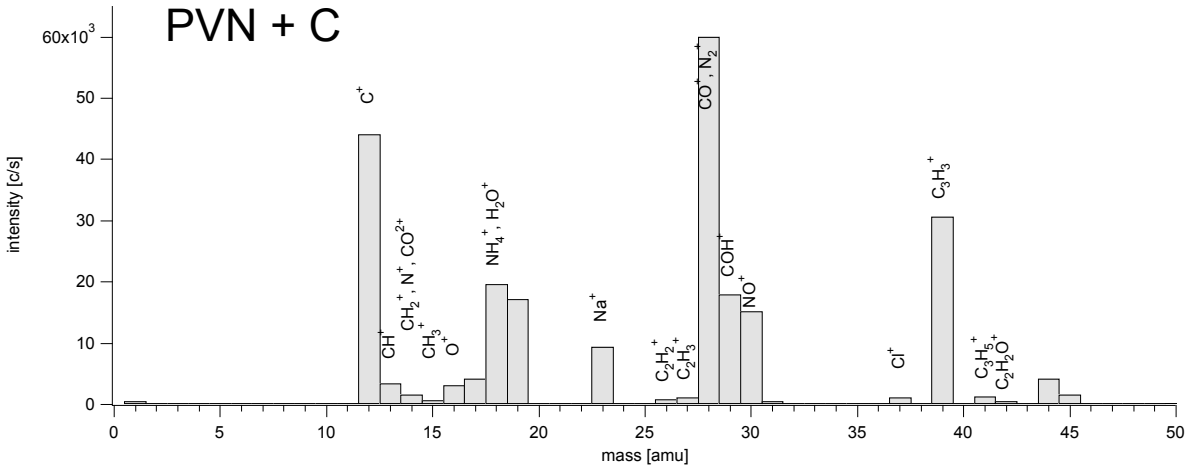

Fig. 51. Mass spectrum of the positive charged ion fragments from PVN+C after irradiation with 22.6 J/cm^2 at 1064 nm

The strongest peaks in the positive ion spectra (shown in Fig. 51) can be assigned to CO^+, C^+ and NO^+. Again no peaks were detected for O_2^+ and NO_2^+, which could be possible fragments in the decomposition of PVN, similarly to the decomposition of inorganic nitrates [34]. A strong signal can be assigned to Na^+, which was already detected for GAP+C and PVC+C. It may therefore be possible to utilize Na for normalizing and comparing the mass spectra for the different carbon doped materials, if a homogeneous distribution through the whole film exists.

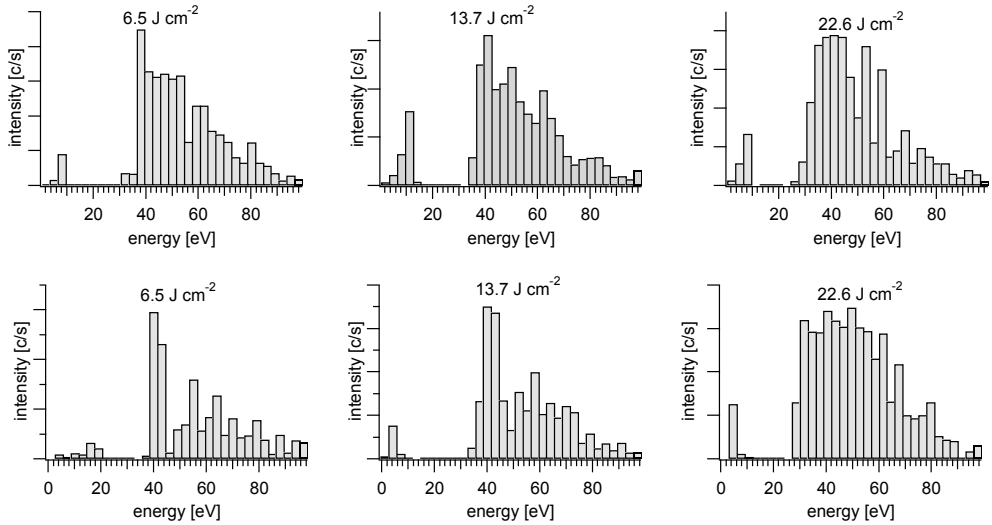

Fig. 52. Kinetic energy distribution for C^+ (top) and N^+ (bottom) from PVN+C for different irradiation fluences with 1064 nm.

The kinetic energy distribution for C^+ (top) and N^+ (bottom) from PVN+C is shown in Fig. 52. For both species the same behavior can be observed as in the case of GAP+C. A weak

peak is detected around 10 eV, and a stronger much broader peak is situated at ~40 to 50 eV. The irradiation fluence increases the amount of ions, but the kinetic energy distribution remains more or less constant.
Also the maximal of the strong peaks at 50 eV is in the same range as for GAP+C and PVC+C.

Summary of the Mass spectrometry measurements

A higher degree of fragmentation has been detected for the energetic polymers GAP and PVN compared to PVC. For all polymers the expected signals had been detected. For the energetic polymers mainly nitrogen containing groups, i.e. HCN and N_2 for GAP and NO for PVN, and fragments from the polymer backbone were detected. The main decomposition products for PVC were also fragments from the polymer backbone and HCl.
A strong signal from the solvent used in the polymer film production was detected for PVN and PVC. Both polymers were solvent cast from dilute (10 to 20 %) polymer solution. In the mass spectra of GAP with both dopants no signal could be assigned to the solvent. The main difference to PVN and PVC is, that GAP is cross-linked from a 70 % polymer solution, and less solvent is present throughout the whole process.
In the carbon doped polymers a strong signal of Na was detected. The signal is too strong to be caused by a contamination of the polymer surface. The carbon is the most probable source of the NaCl, as much less sodium is detected for GAP+IR.

A higher fragmentation was also detected for GAP+IR compared to GAP+C. This is consistent with the shadowgraphy measurements, where no fragments were detected in the ablation plume of GAP+IR.
The kinetic energies of selected positively charged ions show a similar behavior for all carbon doped polymers. Two peaks can be observed, which increase with increasing irradiation fluence. For IR-dye doped GAP the irradiation fluence changes also the intensity ratio between the two peaks. More ions with higher energy are detected at higher fluences.

The kinetic energies are shown in Fig. 53 for an irradiation fluence of 23 Jcm^{-2}. The expansion velocity of the selected species was determined from the energy with the highest intensity (vertical lines in Fig. 53).

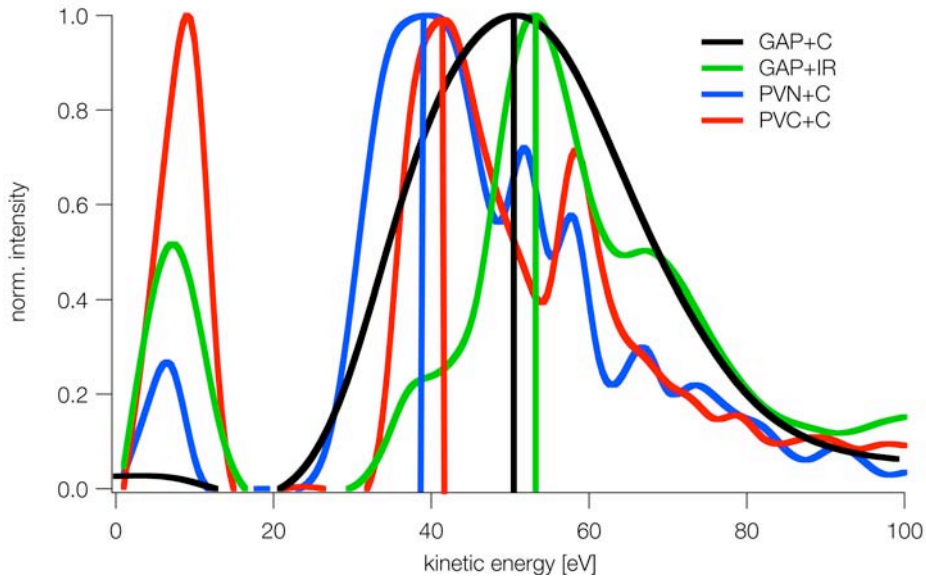

Fig. 53. Kinetic energy versus the normalized intensity of the C^+-ion ns at a irradiation fluence of 22.6 Jcm^{-2}. The velocities shown in Table 4 are calculated from the kinetic energies with the highest intensity.

The highest velocity was observed for GAP+IR, followed by GAP+C. For PVN+C and PVC+C a similar lower velocity for the C^+ was observed (see Table 4). In comparison to the velocities from the emission measurements (see Table 3), velocities that are consistently lower by a factor of 1.2 to 1.8 are obtained. One possible explanation for this is the experimental design, i.e. emission spectroscopy is a non-invasive measurement method, whereas the mass spectrometer and the nozzle can have an influence on the plasma and its expansion, as they are in direct contact with the expanding plasma. Another possible reason could be the fact that in the energy measurements with the mass spectrometer, ions are measured, while the H-Balmer α line corresponds to neutral hydrogen. We have not yet established whether in our experiments the ions and neutrals have the same velocities, but fs experiments show in chapter 6 suggest, that ions travel faster.

To allow a comparison of these two methods, more experiments with the same species have to be performed.

Table 4 Expansion velocities for C^+-ion.

Polymer	**Mass Spectrometry [m/s]**
GAP+C	28600
GAP+IR	29300
PVN+C	25100
PVC+C	25900

4. ms Measurements in Vacuum

4.1. Thrust measurements

Samples of all investigated polymers have been sent to Claude Phipps, where the thrust measurements were performed. The thrust measurements were performed with a ms laser pulse in vacuum. This difference may result in difficulties in the correlation with the results measured under ambient conditions (shadowgraphy and plasma emission spectroscopy).

The target momentum was measured with a torsion balance as described in [35], to analyze the polymers for their performance in a μLPT,. The target momentum was then used to calculate the momentum coupling coefficient C_m:

$$C_m = \frac{m\Delta v}{W} = \frac{F}{P} \text{ [dyn/W]} \quad (2)$$

where $m\Delta v$ is the target momentum produced during the ejection of laser ablated material. W is the incident laser pulse energy, F is the thrust, and P the incident power. The second important parameter for thrusters is the specific impulse I_{sp}, which is defined as:

$$I_{sp} g = v_E = C_m Q^* \text{ [cm/s]} \quad (3)$$

Q^* is the specific ablation energy (incident power/mass ablation rate), v_E is the exhaust velocity, and g is the acceleration due to gravity.

As equation 5 demonstrates, I_{sp} and C_m are not independent. If, for example, a significant amount of incident energy is absorbed as heat in the target rather then producing material ejection, Q^* will be higher and C_m well be proportionally lower. This results in the same exhaust velocity and I_{sp} for both cases .

The ablation efficiency parameter η_{AB} is defined as the efficiency of the conversion of the laser energy into exhaust kinetic energy:

$$\eta_{AB} = C_m \cdot v_E \text{ [\%]} \quad (4)$$

Results

Maximum thrust values

The thrust values given in this section correspond to the maximum values obtained for each polymer, but not the same fluence has been used for C_m and I_{sp}.

GAP shows a higher C_m than both PVC and PVN (Fig. 54). The highest coupling momentum is observed for GAP+IR. The specific impulse for PVN+C is much higher then for GAP and PVC. This result correlates well with the shockwave propagation measurements, where PVN+C showed the fastest shockwave.

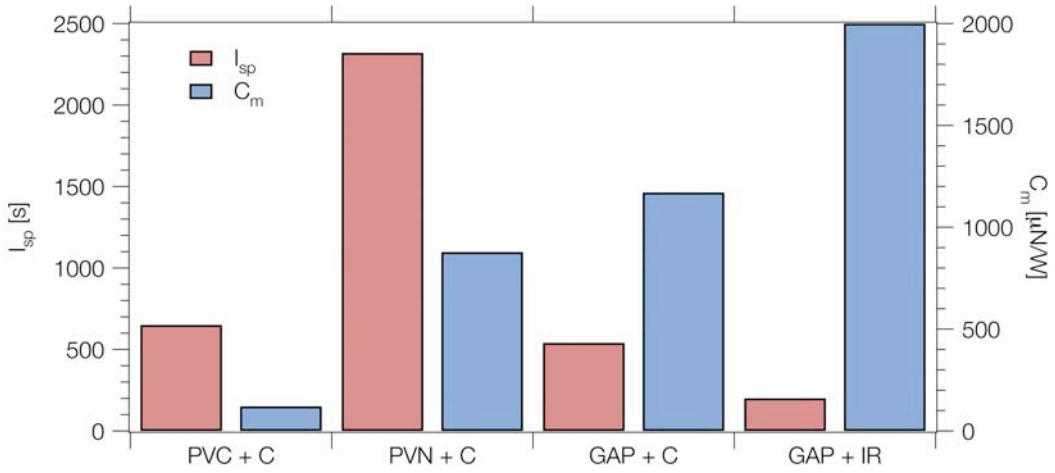

Fig. 54. The maximum C_m and I_{sp} for GAP+C, PVN+C, PVC+C and GAP+IR obtained in the impulse test stand. Note that I_{sp} is plotted on a logarithmic scale.

Table 5 Thrust data acquired by Claude Phipps with the torsion balance

	GAP+C	**PVN+C**	**PVC+C**	**GAP+IR**
Coupling Momentum	1170 µN/W	878 µN/W	120 µN/W	2000 µN/W
Specific Impulse	540 s	2320 s	650 s	200 s

GAP+IR shows an extreme high value for C_m of 2000 µN/W. This correlates well with the shadowgraphy experiments, where no solid fragments are observed, because the coupling momentum is an indicator for the amount of energy that has been transferred. This is in principle surprising, as the thrust experiments are performed at fluences above F_{plasma}, with a different pulse length and in vacuum.

GAP and PVN doped with carbon have a similar C_m, whereas PVC+C shows a much lower value.

Thrust values at optimized fluence

The results present in the this section are from thrust measurements at a optimized fluence for the thruster application.

The thrust measurements reveal the best performance for GAP+C as fuel polymer with η_{AB} of up to 368%. GAP+IR reveals also a η_{AB} value, which exceeds 100% (see Table 6). This means that more energy is released in the form of thrust than deposited in the polymer by the incident laser pulse, suggesting that the μ-LPT with GAP as fuel can be described as a hybrid thruster utilizing chemical-stored and laser energy. For PVC+C and PVN+C η_{AB} values are observed that are significant lower. This was expected for PVC+C, as only a small amount of energy is stored in the polymer.

PVN has the highest decomposition enthalpy of -3829 J/g, but shows the worst performance of all polymers in all experiments at high fluence, i.e. mass-, plasma emission spectrometry, and the thrust measurements. Only in the shadowgraphy measurements the fastest shockwave was observed for PVN+C. One possible explanation for this surprising behavior could be related to the material properties of PVN, as it is a thermoplast with a softening temperature of 30 to 45°C. When this temperature is reached during the decomposition process, the polymer starts to flow and later to melt. For the evaluation of the thrust measurements, the ablated mass has to be determined. The thermal effects such as melting or the observation of fibers on the surface [36] may result in an overestimation of the ablated mass, which will yield a lower momentum coupling coefficients and efficiencies (Equation (2) and (4)). The mass spectra presented in [36] also reveal the presence of solvent in the polymers film. The remaining solvent acts as inert mass during the ablation process, which will not contribute to the thrust.

The thrust date corresponds quite well with the mass spectrometry measurements, where the fastest C^+ fragments were obtained for GAP with both dopants, followed by PVC and finally PVN. This indicates that C^+ plays an important role for the thrust and is probably more important than the influence of neutral hydrogen (plasma emission measurements).

Table 6 Thrust data for all for polymer-absorber systems at optimized experimental conditions, i.e. maximum η_{AB} value.

Polymer	**I_{sp} [s]**	**C_m [μN/W]**	**v_E [m/s]**	**η_{AB} [%]**
GAP+C	867	865	8502	368
GAP+IR	256	1574	2510	198
PVN+C	137	310	1343	21
PVC+C	159	635	1559	49

5. ns and ms Conclusions

Three different polymers (GAP, PVN and PVC) and two different dopants (carbon nanoparticles and IR-dye) have been investigated as fuel in laser plasma thrusters.

The different dopants for GAP seem to have only a small influence on the ablation properties, such as F_{th} and F_{plasma}. The most pronounced differences are observed in the ablation products, which are detected, in the shadowgraphy measurements and the crater appearance. Large fragments of solid and liquid ablation products are observed for GAP+C, while almost no solid fragments are ejected for GAP+IR. It seems, that the ablated material is transferred completely into gaseous products. The SEM images confirm these results, by showing that an ablation crater with steep and smooth walls is obtained for GAP+IR, whereas the crater of GAP+C is quite rough, with deep holes and a very uneven bottom. This difference can be explained by the different distribution of the dopant in the polymer. The IR-dye should be distributed on a molecular level, whereas carbon tends to agglomerate to particles of 10 to 20 µm in size.

The results obtained from shadowgraphy experiments correlate well with maximum thrust measurements on the same polymers performed by Claude Phipps, even though the measurement conditions are quiet different. The thrust experiments were performed with a ms laser pulse, in vacuum and in a much higher fluence range.

PVN+C delivered the best results in the shadowgraphy experiments. A faster shockwave was observed than for GAP+C, GAP+IR and PVC+C results from report [5].

The plasma emission spectroscopy in air showed similar values for all investigated polymers. The energetic polymers show generally a higher maximum temperature, but also a faster decay over time. This indicates, that more energy is released in a shorter time period for the energetic polymers. The emission spectroscopy measurements should be performed in vacuum, to remove the influence of the atmosphere (e.g. CN peaks for PVC).

A correlation between the shadowgraphy and thrust measurements could be established, even though the experimental conditions differed in the laser pulse length, atmosphere and energy range. The emission spectroscopy measurements also indicated the advantages of the energetic polymers.

A slower shockwave was observed for GAP+IR doped with Al- or CuO-nanoparticles. The ablation plume of GAP+IR+CuO showed no large fragments ejected from the polymer and also the ablation crater did not differ to GAP+IR. For GAP+IR+Al, particles with a size of 30

to 50 µm were visible in the polymer film and the ablation plume. The ablation craters were less defined and polymer fragments were redeposited on the polymer surface. No difference could be observed in the plasma emission measurements for GAP+IR doped with CuO- or Al-nanoparticles. A more pronounced influence might be observed in vacuum, i.e. e. with mass spectrometry, plasma emission spectroscopy and thrust measurements. An influence on the energy release has to be determined with thrust measurements. In general, it looks like Al- and CuO-nanoparticles do not improve the decomposition properties in the shadowgraphy measurements, but this may change for the high fluences applied under plasma conditions.

PVN was also doped with an IR-dye to reduce the amount of particles in the ablation plume of PVN doped with carbon nanoparticles. Fewer particles were visible in the ablation plume for PVN+IR than for PVN+C. But strong thermal effects, i.e. “fibers” around the ablation crater, molten crater bottom, and a “strange” shockwave shape were observed. This may be due to the material properties of the polymer. PVN is a thermoplast with a softening of temperature of 30 to 40°C. GAP on the other hand is a cross-linked polymer, which shows no signs of softening at these temperatures.
Doping of PVN+IR with 1% CuO-nanoparticles reduced these thermal effects, but more particles were ejected and the shockwave velocity decreased. Higher laser energies might be necessary to achieve the desired effects of an increase of the decomposition energy.
Thrust data for all polymer/dopant/metal systems have not yet been acquired.

The mass spectrometric measurements showed a higher fragmentation of the energetic polymer GAP and PVN compared to PVC. For all polymers the main decomposition products could be determined. For PVN and PVC strong signals that originated form the solvent used in the preparation step of the polymer films were detected. Both polymers were solvent cast from dilute solution (10-20 wt-%) and larger amounts of solvent were trapped than in the case of GAP, which is cross-linked from a higher concentrated polymer (70 wt-%) solution.

GAP with both dopants decomposes into the same fragments, but in different ratios. Also a higher fragmentation is detected for GAP+IR. The main difference was detected in the fluence dependence of the kinetic energy distribution for selected positively charged ions. In the case of carbon doped polymers, more ions were detected at lower fluences, but the distribution did not change. For the GAP+IR more energetic ions were detected at higher

fluences. This indicates a higher fluence sensitivity for the IR-dye doped polymers and may be explained by the different distribution of the dopant in the polymer.

5.1. Velocities

Only a qualitative correlation can be established between the different methods (see Table 6 and Table 7). GAP+C shows a good performance in all experiments, while GAP+IR reveals good results in the thrust and mass spectrometry measurements, but the velocity of the hydrogen measured by plasma emission spectroscopy is much lower compared to GAP+C and PVC+C. It has to be considered that until now, only a single line in the emission spectra (H-Balmer α) and only one mass in the mass spectrometer (C^+) have been investigated in detail. It is possible, that thrust, which is the sum of different effects, can only be explained by a combination of different measurements.

The longer pulse lengths and shorter irradiation wavelength in the thrust measurements may also have a significant influence on the ablation process. The longer pulse length could increase the influence of the thermal side effects, such as melt ejection, and may therefore result in the worse performances of the thermoplasts, PVN and PVC.
For a quantitative correlation the thrust measurements have to be performed with the same experimental conditions, i.e. pulse length and irradiation wavelength.

Table 7 Expansion velocities for the shockwave, C^+-ions and hydrogen from the H Balmer α line.

Polymer	**Shadowgraphy (from shockwave) [m/s]**	**Mass Spectrometry (from the kinetic energy of C^+) [m/s]**	**Plasma emission (from the H Balmer α line) [m/s]**
GAP+C	710	28600	46000
GAP+IR	850	29300	36700
PVN+C	1080	25100	31100
PVC+C	630	25900	48300

The best overall performance from the studied polymers is observed for GAP+C, but only a qualitative correlation can be established between the different spectroscopy methods and the measured thrust. GAP+C clearly indicates the importance and possibility of the utilization of

the chemical energy stored in the polymer, as 3.7 times more energy was released as thrust than deposited by the laser pulse. Energy could also be gained from decomposing GAP+IR, while PVN, the polymer with the highest decomposition enthalpy, exhibits the worst performance in all experiments at high irradiation fluences. This is probably caused by the thermal properties of the polymer, i.e. the ejection of molten polymer, which is lost for the decomposition process and a pronounced amount of remaining solvent in the polymer film.
An ablation efficiency of ~50% was achieved for PVC+C, which is not surprising, as only a small amount of energy is gained from the decomposition of the polymer.

6. fs Experiments in Vacuum

6.1. Motivation

From [37]: *"Need for fs data in laser ablation propulsion*

Knowledge of two parameters is critical for designing successful laser space propulsion applications [35, 38]*. The first of these is the so-called laser momentum coupling coefficient* C_m *(N s/J) = J/W which is the ratio of momentum J transferred to an object by laser ablation and the incident laser energy W. The second is the optimum coupling fluence* Φ_{opt} *(J/m*^{2}*) for which* C_m *is maximized, and this is a critical parameter because the fluence range for optimum coupling is fairly narrow. In particular, the leading-edge slope of an experimental plot of* C_m *versus* Φ *is very steep, corresponding to the onset of intense vapor generation.* C_m *then rises to a maximum at the vapor–plasma transition and decreases somewhat less rapidly at higher laser pulse fluence due to plasma shielding. Fig. 55 shows data* [39] *which illustrates this point.*

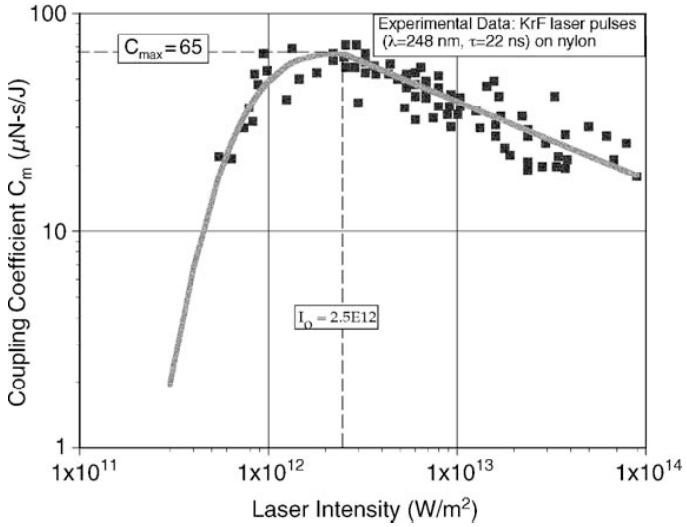

Fig. 55. Data illustrating the concept of optimum coupling fluence. In this case, the optimum intensity is 2.5 TW/m^2 *and* Φ_{opt} *= 55 kJ/m*^{2}*.*

For applications such as the ORION laser-space-debris clearing concept [38]*, for which laser systems with tens of kilowatt average power have been proposed, an incorrect value of* Φ_{opt} *can affect system design and cost unfavorably, or make the whole concept unworkable because correcting the error runs into other limitations such as reaching the threshold for stimulated Raman scattering (SRS) in the atmosphere. Isolated measurements of* C_m *or ablation rate alone are not sufficient; rather, a clear experimental demonstration that the* C_m *versus* Φ *maximum has been achieved is required, and this has not often been done in the*

literature. In the range 100 ps < t < 1 ms, we have shown [35] *that* Φ_{opt} *varies approximately as predicted by 1-D thermal transfer theory* [40]*:*

$$\Phi_{opt}\left(J/cm^2\right) = B\tau^m \qquad (5)$$

with m = 0.5 and B = 480 MJ/m^2*. However, the precise result is material-, wavelength- and pulse width-dependent and, previous to this work, information on* Φ_{opt} *and the associated* C_m *did not exist for pulses shorter than 100 ps, and no proven model existed for predicting the parameters. Yet, interesting applications for femtosecond-pulse momentum transfer exist.*

Aside from these practical concerns, a second motivation for this work was to discover where the short-pulse breakdown would occur in our theoretical model [39, 41] *for* C_m*, exhaust velocity* v_E*, electron density* n_e *and temperature* T_e *in the range 100 ps <* τ *< 1 ms. In particular, the authors of ref.* [42] *have shown that this breakdown point is probably* τ *= 10 ps. Specific impulse is defined by the relationship* I_{sp} *1/4* v_E*=go, where go is the standard acceleration of gravity at sea level."*

In Fig. 56 the optimum coupling fluence for some metals and GAP+IR is plotted versus the laser pulse duration. It is visible that the optimum coupling fluence at 130 ns is essentially the same as for 100 ps. To compare these results with data acquired for ns laser pulses, plasma studies for fs laser pulse irradiation were performed. This data allowed a comparison of thrust and plasma emission with the same pulse length, which was until now not possible, as the thrust data was acquired with ms pulses, and the spectroscopic date was obtained with ns irradiation.

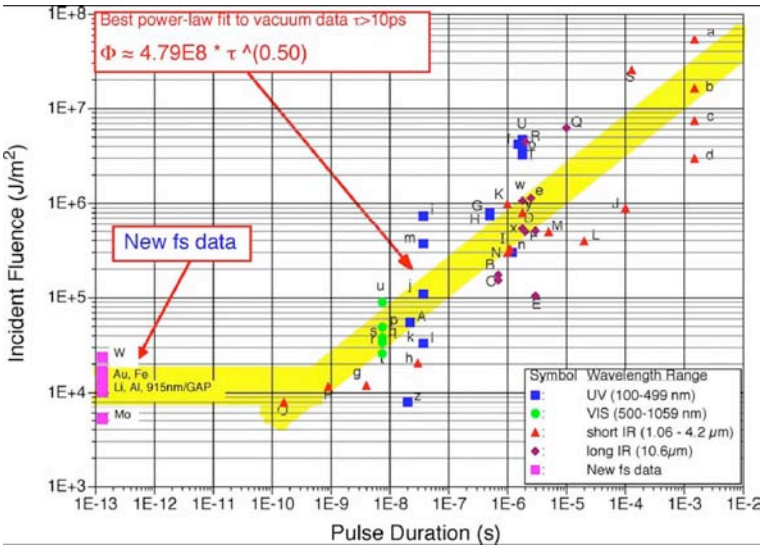

Fig. 56. Optimum coupling fluence plot shows purely thermal behavior down to 100 ps, and a flat behavior for shorter pulses. The letters next to data points in the figure are references to the literature explained in [35]. Figure copied from [37].

The plasma expansion as a function of the target material-absorber system and the irradiation laser fluence has been investigated by plasma imaging. Selected emission lines have also been recorded and were used to calculate plasma properties, such as electron density and plasma temperature. Also the expansion of selected material specific decomposition products for each material-absorber system have been investigated.

6.2. fs thrust measurements

The fs thrust measurements in Table 8 were performed by Claude Phipps and are presented here for comparison. GAP+C and GAP+IR with two different IR-dyes were investigated for the optimal fluence (Φ_{opt}) for the thruster application. For GAP+C the lowest Φ_{opt} and the highest C_m was measured. A small difference was observed for GAP+IR with the two different dyes.

Table 8 Cm and the optimal laser fluence obtained for fs laser irradiation (from [37])

Polymer	**Φ_{opt} (kJ/m^2)**	**$C_{m\ opt}$ (µN/W)**
GAP+C	10.4	80
GAP+IR/915nm	13.0	32
GAP+IR/935nm	13.0	40

6.3. Experimental Setup

The fs laser pulse were performed at the LP3 Laboratory in Marseille. The ultra short laser pulses of 100 fs duration were delivered by a Ti:sapphire laser system (Spectraphysics, model Hurricane) at wavelength of 800 nm and 100 Hz repetition rate. The energies of the femtosecond laser pulses were varied using calibrated attenuating plates. In the plasma imaging experiments, the center part of the laser beam was selected using a square mask of 2 mm x 2 mm, to get an almost uniform laser energy distribution. A spot of about 30 µm x 30 µm area was obtained by projecting the mask image onto the sample surface with the aid of a plano-convex lens of 50 mm focal length. In order to reach higher irradiation fluences than 4.4 J/cm^2, the mask was omitted and the whole laser beam was focused to an ablation spot size of 50 µm diameters. A mechanical shutter controlled the number of applied laser pulses. Target holder and focusing objective were placed on motorized translation axes. The focusing distance and the target position were controlled by a micro-computer and visualized by a CCD camera that captured the image of the targets surface through the focusing objective

(experimental setup is shown in Fig. 57). All fs experiments were performed at a pressure of ~5 • 10^{-5} mbar at room temperature.

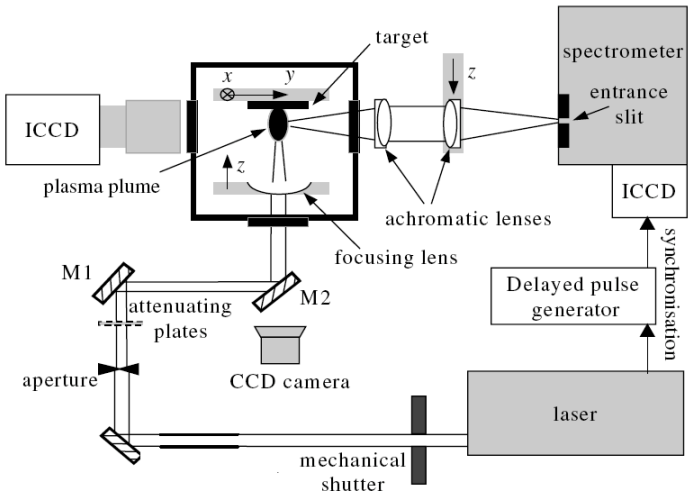

Fig. 57. Experimental setup for the plasma imaging and plasma emission spectroscopy measurements with fs laser pulses.

Plasma imaging

A fast intensified charge coupled device (ICCD) (iStar from Andor) with a 5 ns gate width and an objective (Tamron 70–210 mm; 1:3,8-4) were used for imaging. The spatial resolution of the system was of about 20 μm. The time delay to the laser pulse was varied with a delay generator to observe the plasma expansion.

Plasma emission spectroscopy

The plasma was imaged on the entrance slit of the spectrometer (Spectra Pro 300i from Acton research). The spectral and special resolved images were then recorded with a fast intensified charge coupled device (ICCD) (iStar from Andor) with a 5 ns gate width. For all polymers neutral, ionic and diatomic species were observed at varying time delays to the ablation laser pulse.

6.4. Results

Plasma Imaging

For all polymer-absorber systems, plasma images at varying time delays have been recorded at irradiation fluences of 4.4 and 7.6 J/cm^2. At a time delay of 100 ns after the laser pulse, a series of plasma images with different irradiation fluences from 0.44 to 4.4 J/cm^2 have been

recorded for all polymers. All plasma images are digitally enhanced to optimize the visibility of the features to be explained.

The maximum intensity of a line profile through the center of the ablation plume was used to calculate the expansion velocity.

GAP+C

An egg-shaped plasma plume is visible for GAP+C at an irradiation fluence of 4.4 J/cm^2 20 ns after the laser pulse in Fig. 58. This first domain of the plasma plume expands and simultaneously moves away from the sample surface, which is located on the right side of the images. After 50 ns a second domain with a lower intensity becomes visible as a connection between the first domain and the sample surface. This second domain also expands and moves perpendicular to the sample surface, but at a lower velocity. 100 ns after the laser pulse a third domain appears on the sample surface. The propagation of this third domain is slower, but its expansion is much faster. It is also well separated from the second domain. The expansion perpendicular to the sample surface is slower than parallel to the surface, which leads to a broader expansion angle of the plasma plume at later times. After 400 ns the first domain has traveled out of the field of vision and is completely separated from the second domain. During the whole observation time, the highest intensity is observed in a small region directly on the sample surface.

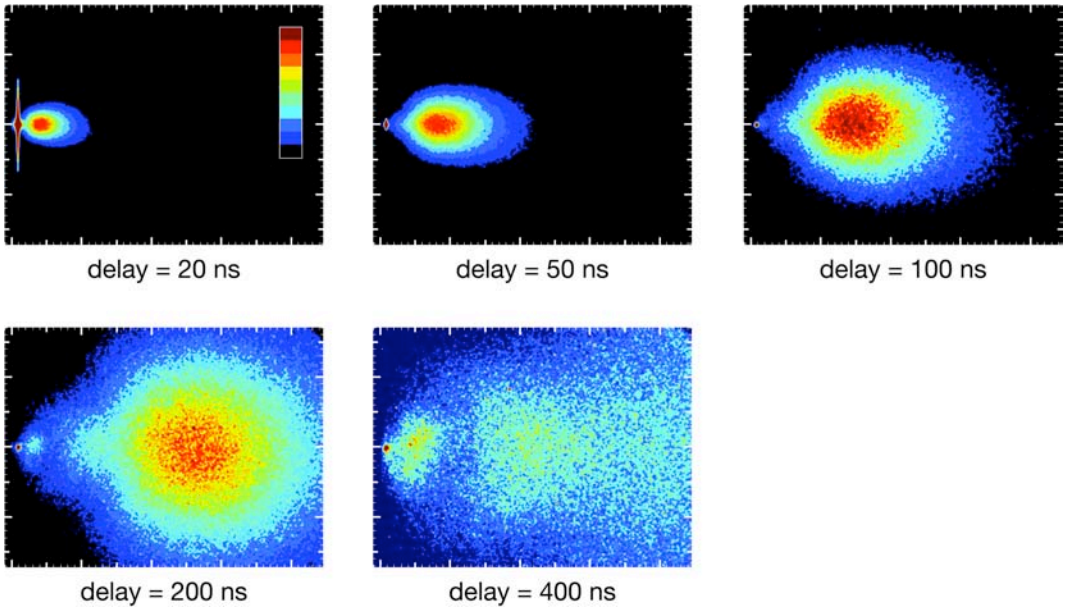

Fig. 58. Plasma image of GAP+C for an irradiation fluence of 4.4 J/cm^2.

In Fig. 59, the distance of the maximum of each domain to the sample surface is plotted versus the time delay to the laser pulse. For the two investigated fluences of 4.4 and 7.6 J/cm^2, no significant differences can be observed. The first domain travels with a velocity of 26200

m/s at an irradiation fluence of 4.4 J/cm^2, and 29300 m/s with Φ = 7.6 J/cm^2. The propagation velocity of the second domain is similar for both irradiation fluences with ~10000 m/s. The third domain appears 200 ns after the laser pulse for the lower fluence but is much less intense and can only be observed for until ~400 ns after the laser pulse, whereas for the higher laser fluence, the third domain is visible for 1 µs. The propagation velocity of domain II is ~1750 m/s for both fluences

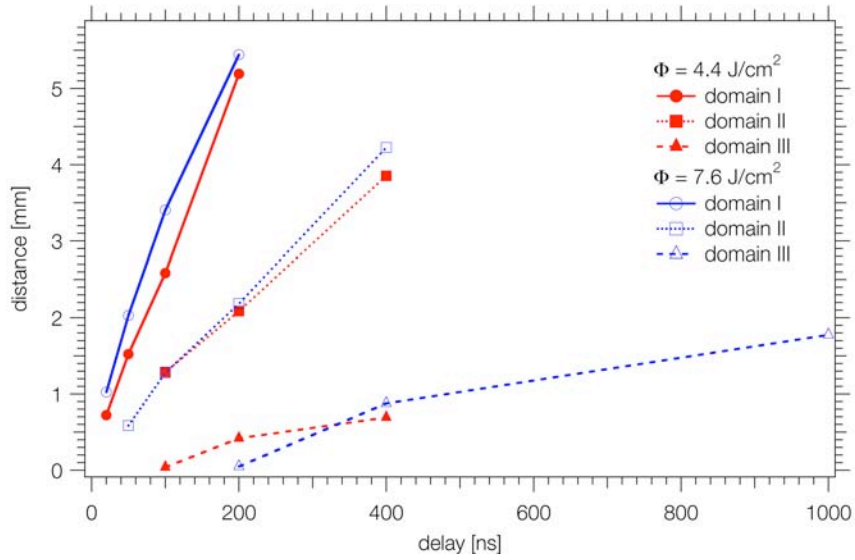

Fig. 59. The expansion of the different domains of the plasma plume of GAP+C versus the delay to the laser pulse.

The dependence of the plasma plume appearance on the irradiation fluence is shown in Fig. 60. Images were recorded at fluences ranging from 0.44 to 4.4 J/cm^2 at a time delay of 100 ns after the laser pulse. In all images the highest intensity is observed on the sample surface in a very confined round region. At 0.44 J/cm^2 only a very small circular plasma plume is visible ~1 mm from the sample surface. With increasing laser fluence, the intensity and the expansion of this domain increase. At 1.32 J/cm^2, a second domain appears farther away from the surface. The intensity of this second domain increases faster with increasing fluence than the intensity of the first domain. At Φ > 1.76 J/cm^2 this second domain is more intense than the first domain. With increasing fluence the second domain increases in size and the position of the maximum intensity moves further from the sample surface.

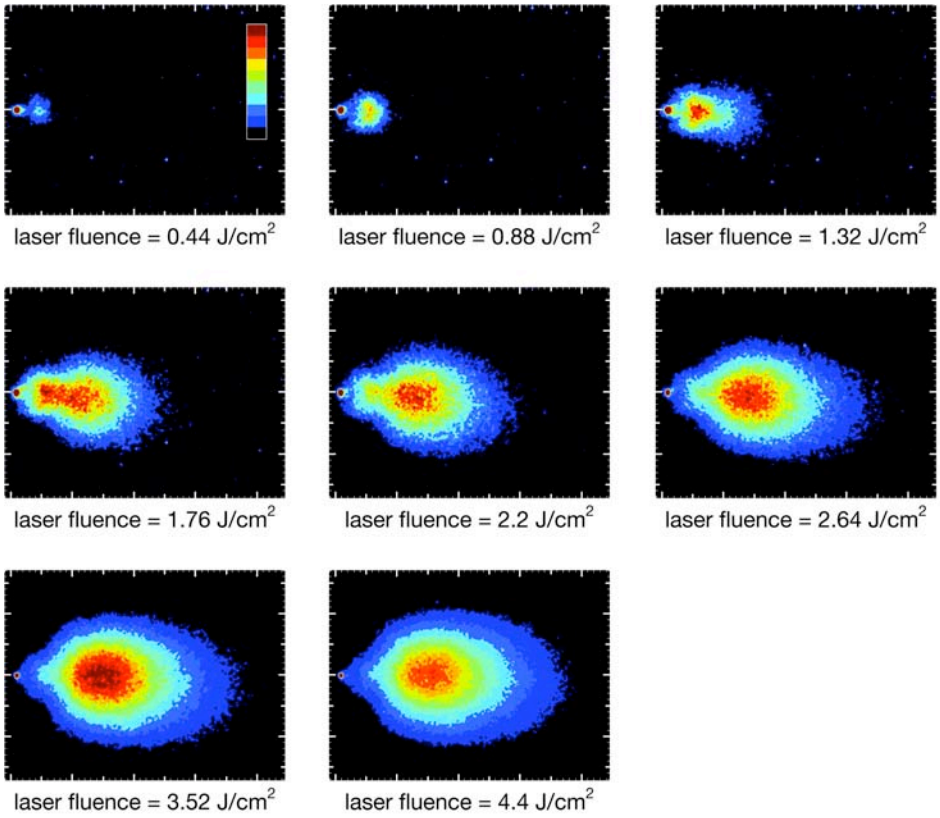

Fig. 60. Plasma image of GAP+C for different irradiation fluences 100 ns after the laser pulse.

The velocity of the maximum intensity versus the irradiation fluence is plotted in Fig. 61. The maximum of domain I remains within 1.4 mm distance to the surface for all irradiation fluences. Domain II appears at fluences over 1.76 J/cm^2 and shows a much stronger dependence on the irradiation fluence than domain I.

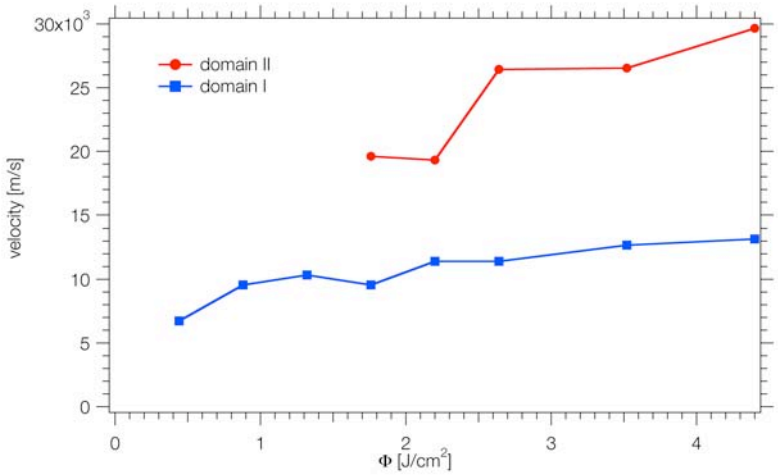

Fig. 61. The propagation of the maximum intensity 100 ns after the laser pulse of the different domains of the plasma plume of GAP+C versus the delay to the irradiation laser fluence.

GAP+IR

The plasma plume for GAP+IR is egg-shaped, and only one domain is visible 20 ns after the laser pulse for an irradiation fluence of 4.4 J/cm^2 (see Fig. 62). With increasing time this domain moves away from the surface and expands in all directions. A second domain appears after 50 ns but overlaps strongly with the first domain. After 200 ns the two domains are separated. The highest intensity is observed in a confined stationary area close to the sample surface, as observed also for GAP+C. The shape and size of the two domains for GAP+IR is very similar to domains I and II observed for GAP+C, but no third domain is visible for GAP+IR at both laser fluences. The main difference between GAP+C and GAP+IR is the size and distribution of the absorber in the polymer. The IR-dye used as absorber in GAP+-IR is distributed on a molecular level, whereas the carbon nanoparticles form clusters of nanometer to micrometer size. This nanometer sized carbon nanoparticles can produce a continuum black-body like emission [43], which has also been observed for other materials such as Mo, Nb and Hf after ns-pulse laser irradiation [44] and TiO after fs-pulse laser irradiation [45, 46].

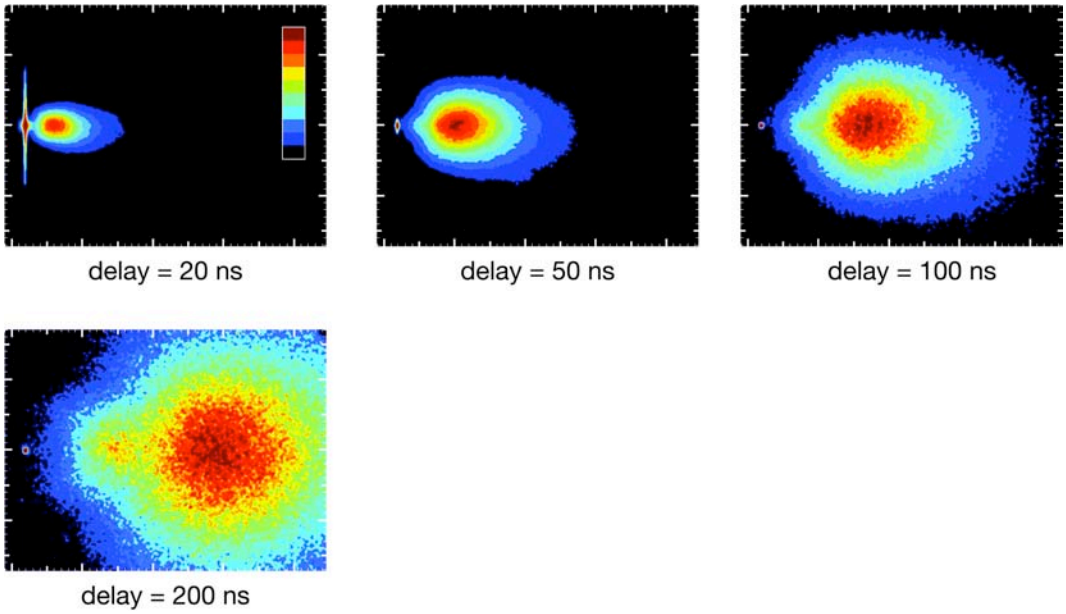

Fig. 62. Plasma image of GAP+IR for an irradiation fluence of 4.4 J/cm^2.

The same behavior for the first domain is observed for GAP+IR at both fluences (see Fig. 63). The expansion velocities of GAP+IR of 27900 m/s at Φ = 4.4 J/m^2 and 32200 m/s at Φ = 7.6 J/cm^2 are 5 %, respectively 10% higher than for GAP+C. A second domain is visible at both irradiation fluences, but the expansion velocity could only be determined at the higher fluence, as for 4.4 J/cm^2, no clear separation of the two domains at early times was detectable. The expansion velocity of 12100 m/s at Φ = 7.6 J/cm^2 is about 10 % higher than the velocity of the second domain observed for GAP+C at the same irradiation fluence.

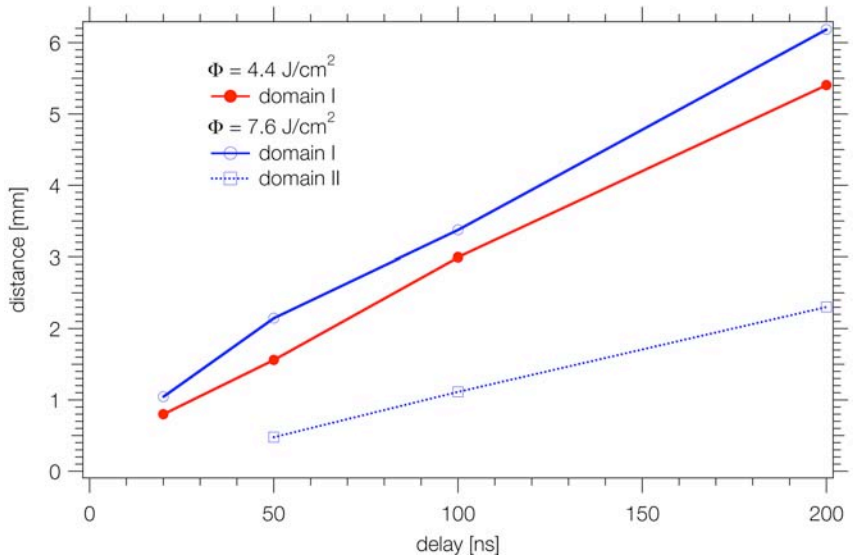

Fig. 63. The expansion of the different domains of the plasma plume of GAP+IR versus the delay to the laser pulse.

PVC+C

The intensity of the plasma plume of PVC+C is higher than for GAP with both absorbers. It was therefore possible to observe the plumes for a time delay of 1 µs for both irradiation fluences. At delay times of up to 20 ns, only one egg-shaped domain is visible (see Fig. 64).

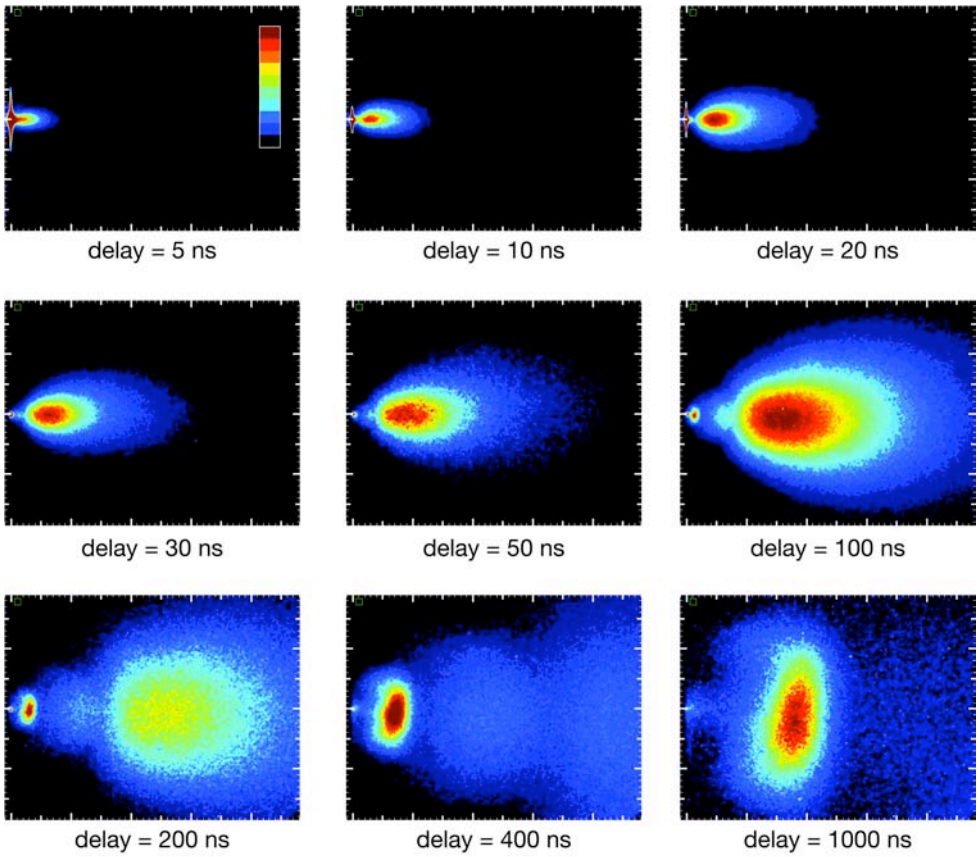

Fig. 64. Plasma image of PVC+C for an irradiation fluence of 4.4 J/cm^2.

This domain expands more directed, perpendicular to the surface and is confined to a narrower expansion angle than for GAP with both absorbers. After 30 ns the maximum of the first domain has moved far enough from the surface, so that a second domain becomes distinguishable. This second domain also moves away from the surface and expands more uniform than the first domain in all directions. After 100 ns a third domain is formed on the sample surface. This domain has the highest intensity, is well separated from the other two domains and can be explained by continuum black-body like emission of e.g. carbon nanoparticles, which function as absorber in PVC+C. Similar to GAP+C, the expansion of the third domain is faster parallel to the surface, than in the propagation direction. This leads to an almost disc-shaped third domain, with a more intense front region and a broader expansion angle of the plasma plume.

No difference can be observed in the expansion velocity of the different domains for PVC+C for the two fluences (see Fig. 65). The first domain has an expansion velocity of 23000 m/s, which is slower than the same domain for GAP with both absorbers (10 % slower than GAP+C and almost 30 % slower than GAP+IR). The second domain (10500 m/s) has a similar velocity like GAP+C but is slower than for GAP+IR. The third domain with a velocity of 3500 m/s is twice as fast as the third domain of GAP+C.

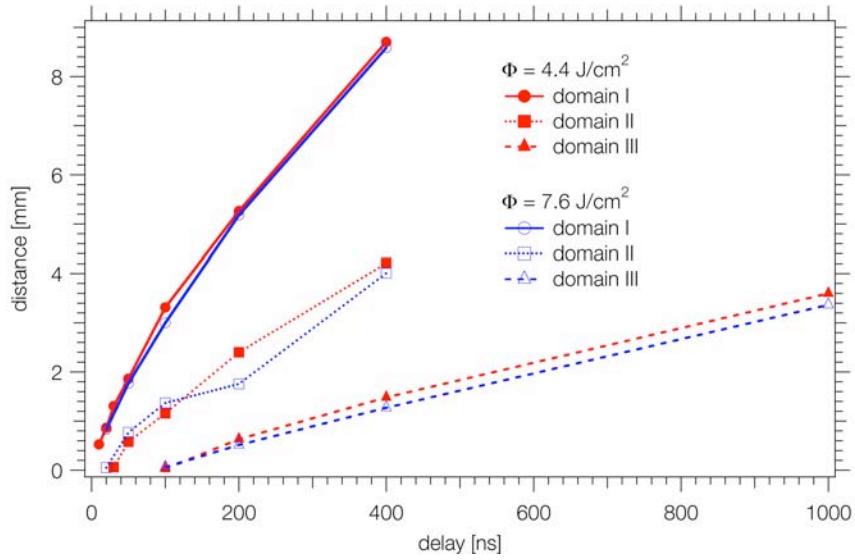

Fig. 65. The expansion of the different domains of the plasma plume of PVC+C versus the delay to the laser pulse.

Even though the experiments were performed at a pressure of $5 \cdot 10^{-5}$ mbar, where the mean free path for atoms and ions is much larger than the field of view of the ICCD, the velocity is decreasing with increasing distance from the surface. A possible explanation for this is

collisions of particles in the plasma. Such collisions of particles with similar velocities and direction would lead to a broadening and slowing of the plasma plume, as more particles are scattered and lose a part of their directionality. This effect would be more pronounced in a denser, more directional plasma, as it is observed for PVC+C, compared with GAP+C, where this effect is less pronounced.

PVN+C

For PVN+C the plasma plume with the lowest intensity was observed. Even at a fluence of 7.6 J/cm^2, only one domain could be assigned. In Fig. 66 the plasma images after irradiation with 4.4 J/cm^2 are shown. The plasma plume of PVN+C is smaller and remains closer to the surface than the first domain of the plasma plumes of the other polymers and has a "flat" backside. A second domain becomes visible after 200 ns, but cannot be separated from the first domain.

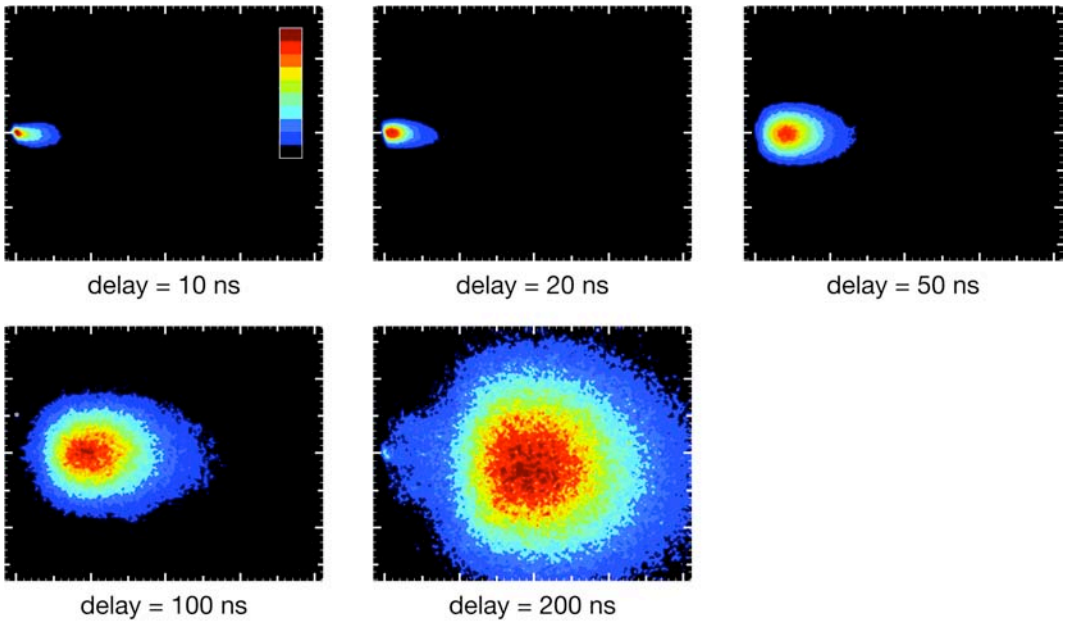

Fig. 66. Plasma image of PVN+C for an irradiation fluence of 4.4 J/cm^2.

The expansion velocity of the plasma of PVN+C of 20000 m/s at Φ = 4.4 J/cm^2 is the lowest value of all polymers. At a fluence of 7.6 J/cm^2, the propagation velocity reaches 24600 m/s and is in the range of PVC+C. During the first 200 ns after the laser pulse, the plasma plume is not slowed down, and at later times it was not possible to determine the position of the maximum intensity (see Fig. 67).

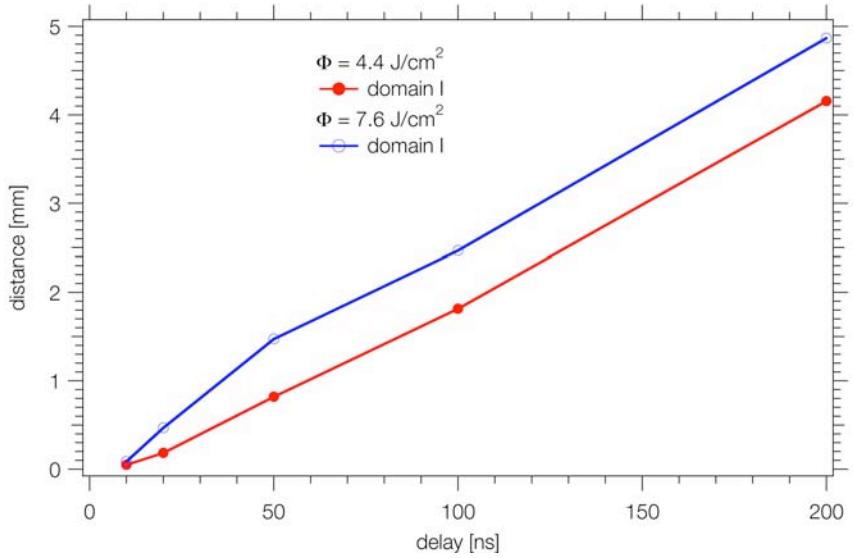

Fig. 67. The expansion of the first domain of the plasma plume of PVN+C versus the delay to the laser pulse.

Summary of the fs-plasma imaging experiments

For GAP+C and PVC+C three different domains are visible at both irradiation fluences and can be observed for up to 1 µs after the laser pulse. The plasma plume of PVN+IR is to weak to separate the individual domains and can only be observed for 200 ns before the signal to noise ratio becomes to small.

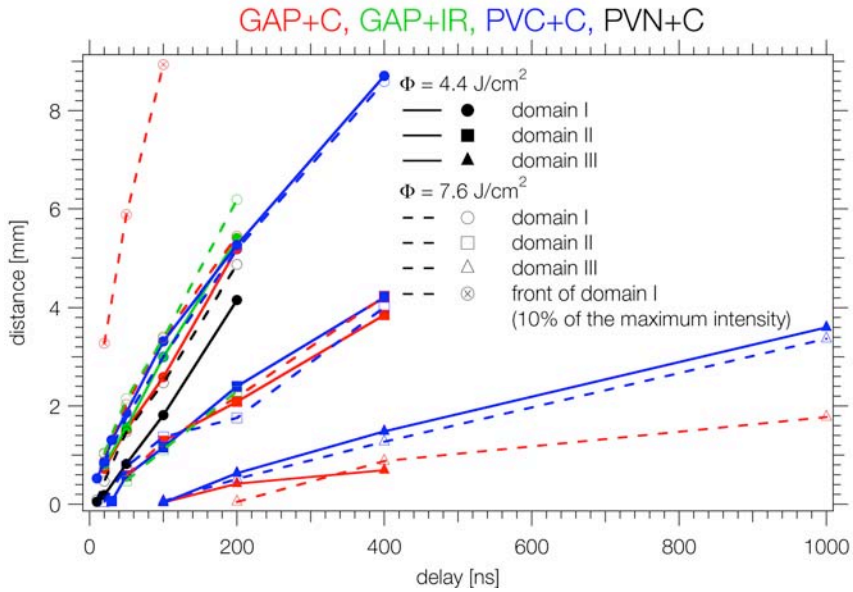

Fig. 68. The expansion of the different domains of the plasma all polymers versus the delay to the laser pulse. The different colors represent the different polymer-absorber systems. The marker symbols represent the three domains, and the dashed line indicates the higher fluence.

For GAP+IR only two domains are present. The third domain observed for GAP+C and PVC+C could be due to a continuum black-body like emission of the carbon nanoparticles, which were added to the polymers as absorbers. In Fig. 68, the propagation of the maximum intensities of all domains for the different polymers at both irradiation fluences are displayed versus the time delay to the laser pulse. Additionally the front of domain I of GAP+C is displayed in the graph to indicate the maximal expansion of the plasma plume. The front was defined as the position of the domain, where the intensity has reached 10 % of the maximal domain intensity. For the more intense plasmas of GAP+C and PVC+C a decrease of the propagation velocity with increasing time can be observed. This decrease could be caused by collisions of plasma particles and scattering of these particles.

The first and second domain of GAP+IR have the largest propagation velocity, followed by GAP+C, PVC+C and PVN+C. This order changes for third domains, which propagate faster for PVC+C than for GAP+C.

The shape of the first domain is very similar for GAP with both absorbers and has an egg-like shape. Domain I of PVC+C expands at a smaller angle than for GAP.
The second domain is very similar for all polymers and is visible as a round zone that partly overlaps with the first domain.
The third domain, observed for GAP+C and PVC+C, expands faster parallel to the sample surface than perpendicular to it. It is therefore more disc-shaped, with the maximum intensity closer to the front edge.

Spectroscopic fs-Plasma Emission Spectroscopy

All plasma emission experiments were performed at an irradiation fluence of 7.6 J/cm^2 at room temperature and a pressure of $5 \cdot 10^{-5}$ mbar. On each recorded image the horizontal axis represents the spectral axis. The vertical axis is the spatial axis, where the sample surface is close to the lower edge and is indicated as dashed white line. Each image has been digitally enhanced to optimize the visibility of the interesting features. The color scale is represented on the left side of each image and ranges from white (highest intensity) to black (background). Red or green horizontal lines represent the position of selected profiles that are shown on the right side of the spectroscopy image to emphasize the discussed features. Below each image the time delay to the ablation laser pulse is indicated. The overview spectra were recorded with a 150 pitch/mm grating. Selected regions, in which the main decomposition products are present, were investigated with a high-resolution grating (1800 pitch/mm).

GAP+C

In the overview spectra of GAP+C presented on the right side of Fig. 69, ionic atoms, neutral atoms and neutral diatomic species are visible. In the red profile, that represents the spectrum in a distance of ~ 0.5 mm seven lines can be clearly distinguished. The most prominent line can be assigned to the neutral H Balmer β line at 486.2 nm, which corresponds to *2p – 4d* transition. The second strongest line is due to ionic carbon at 392 nm and corresponds to a $2s^2 3p - 2s^2 4s$ transition. The other lines could not yet be assigned, as the spectral resolution of the used grating is not sufficient to separate lines that are too close. The green profile was recorded close to the sample surface and the visible peaks can be assigned to diatomic systems like C_2 Swan [47] and CN Violet.

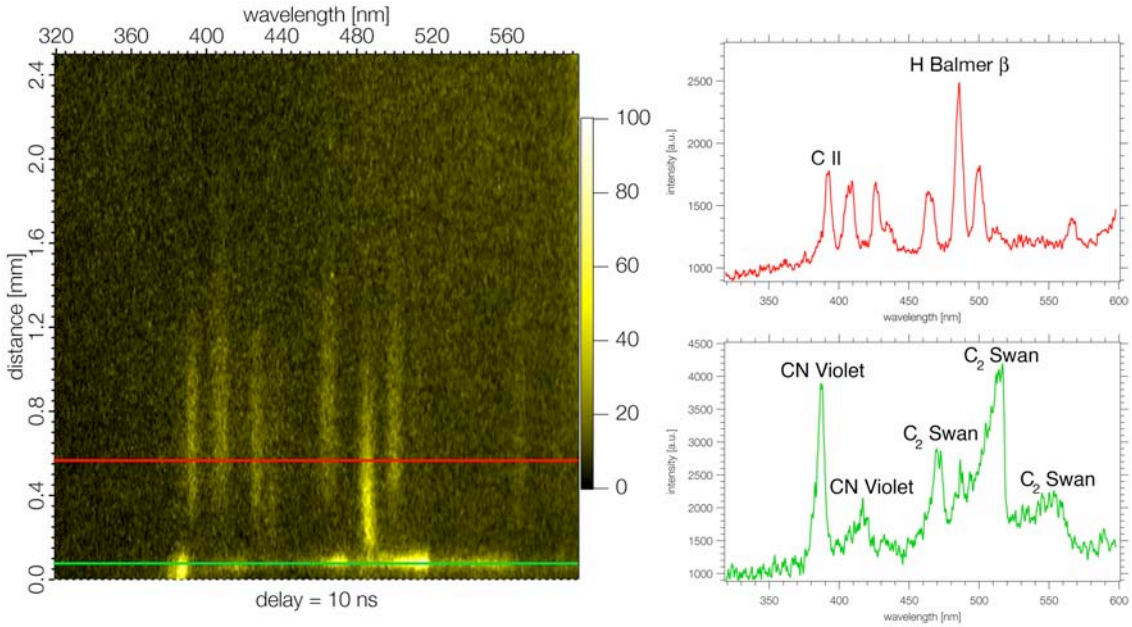

Fig. 69. Overview plasma emission spectra for GAP+C, 10 ns after the laser pulse. The spectra on the right side represent selected profiles, that are recorded at different positions from the sample surface, that are indicated as horizontal lines in the spectral image. Neutral atomic (H), ionized atomic (C II) and neutral diatomic (CN and C_2) species are visible.

For all polymer-absorber systems three spectral regions were investigated in detail. The first region ranges from 382 nm to 393 nm and is shown for GAP+C, 20 ns after the laser pulse in Fig. 18. The red profile represents the spectra in a distance of 1.4 mm from the sample surface. Multiple peaks are visible, but until now only C II at 392 nm could be assigned.

The green spectrum has been recorded in a distance of 0.25 mm. The line system corresponds to the emission of CN and was used to calculate the rotational-vibrational temperature as described in [5]. The position of the maximum intensity of the strongest peak of the CN

Violet system at different time delays was also used to calculate the propagation velocity of the CN system.

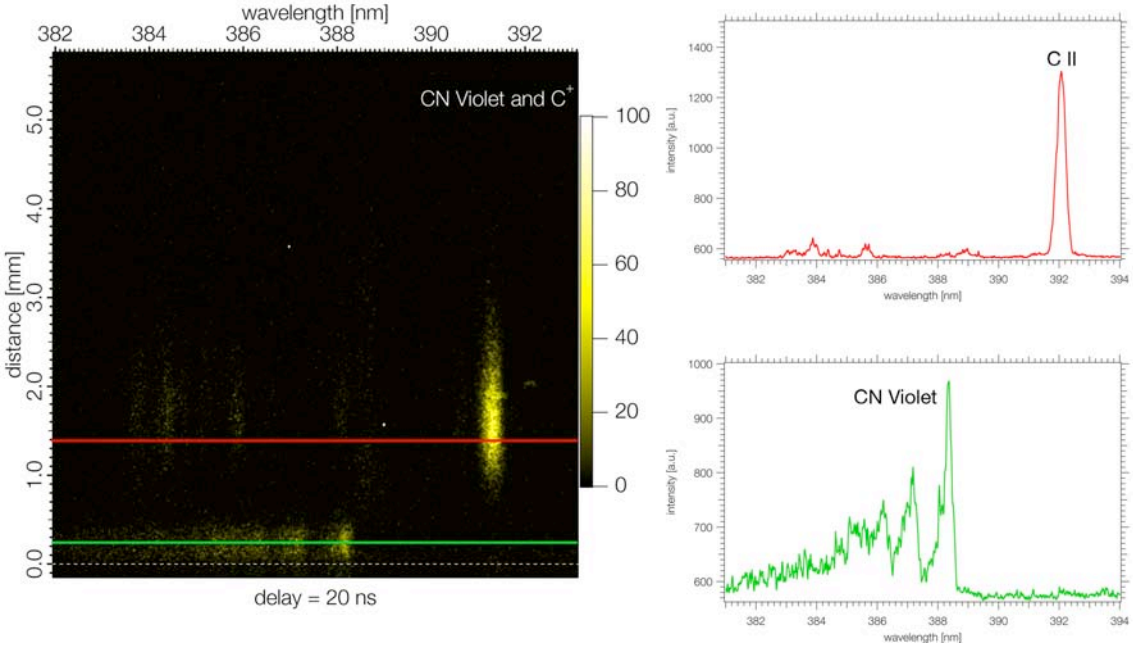

Fig. 70. Plasma emission of CN Violet and C II for GAP+C 20 ns after the laser pulse. The spectra on the right side represent selected profiles, that are recorded at different positions from the sample surface, that are indicated as horizontal lines in the spectral image.

The highest rotational-vibrational temperature of the CN Violet system of 9000 K was calculated from a spectrum recorded 10 ns after the laser pulse on the sample surface. At a delay of 20 ns the plasma temperature has dropped to 6800 K on the sample surface and to 5500 K in a distance of 0.3 mm from the surface. 50 ns after the laser pulse, a maximum of 6500 K is measured in a broad region ranging from 0.9 mm to 1.4 mm. Closer to the sample surface, the temperature decreases to 5200 K at 0.6 mm.

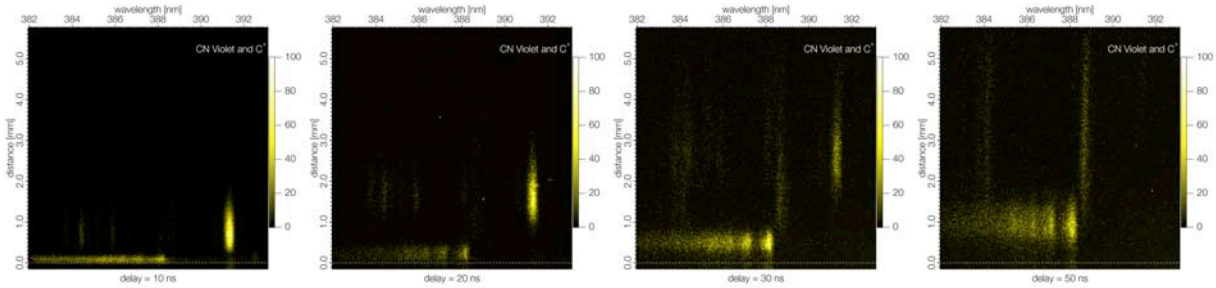

Fig. 71. Plasma emission of CN Violet and C II for GAP+C for different delay times after the laser pulse.

In Fig. 71 the expansion of C II and CN Violet is shown. The diatomic CN moves slower than the ionic carbon, which leaves the field of vision after 50 ns. The emission lines of the CN

molecule are visible as a series of lines with increasing intensity at higher wavelengths, that propagate all at the same velocity, but which are clearly slower than the C II line. Other lines, that could not be assigned yet, propagate at a velocity between the diatomic CN and the ionic carbon. They are most probable neutral atomic species, as they show a behavior similar to hydrogen.

The H Blamer β line at 486 nm is the strongest line observed for GAP+C. In the profile shown in Fig. 72, no other peaks are visible. The hydrogen Balmer β line was used to calculate the electron density (ρ_{el}) in the plasma as described earlier in this report.

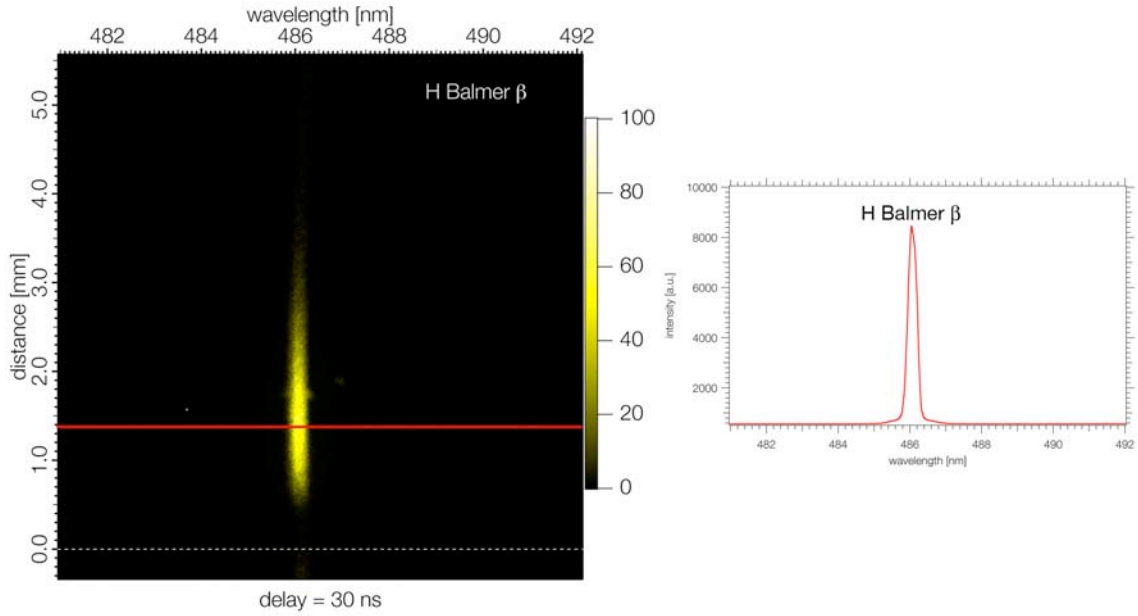

Fig. 72. Plasma emission of H Balmer β for GAP+C 30 ns after the laser pulse. The spectrum on the right side represents a line profile, that is recorded at a distance of 1.3 mm from the sample surface, that is indicated as horizontal line in the spectral image.

In Fig. 73 the electron density versus the distance from the sample surface is shown for different time delays. The dotted lines represent the intensity of the H Balmer β line as function of the distance to the sample surface. 10 ns after the laser pulse the highest electron density of $1.25 \cdot 10^{22}$ m^{-3} was measured at a distance of 0.11 mm from the sample surface. ρ_{el} decreases in direction of the sample surface to $4.85 \cdot 10^{21}$ m^{-3}. Further away the electron density decreases to a constant value of $1.75 \cdot 10^{21}$ m^{-3}. At a time delay of 20 ns after the laser pulse, the maximum electron density of $2.8 \cdot 10^{21}$ m^{-3} is again observed at the backside of the plasma plume, closest to the surface. At increasing distances ρ_{el} decreases to $1.5 \cdot 10^{21}$ m^{-3}. 30 ns after the laser pulse, only a small increase of ρ_{el} can be observed at the backside of the

plasma plume, before the it decreases to a value of $1.4 \cdot 10^{21}$ m^{-3}. At later time delays, ρ_{el} remains constant in the whole plasma plume at $1.35 \cdot 10^{21}$ m^{-3}.

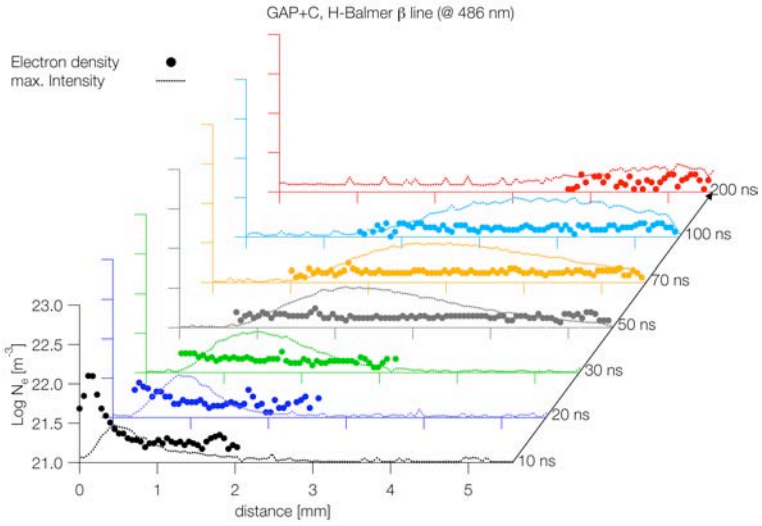

Fig. 73. The electron density as a function of distance from the sample surface and time delay to the laser pulse for GAP+C, calculated form the Stark broadening of the H Blamer β line at 486 nm.

The emission lines of C_2 are shown in Fig. 74. The strongest peak of this C_2 Swan emission at 517 nm has been used to calculate the expansion of this neutral diatomic system. The other emission lines, that move faster than the C_2 Swan lines, could not yet be assigned.

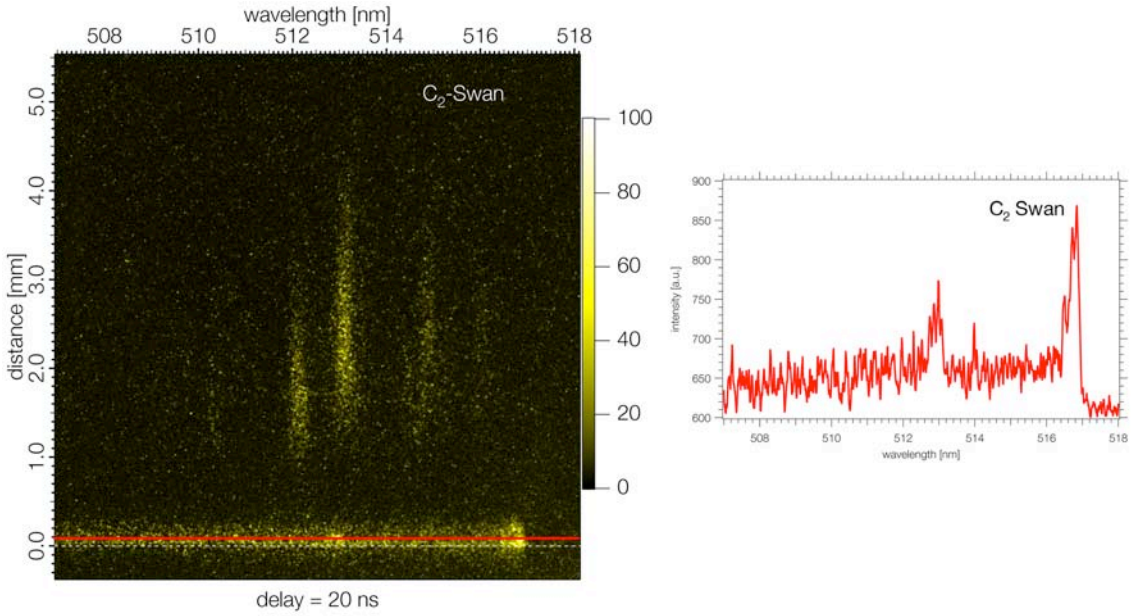

Fig. 74. Plasma emission of C_2 Swan for GAP+C 20 ns after the laser pulse. The spectrum on the right side represents a line profile, that is recorded at a distance of 0.5 mm from the sample surface, that is indicated as horizontal line in the spectral image.

The expansion velocities for different species in the plasma plume of GAP+C are shown in Fig. 75. The highest velocity of 78200 m/s is observed for positive charged carbon, which moves at a constant velocity over the whole measurements period. For the neutral hydrogen a small decay of the expansion velocity is observed at later times. During the first 50 ns a propagation velocity of 39000 m/s is obtained. The diatomic species C_2 and CN move much slower and reach velocities of 9400 m/s and 17000 m/s.

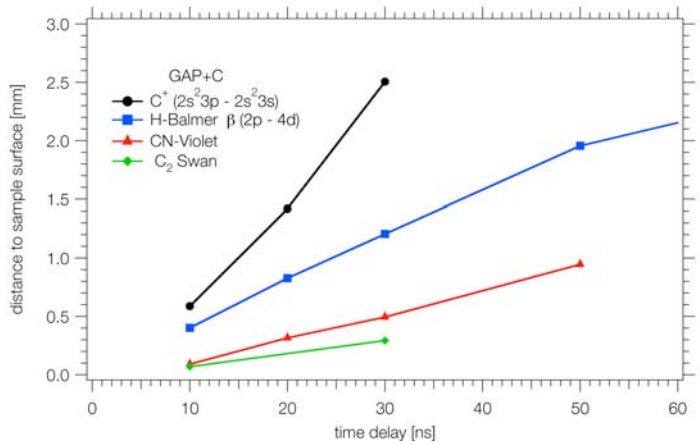

Fig. 75. The plasma expansion of positive charged ions (C II), neutral atoms (H) and diatomic species (CN and C_2) for GAP+C.

GAP+IR

The same peaks as for GAP+C are visible in the overview spectra of GAP+IR. Again the H Balmer β is the most intense peak at a distance of 0.6 mm from the sample surface (red profile in Fig. 76). A second peak could be assigned to C II. The other peaks in the red profile have not yet been assigned.

In the green profile, close to the sample, the emission of the same diatomic species as for GAP+C can be observed (C_2 Swan and CN Violet).

The CN Violet system was used to calculate the rotation-vibration temperature, which is assumed to be the plasma temperature (T_{plasma}). The highest temperature of 8500 K was measured 10 ns after the laser pulse on the sample surface. At 20 ns T_{plasma} on the sample surface has dropped to 6600 K. The maximum temperature is measured 0.16 mm from the sample surface and reaches a value of 7000 K. After 50 ns the maximum temperature is still 7000 K and is measured in a distance of 1.2 to 1.5 mm from the sample surface. Closer to the surface the temperature has dropped to 5500 K. Compared to GAP+C, a slightly lower initial temperature has been measured, but the temperature decay with increasing time delays is slower.

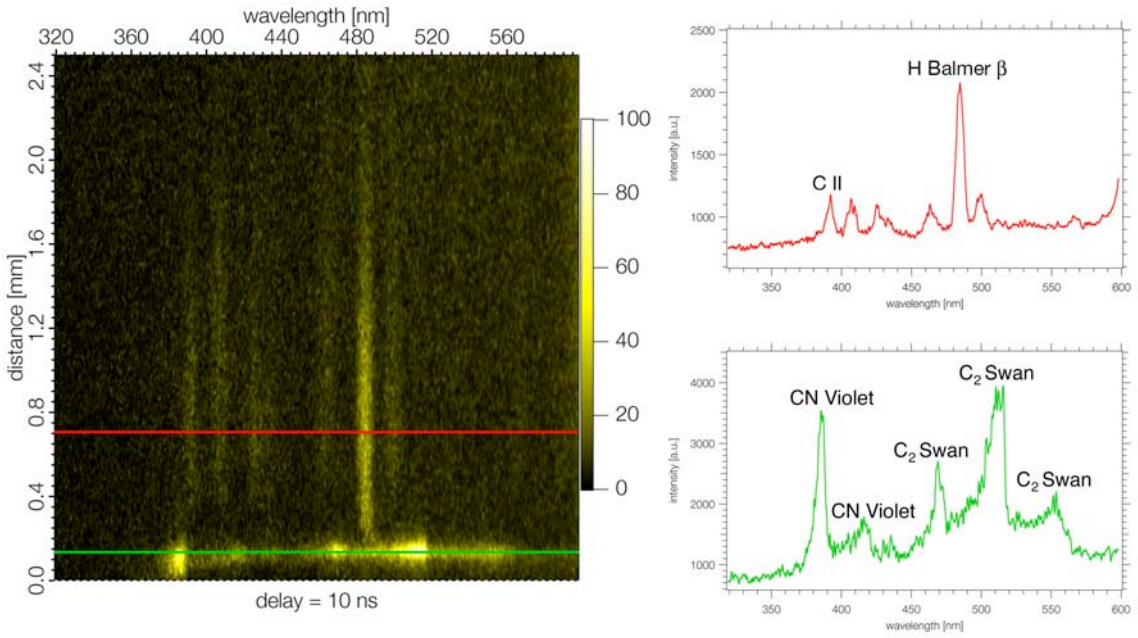

Fig. 76. Overview plasma emission spectra for GAP+IR, 10 ns after the laser pulse. The spectra on the right side represent selected profiles, that are recorded at different positions from the sample surface, that are indicated as horizontal lines in the spectral image. Neutral atomic (H), ionized atomic (C II) and neutral diatomic (CN and C_2) species are visible.

The electron density (ρ_{el}) in the plasma was calculated from the Stark broadening of the H Balmer β line at 486.2 nm and is shown in as a function of distance to the sample surface and delay time to the laser pulse.

The dashed line represents the intensity of the H Balmer β line.

The maximum ρ_{el} of $6.75 \cdot 10^{21}$ m^{-3} for GAP+IR was measured 10 ns after the laser pulse in a distance of 0.12 mm from the sample surface. With increasing distance it decreases to a $1.66 \cdot 10^{21}$ m^{-3}. At a delay of 20 ns, ρ_{el} reaches a maximum of $2.45 \cdot 10^{21}$ m^{-3} in a distance of 0.46 mm from the sample surface and decreases to a constant value of $1.4 \cdot 10^{21}$ m^{-3} at larger distances. After 30 ns only a small increase of ρ_{el} at the backside of the H Balmer β line is observed, before it remains constant at $1.35 \cdot 10^{21}$ m^{-3} over the whole H Balmer β line for later times.

The maximum electron density for GAP+IR is only half of the value reached for GAP+C. With increasing distance and time delays, ρ_{el} reaches similar values for both polymers. The increase of the electron density at the rear of the H Balmer β line close to the sample surface is present for a longer time in the case of GAP+IR than for GAP+C.

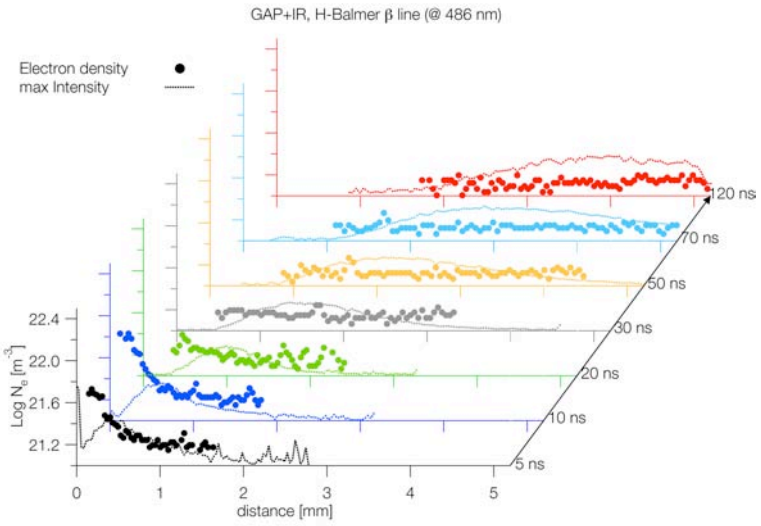

Fig. 77. The electron density as a function of distance from the sample surface and time delay to the laser pulse for GAP+IR, calculated form the Stark broadening of the H Blamer β line at 486 nm.

In Fig. 78 the propagation of the maximum intensity is displayed versus the time delay to the laser pulse. The highest propagation velocity is observed for ionic carbon with 83700 m/s. The propagation velocity is constant over the complete field of view. The propagation of the neutral hydrogen is slower and is slowed down with increasing time delays. During the first 50 ns the velocity remains almost constant at a value of 39500 m/s. For CN a propagation velocity of 17200 m/s has been measured during the first 50 ns after the laser pulse. At later time the CN Violet signal was to weak to be measured.

The expansion velocity for neutral hydrogen and CN of GAP+IR are identical to the values measured for GAP+C, but the ionic carbon is expanding slightly faster for GAP+IR.

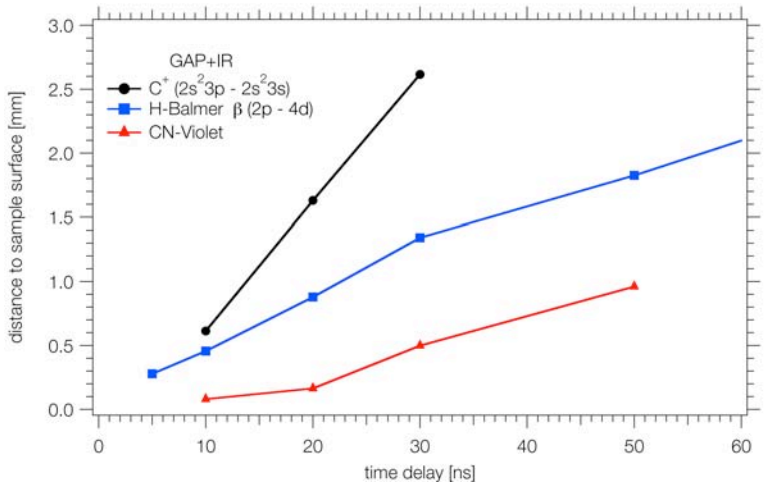

Fig. 78. The plasma expansion of positive charged ions (C II), neutral atoms (H) and diatomic species (CN) for GAP+IR.

PVC+C

The most intense plasma was observed for PVC+C (see Fig. 79). In the red profile 0.6 mm from the sample surface, the H Balmer β line is the most prominent feature, as already observed for GAP with both absorbers. The second most intensive peak can be assigned to three line from Cl II, that are not resolved with the 150 grating. Close to the surface (see green profile), strong signals can be assigned to C_2. Compared with the emission spectra of GAP with both absorbers, no CN emissions are visible as expected from the structure and by performing the experiments in vacuum. This is different to the ns experiments in air, where CN was clearly detectable for PVC+C. The plasma temperature could therefore not yet be determined. A possible solution could be to calculate the temperature of the C_2 Swan system, but the method has not yet been implemented in our analytical software, which has been used to process to the current results.

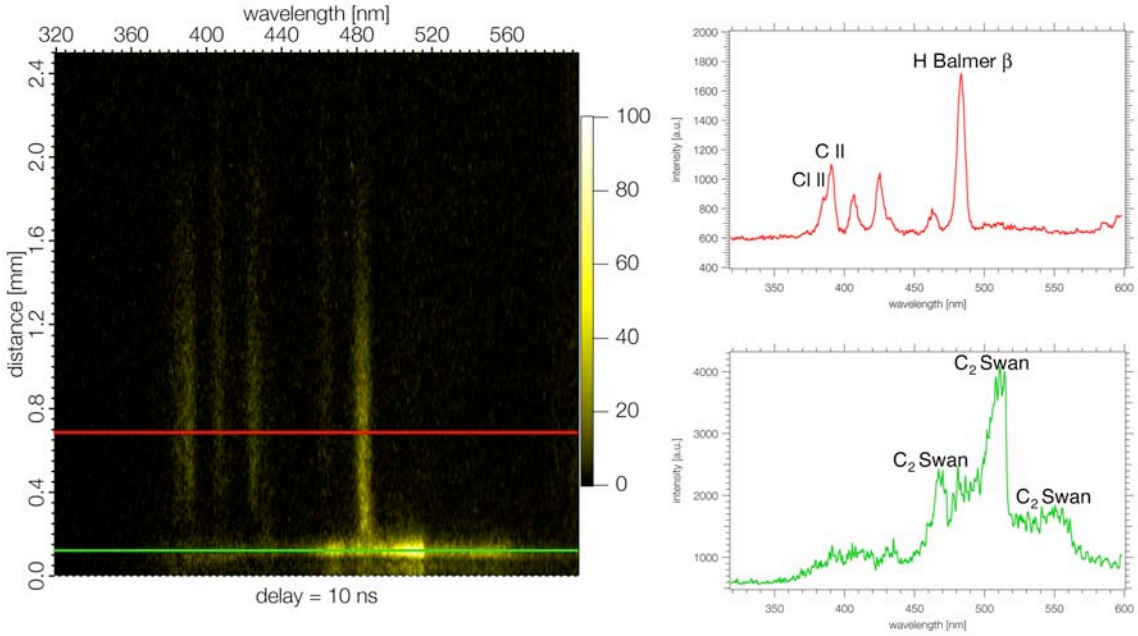

Fig. 79. Overview plasma emission spectra for PVC+C, 10 ns after the laser pulse. The spectra on the right side represent selected profiles, that are recorded at different positions from the sample surface, that are indicated as horizontal lines in the spectral image. Neutral atomic (H), ionized atomic (C II and Cl II) and neutral diatomic (C_2) species are visible.

In Fig. 80, a high-resolution image of the spectral region between 381 nm and 394 nm is shown. The strongest peak at 392 nm can be assigned to C II. The three peaks at 384.56 nm, 385.09 nm and 386.08 nm correspond to the emission of Cl II ($3s^2 3p^3(4S°)4p$-$3s^2 3p^3(4S°)4d$). The strongest of these three Cl II lines was used to calculate the propagation velocity of Cl II.

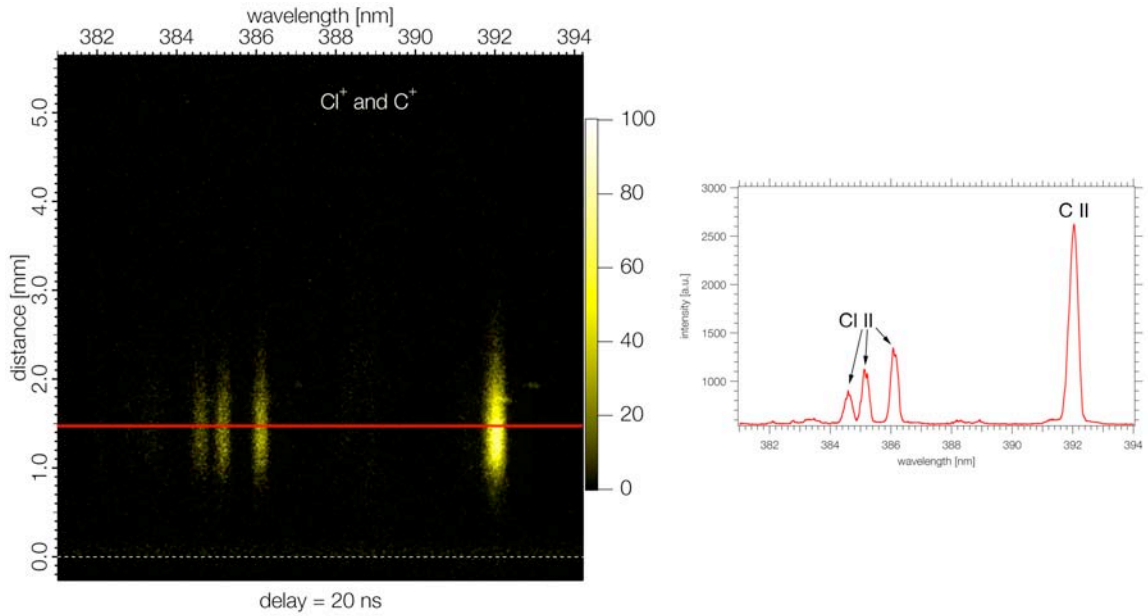

Fig. 80. Plasma emission of Cl ll and C II for PVC+C, 20 ns after the laser pulse. The spectrum on the right side represents a line profile, that is recorded at a distance of 1.5 mm from the sample surface, that is indicated as horizontal line in the spectral image.

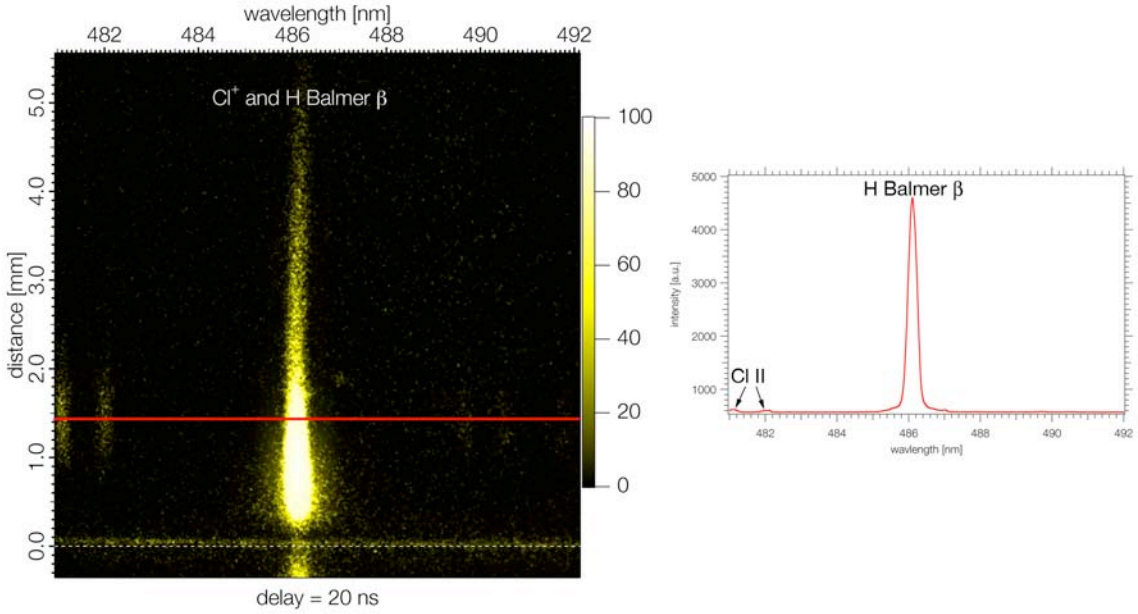

Fig. 81. Plasma emission of H Balmer β and C II for PVC+C, 20 ns after the laser pulse. The spectrum on the right side represents a line profile, that is recorded at a distance of 1.5 mm from the sample surface, that is indicated as horizontal line in the spectral image.

The strongest emission line at 486.13 nm in Fig. 81 is the H Balmer β line. Two weak Cl II lines ($3s^2 3p^3(4S°)4s$-$3s^2 3p^3(4S°)4p$) are visible at 481 nm and at 481.94 nm after strong digital

enhancement of the spectral image. The emission line at 481 nm was used to investigate the propagation of this transition of Cl II.

The H Balmer β line was used to calculate the electron density as a function of distance to the sample surface and the time delay to the laser pulse (Fig. 82). The dashed line represents the intensity of the H Balmer β line.

The highest ρ_{el} of 2.42 • 10^{22} m^{-3} is measured in a distance of 0.15 mm, 10 ns after the laser pulse. With increasing distance to the sample surface, it drops to 1.84 • 10^{21} m^{-3}. At time delay of 20 ns the maximum has ρ_{el} dropped to 3.45 • 10^{21} m^{-3} at a distance of 0.27 mm. The electron density in the plasma is reduced to 1.49 • 10^{21} m^{-3} with increasing distance. 30 ns after the laser pulse, the ρ_{el} has a maximum of 2.46 • 10^{21} m^{-3}, 0.5 mm from the sample surface, before it drops to 1.41 • 10^{21} m^{-3}at larger distances. For larger time delays, ρ_{el} remains constant at 1.32 • 10^{21} m^{-3} within the whole plume.

The maximum ρ_{el} is higher for PVC+C than for GAP with both absorbers. The increase of the electron density at the backside of the H Balmer β line, close to the sample surface, can be observed up to 30 ns after the laser pulse, as it is also the case for GAP+IR, but not for GAP+C.

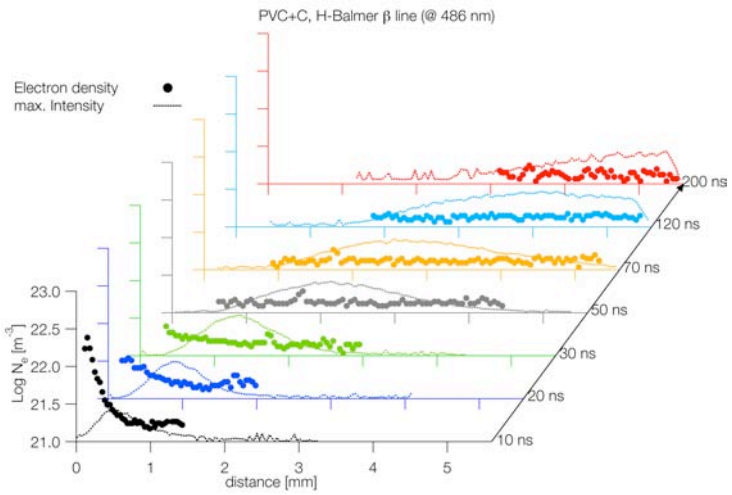

Fig. 82. The electron density as a function of distance from the sample surface and time delay to the laser pulse for PVC+C, calculated form the Stark broadening of the H Blamer β line at 486 nm.

The highest velocity for PVC+C of 74200 m/s is observed for Cl II (*$3s^2 3p^3(4S°)4s$-$3s^2 3p^3(4S°)4p$*). For the other investigated Cl II line (*$3s^2 3p^3(4S°)4p$-$3s^2 3p^3(4S°)4d$*) and C II a slightly lower velocity of 69500 m/s has been measured. The velocity of all ionic species remains constant in the whole investigation period. The neutral hydrogen propagates at a

velocity of 36500 m/s during the first 50 ns, before it is continuously slowed down. The expansion velocity of C_2 is constant at 7600 m/s as long as the system is visible.

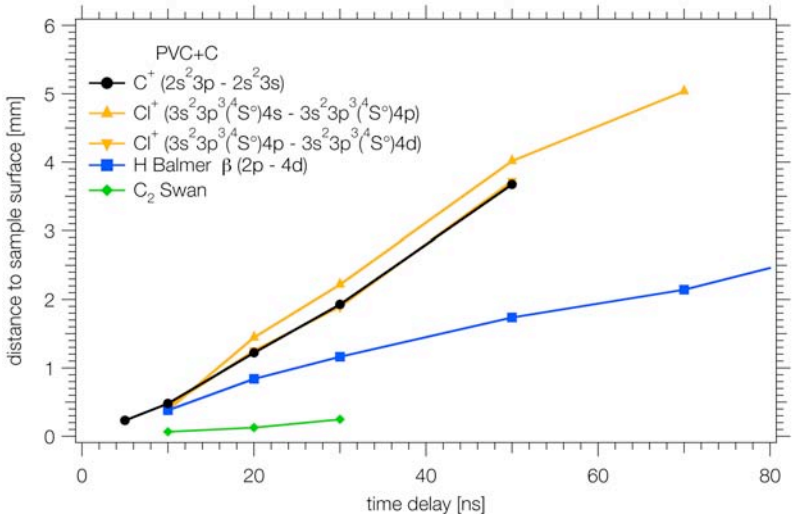

Fig. 83. The plasma expansion of positive charged ions (C II and Cl ll), neutral atoms (H) and diatomic species (C_2) for PVN+C.

Compared to GAP, the expansion velocities are lower for PVC+C for all investigated species. The difference is more pronounce for the ionic carbon with ~20% than for the neutral hydrogen and C_2.

PVN+C

The plasma emission of PVN+C was very weak and only few peaks are visible in Fig. 84.
In the red profile, only H Balmer β and C II can be assigned. In the green profile that has been recorded close to the sample surface no clear diatomic species can be assigned, due to a signal that was to weak.

In the high-resolution spectra of PVN+C (Fig. 85) CN Violet at 386 nm, C II at 382 nm and H Balmer β are visible, but no other peaks could be detected. From the CN Violet system a plasma temperature of 7500 K on the sample surface, 10 ns after the laser pulse and 7000 K in a distance of 0.2 mm from the sample surface and a time delay of 20 ns were determined. The initial temperature is well below the plasma temperatures measured for GAP with both absorbers, but the cooling is slower and after 20 ns similar temperatures are reached for all polymer-dopant systems.

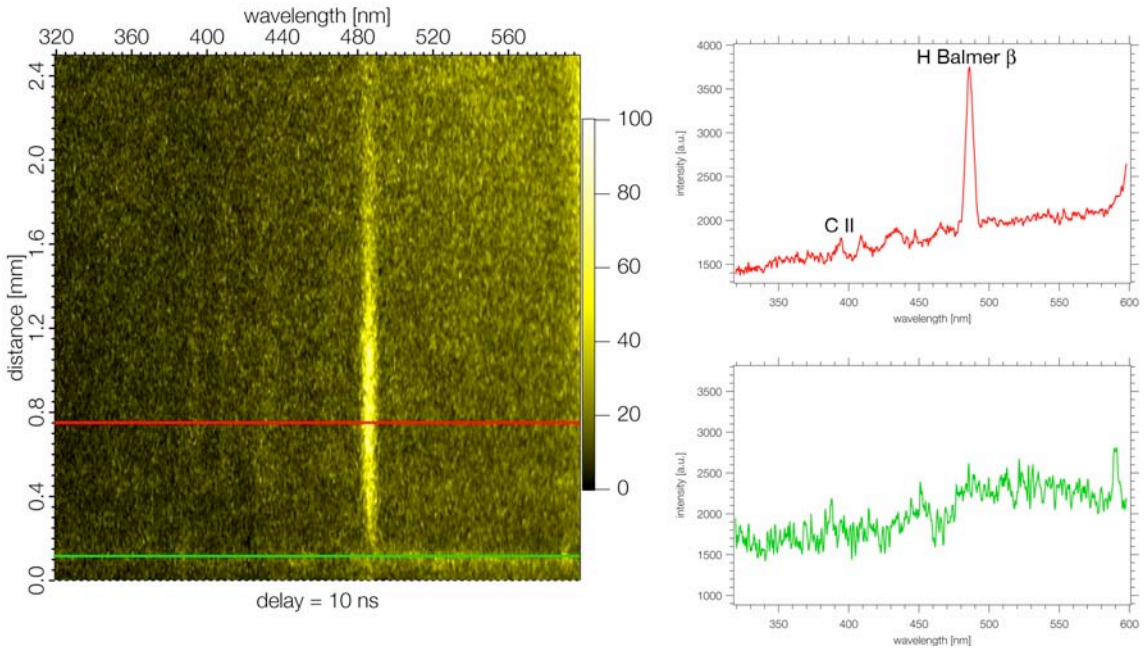

Fig. 84. Overview plasma emission spectra for PVN+C, 10 ns after the laser pulse. The spectra on the right side represent selected profiles, that are recorded at different positions from the sample surface, that are indicated as horizontal lines in the spectral image. Neutral atomic (H), ionized atomic (C II) are clearly visible, neutral diatomic (CN and C_2) species cannot be distinguished from the background.

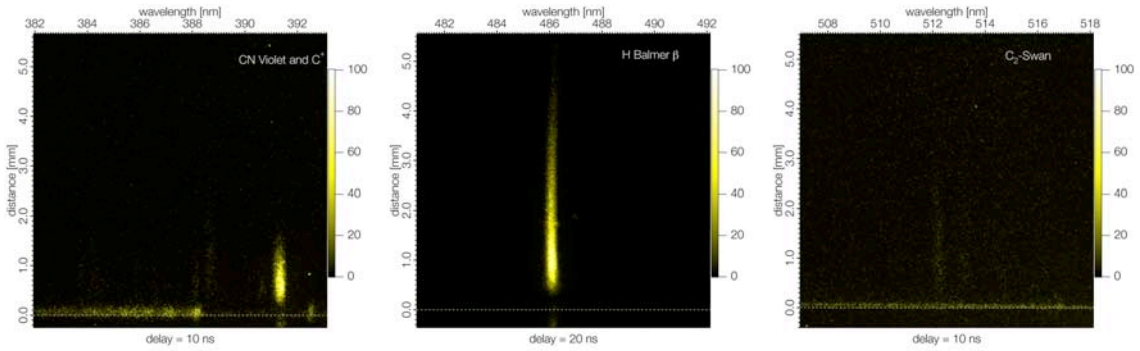

Fig. 85. In the high-resolution plasma emission spectra for PVN+C CN Violet, C II (left) and hydrogen (middle) are visible, but no signal from C_2 (right) could be distinguished from the background.

The electron density in the plasma (ρ_{el}) for PVN+C as a function of the distance to the sample surface and the time delay is shown in Fig. 86. The dashed line represents the intensity of the H Balmer β peak.

The highest ρ_{el} of $4.57 \cdot 10^{21}$ m^{-3} for PVN+C is observed after 10 ns in a distance of 0.25 mm from the sample surface. With increasing distance, it decreases to a value of $1.49 \cdot 10^{21}$ m^{-3}. 20 ns after the laser pulse, the highest ρ_{el} is located in 0.31 mm from the sample surface and

has a value of 2.56 • 10^{21} m^{-3}, that decreases to 1.40 • 10^{21} m^{-3} further away from the surface. At later times, the electron density remains constant at 1.32 • 10^{21} m^{-3} for all distances.
The electron densities observed for PVN+C show the lowest values of all polymers and also the fastest decrease.

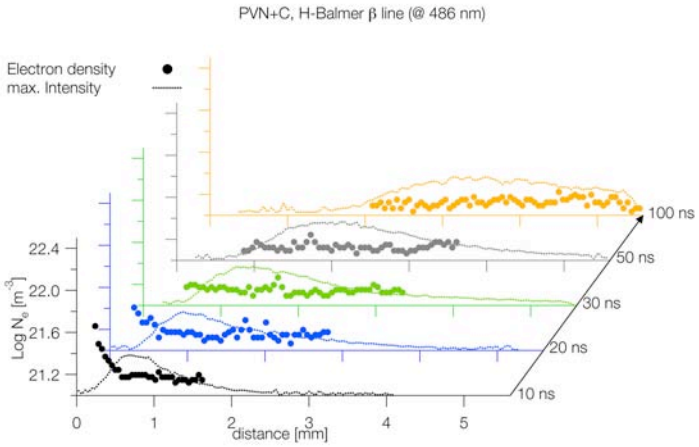

Fig. 86. The electron density as a function of distance from the sample surface and time delay to the laser pulse for PVN+C, calculated form the Stark broadening of the H Blamer β line at 486 nm.

The propagation velocities of different species from PVN+C are shown in Fig. 87. For the ionic carbon the lowest velocity of all energetic polymer-absorber systems of 66200 m/s was observed. Also the values for H Balmer β of 34100 m/s and for CN of 10500 m/s are below the velocities measured for GAP, but similar to PVC+C. The values given for C II and CN are determined from two points and might therefore include a significant error. With increasing time delay to the laser pulse, a decrease in the propagation velocity of the H Balmer β line is observed.

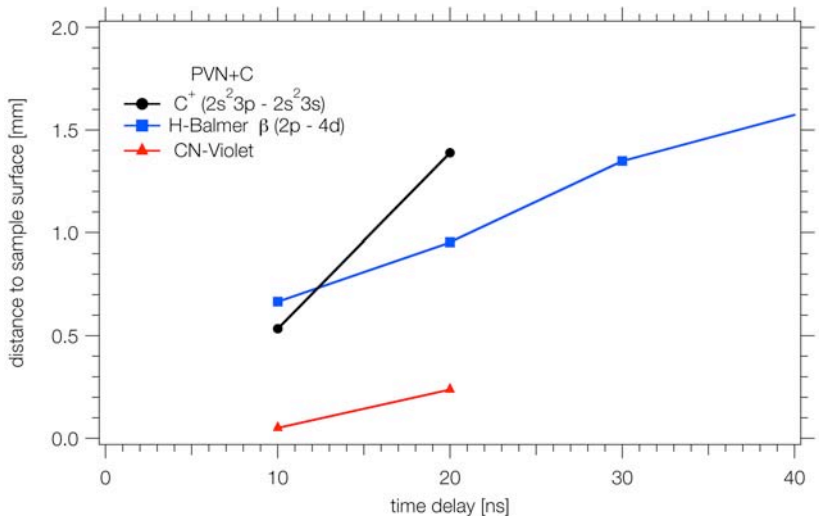

Fig. 87. The plasma expansion of positive charged ions (C II), neutral atoms (H) and diatomic species (CN) for PVN+C.

Summary of the fs-plasma emission spectroscopy experiments

Neutral, atomic and diatomic species have been investigated for all polymer-absorber systems. The expansion velocities of these species are displayed in Fig. 88. Three different regions can clearly be distinguished. The fastest region contains all ionic atomic species (Cl^+ and C^+), the intermediate region the neutral atomic species (H) and the third region the neutral diatomic species (C_2 and CN).

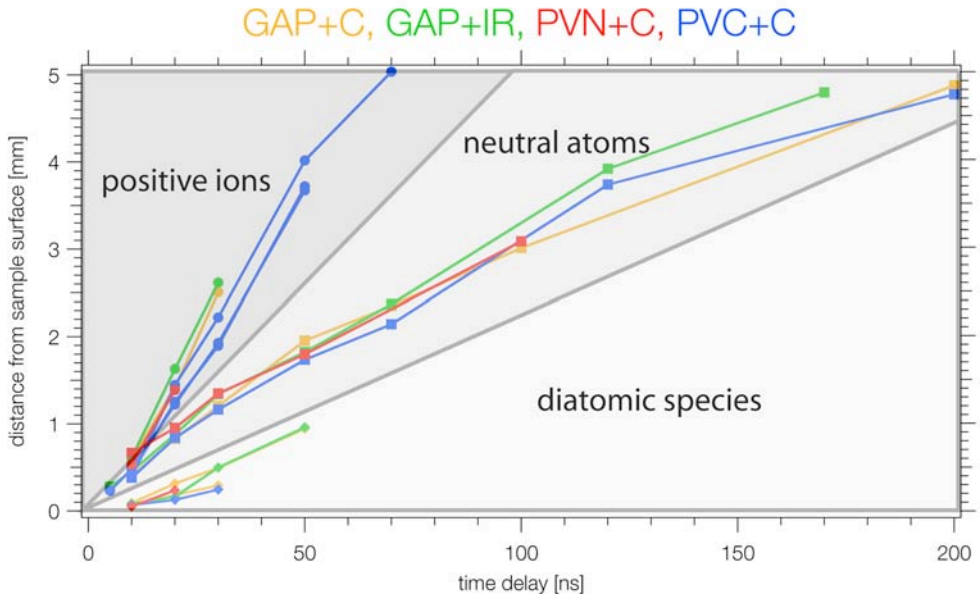

Fig. 88. The plasma expansion of positive charged ions, neutral atoms and diatomic species for GAP+C, GAP+IR, PVN+C and PVC+C.

For all ionic species a constant propagation velocity was measured. The fastest ions are observed for GAP+IR (83700 m/s), followed by GAP+C (78200 m/s), PVN+C (74200 m/s for Cl II and 69500 m/s for C II) and PVC+C (66200 m/s). These fast ions are ions that were accelerated by the Coulomb explosion that is occurring on the substrate due to multi-photon absorption induced by the high peak power delivered by the femtosecond pulse [48, 49].
The highest velocity of the H Balmer β line was observed for GAP (~ 39000 m/s) with both absorbers, followed by PVC+C (36500 m/s) and PVN+C (34100 m/s). Also the diatomic species from GAP (~ 17000 m/s for CN and 9400 m/s for C_2) were faster than for PVC+C (7600 m/s for C_2) and PVN+C (10500 m/s for CN).

From the H Balmer β line at 486.1 nm, the electron density was calculated as described earlier. The highest electron density was observed for PVC+C ($2.42 \cdot 10^{22}$ m^{-3}), followed by GAP+C ($1.25 \cdot 10^{22}$ m^{-3}), GAP+IR ($6.75 \cdot 10^{21}$ m^{-3}) and PVN+C ($4.57 \cdot 10^{21}$ m^{-3}). This correlates also well with the intensity of the H Balmer β line, where the highest intensity was

also observed for PVC+C. The high electron densities are confined to a small area close to the sample surface and to short time delays after the laser pulse. With increasing distance and time delays, the electron density for all polymer-absorber systems approaches a constant value of $1.32 \bullet 10^{21}$ m^{-3}.

From the CN Violet peak system, the plasma rotational-vibrational temperature of the CN molecule was calculated with the LIFBASE program [23]. The highest initial plasma temperature has been observed for GAP+C (9000 K), followed by GAP+IR (8500 K) and PVN+C (7500 K), but after 20 ns similar temperatures (~7000 K) were calculated for all energetic polymers. This is the same order and behavior as observed for the electron density. In the PVC+C emission spectrum, no CN emissions are present, and the plasma temperature could not yet be determined.

6.5. fs-Conclusions

The properties of a plasma produced by the irradiation of GAP+C, GAP+IR, PVC+C and PVN+C with 100 fs laser pulses has been investigated by time resolved plasma imaging and time and space resolved plasma emission spectroscopy. The expansion velocities of different domains of the plasma plume and of selected emission lines of neutral and ionized elements, and diatomic species have been measured and are displayed in Fig. 89 and Table 9 .

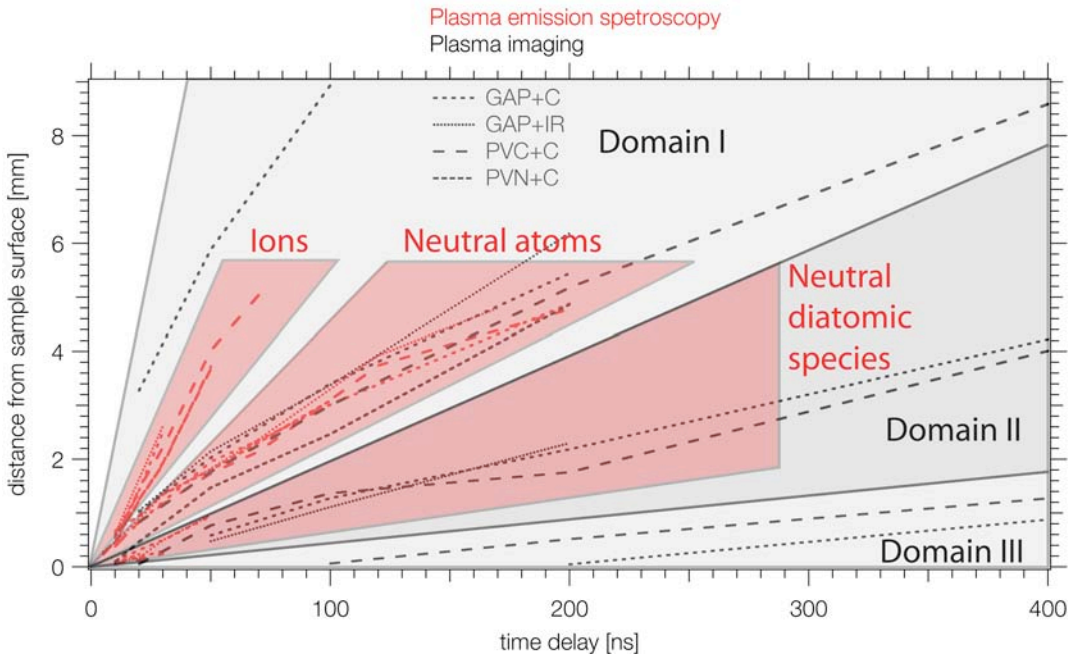

Fig. 89. The plasma expansion of positive charged ions, neutral atoms and diatomic species (red) and of the different domains observed in plasma imaging (gray).

The gray areas in Fig. 89 mark the three domains observed in the plasma by plasma imaging. The red areas represent the three regions that have been defined with the plasma emission spectroscopy measurements. The first region can be assigned to ionized elements that have been accelerated by a fs laser pulse induced coulomb explosion on the sample surface. The second region contains the neutral atoms, the third region is populated by diatomic species.

Table 9 The expansion velocities of selected species for GAP+C, GAP+IR, PVC+C and PVN+C. The unit of all velocities is m/s. The letters in the brackets indicate from which species the velocity was calculated.

	Plasma Emission Spectroscopy			**Plasma Imaging**
	Domain I		**Domain II**	**Domain III**
Polymer	**Positive ions**	**Neutral atoms**	**Diatomic species**	**Nanoparticles**
GAP+C	78200 ±3% (C II)	39000 ±3% (H)	17000 ±3% (CN) 9400 ±3% (C_2)	1750 ±3%
GAP+IR	83700 ±3% (C II)	39500 ±3% (H)	17200 ±3% (CN)	
PVC+C	74200 ±3% (Cl II) 69500 ±3% (C II)	36500 ±3% (H)	7600 ±3% (C_2)	3500 ±3%
PVN+C	66200 ±3% (C II)	34100 ±3% (H)	10500 ±3% (CN)	

The three domains obtained from plasma imaging show a good correlation with the three regions defined by the plasma emission measurements:

- Domain I contains the neutral and ionized elements. The difference in the expansion velocity is not large enough to separate the plasma plume in the plasma imaging measurements into two domains. In both experiments, this domain is the most intense.
- Domain II is formed by uncharged diatomic species. These diatomic species have a lower intensity than the atomic and neutral elements.
- Domain III is only visible for GAP+C and PVC+C and might be produced by a continuum black-body like emission by the carbon nanoparticles The emission of PVN+C is too weak to observe anything at longer timed delays, at which this domain appears. The emission of the carbon nanoparticles can be confirmed with plasma emission spectroscopy experiments at longer time delays (in the µs range).

The highest expansion velocities for the first and second domain have been measured for GAP+IR, followed by GAP+C, PVC+C and PVN+C with both methods. The third domain is faster for PVC+C than for GAP+C.

The electron density in the plasma has been calculated from Stark broadening of the H Balmer β line and is presented in Table 10 The highest value has been calculated for PVC+C, followed by GAP+C, GAP+IR and PVN+C. This correlates well with the intensity of the different domains in the plasma imaging experiments and the intensity of the H Balmer β line. The maximum was located close to the sample surface at the backside of the H Balmer β line and decreased to similar values for all polymers with increasing distance to the sample surface and/or delay times to the laser pulse.

The rotational-vibrational temperature of the CN molecule has been calculated from the CN Violet emission at 386 nm and was assumed to be the general temperature in the plasma. The highest initial temperature was measured for GAP+C, followed by GAP+IR and PVN+C (see Table 10). This is the same order as observed for the maximum electron density. The plasma temperature of PVC+C could not be calculated yet, as no CN emission lines are present in the emission plume.

Table 10 The plasma properties of GAP+C, GAP+IR, PVN+C, PVC+C.

Polymer	$\mathbf{T_{plasma}}$ **(K)**	$\mathbf{\rho_{el}}$ **(m^{-3})**
GAP+C	9000 ±300	$1.25 \cdot 10^{22}$ ±3%
GAP+IR	8500 ±300	$6.75 \cdot 10^{21}$ ±3%
PVC+C		$2.42 \cdot 10^{22}$ ±3%
PVN+C	7500 ±300	$4.57 \cdot 10^{21}$ ±3%

7. Conclusions

The laser plasma thruster is a device for the steering of small satellite. Due to specific demands on the fuel material, polymers were used. With commercially available polymers the mission targets could not be reached.

Therefore three different polymers (GAP, PVN and PVC) with two different absorbers (carbon nanoparticles and an IR-dye (Epolite 2057)) have been investigated as fuel for the micro laser plasma thruster. Additionally, CuO- and Al-nanoparticles have been added to the IR-dye doped polymers to achieve a better control over the energy release during the ablation process. GAP and PVN are energetic polymers with a high decomposition enthalpy of -3829 J/g (PVN) and -2053 J/g (GAP). PVC was used as a less energetic (the decomposition enthalpy of -418 J/g is much lower than for the other two polymers) commercially available reference.

Experiments at low fluences (shadowgraphy (in air)) and at high fluences (thrust measurements (in vacuum), plasma emission spectroscopy (in air and vacuum) and mass spectrometry (in vacuum)) have been performed. Also different laser pulse lengths (ranging from fs to μs) were applied.

The shadowgraphy measurements were performed with ns laser pulses at a fluence below the plasma formation threshold fluence. The main advantage of this method is the relative simple setup, as the experiments are performed in air. The main features that can be observed are the propagation of the shockwave and the composition and propagation of the particle plume.

The shadowgraphy measurements were in good correlation with the energetic properties of the polymers. The fastest shockwave was observed for PVN+C, followed by GAP with both absorbers and PVC+C. For all carbon doped polymers, a big amount of solid or liquid polymer fragments were visible in the ablation plume. In the plasma plume of GAP+IR no large fragments were visible. This indicates a higher degree of fragmentation for GAP+IR, and therefore also more chemically stored energy that is released.

For PVN+IR strong thermal features were observed (formation of fibers and melting). This features could be reduced by an additional doping with CuO-nanoparticles, but no improvements on the shockwave and particle propagation compared to PVN+C could be observed. Also for GAP an additional doping with CuO- or Al-nanoparticles did not improve the performance in the thrust measurements.

Plasma emission spectroscopy in air was used to investigate the influence of the atmosphere. The experiments can be compared to the shadowgraphy measurements, that were also performed in air, but at much lower irradiation fluences and with the plasma emission measurements in vacuum. Plasma properties such as electron density and plasma temperature were calculated from specific emission lines (H Balmer α and CN Violet).

In the emission spectroscopy measurements in air with ns laser pulses, the same peaks were observed for all polymers. Also similar maximum values or the electron density (~10^{24} m^{-3}) and a fast decay during the first microsecond were measured for all polymers. The plasma temperature reached maximum values of 7500 K after one microsecond. This increase is in the same time range in which the electron density decreased, and may be related to a recombination of CN radicals with electrons in the plasma.

The same experimental conditions were used for the ns plasma emission spectrometry in vacuum and the mass spectrometry setup. Both experiments were performed in UHV and at high laser fluences (~23 J/cm^2).

The plasma emission spectroscopy experiments with ns laser pulses were used to calculate the propagation velocity of the H Balmer α line. The highest velocity was observed for GAP+C and PVC+C, followed by GAP+IR and PVN+C. This is a different order as observed in the shadowgraphy measurements. This may caused by the two different fluences or the influence of the atmosphere.

A higher degree of fragmentation was observed for the energetic polymers with the mass spectrometer after ns pulse irradiation. In mass spectra of PVC+C and PVN+C, strong signals could be assigned to the solvent that was used to solvent cast the polymers. This trapped solvent acts as inert material during the ablation process and can therefore have a negative influence on the thrust properties of the two polymers.

The mass spectrometry measurements were also used to calculate the velocity of selected species from the kinetic energy and to measure the fragmentation of the different polymers. The expansion velocity was determined from the kinetic energy of C^+. The highest velocity was measured for GAP, followed by PVC and PVN. This correlates well with the thrust measurements and qualitatively also with the femtosecond emission spectrometry results, but at a much lower velocity. A correlation with the emission spectroscopy could not yet be established, as different species were measured with the two different methods.

The influence of the pulse length was investigated with plasma emission spectroscopy measurements. They were performed with fs and ns laser pulses in vacuum. In fs experiments three domains with different velocities could be observed. The domain with the highest propagation velocity is formed by ionized species. They are accelerated by a coulomb explosion on the sample surface. A second domain could be assigned to neutral atoms. The third domain is formed by diatomic species. A forth domain which was observed with plasma imaging, consists most probably of nanoparticles. These nanoparticles were only observed for the polymers with carbon nanoparticles as absorbers. This correlates well with the shadowgraphy measurements, where also no particles were observed in the ablation plume for GAP+IR.

Lower electron densities are measured for the fs experiments than in the ns experiments, but the maximum plasma temperatures are higher. The highest electron density after fs irradiation has been observed for PVC+C, which also had the most intense plasma. The maximum plasma temperature of 9000 K was obtained with GAP+C. The plasma temperature of PVC+C has not yet been determined, as no CN Violet emission was observed for this polymer in vacuum.

The highest expansion velocity was observed for GAP+IR, followed by GAP+C, PVC+C and PVN+C. This is in good correlation with the fs pulse thrust measurements, where also GAP+IR showed the better result than GAP+C.

The highest ms thrust values were obtained for GAP+C, followed by GAP+IR. For both polymer-absorber systems efficiencies of over 100 % (370 % for GAP+C and 200 % for GAP+IR) were measured. For PVC+C a efficiency of 50 % was obtained. The lowest values were measured for PVN+C with only 21 %. This low value for the most energetic polymer is probably caused by trapped solvent in the film and by thermal effects observed for this polymer (melting, splashing).

Thrust origins most probably from a combination of volume explosion from the polymer decomposition, Coulomb repulsion and impulse from larger, fast traveling fragments, and can not yet be quantitatively correlated with any other method. A qualitative correlation is possible with a whole variety of measurements.

8. Additional experiments

With the permission of Ingrid Wysong, a GAP+C sample was sent to the group of Prof. Akihiro Sasoh at the Institute of Fluid Science at Tohoku University. The thrust data was acquired as shown in the illustration of the setup in Fig. 90 for CO_2 laser irradiation.

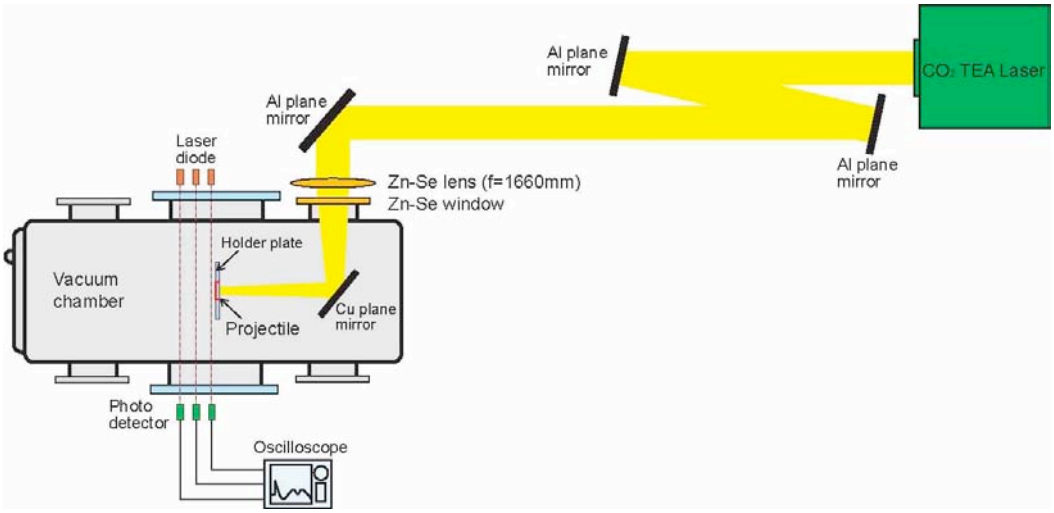

Fig. 90. Experimental Setup to measure the propagation speed of the projectile.

Table 11 Data acquired by Prof. Akihiro Sasoh for polyacetal and GAP+C

	Polyacetal	**Polyacetal and GAP+C**
Flyer mass (before shot)	1.36 g	1.99 g
Ablated mass	10.6 mg	22.1 mg
Launch speed	13.2 m/s	17.4 m/s
Momentum	0.0178 kg • m/s	0.0342 kg • m/s
Laser energy	42 J	37 J
Momentum coupling coefficient	420 µN • s/J	920 µN • s/J
Specific Impulse	171 s	158 s

GAP+C produces a much higher launch speed of the flyer at a higher flyer mass a lower laser energy. This leads to a similar C_m as measured in the torsion balance measurements by Claude Phipps. The I_{sp} are completely different values. A reason could be, that not only GAP was ablated, but also Polyacetal. This would lead to a lower specific ablation energy and a lower I_{sp}. Another reason for the different results might be the different wavelength of the CO_2 laser (10.6 µm). Carbon may not be necessary for the ablation of GAP, as the undoped polymer shows absorption at 10.6 µm, but may influence the ablation process,.

9. Possible measurements to answer remaining questions

- Time and space resolved plasma emission spectroscopy measurements will be performed in vacuum for more species.
- The same products will be investigated with mass spectroscopy measurements.
- A micro thrust stand (same as Claude Phipps) is being set up at our laboratory, to have the same measurement conditions as in all other experiments.
- More detailed studies on the fragmentation and the energy distribution of the ionic fragments of the different polymers will be performed
- New energetic polymers will be tested as fuel for the plasma thruster. Possible candidates are Poly(bis-azidomethyl oxetane) (BAMO) and Poly(azidomethyl methyloxetan) (AMMO).

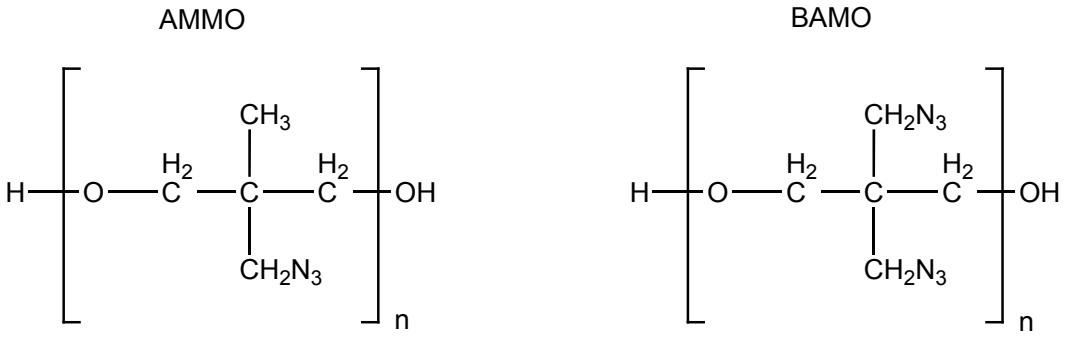

Fig. 91. Chemical structure of AMMO (left) and BAMO (right)

10. Acknowledgments

The cooperation of Claude Phipps, who performed all the thrust measurements and who supplied us with the thrust stand, is gratefully acknowledged.

11. References

1. T. Lippert, C. David, M. Hauer, T. Masubuchi, H. Masuhara, K. Nomura, O. Nuyken, C. Phipps, J. Robert, T. Tada, K. Tomita, and A. Wokaun, *Novel applications for laser ablation of photopolymers*, Appl. Surf. Sci., 186 (2002) 14-23.
2. T. Lippert, M. Hauer, C.R. Phipps, and A. Wokaun, *Fundamentals and applications of polymers designed for laser ablation*, Appl. Phys. A-Mater. Sci. Process., 77 (2003) 259-264.
3. C. Phipps, J. Luke, and T. Lippert, *Laser ablation of organic coatings as a basis for micropropulsion*, Thin Solid Films, 453-54 (2004) 573-583.
4. C.R. Phipps, J.R. Luke, G.G. McDuff, and T. Lippert, *Laser-driven micro-rocket*, Appl. Phys. A-Mater. Sci. Process., 77 (2003) 193-201.
5. T. Lippert, *Polymers used as Fuel for Laser Plasma Thrusters in Small Satellites*. 2003, PSI: Villigen.
6. J. Köhler and R. Meyer, Explosivstoffe, Wiley-VCH, Weinheim, 1998.
7. R.A. Strecker and F.D. Verdderame, US Patent 3965081, 1976.
8. W. Diepold, *Herstellung, Stabilisierung und Eigenschaften von Polyvinylnitrat*, Explosivstoffe, 1 (1970).
9. B. Gaur, B. Lochab, V. Choudhary, and I.K. Varma, *Azido polymers - Energetic binders for solid rocket propellants*, Journal of Macromolecular Science-Polymer Reviews, C43 (2003) 505-545.
10. K. Menke, J. Bohnlein-Mauss, and H. Schubert, *Characteristic properties of AN/GAP-propellants*, Propellants Explosives Pyrotechnics, 21 (1996) 139-145.
11. G. Sivalingam, R. Karthik, and G. Madras, *Effect of metal oxides on thermal degradation of poly(vinyl acetate) and poly(vinyl chloride) and their blends*, Industrial & Engineering Chemistry Research, 42 (2003) 3647-3653.
12. M. Blazso and E. Jakab, *Effect of metals, metal oxides, and carboxylates on the thermal decomposition processes of poly (vinyl chloride)*, Journal Of Analytical And Applied Pyrolysis, 49 (1999) 125-143.
13. B.D. Patterson, C. Bronnimann, D. Maden, F. Gozzo, A. Groso, B. Schmitt, M. Stampanoni, and P.R. Willmott, *The materials science beamline at the Swiss Light Source*, Nucl. Instrum. Methods Phys. Res. Sect. B-Beam Interact. Mater. Atoms, 238 (2005) 224-228.

14. A. Groso, M. Stampanoni, R. Abela, P. Schneider, S. Linga, and R. Muller, *Phase contrast tomography: An alternative approach*, Appl. Phys. Lett., 88 (2006).
15. R. Srinivasan and B. Braren, *Ablative Photodecomposition Of Polymer-Films By Pulsed Far-Ultraviolet (193 nm) Laser-Radiation - Dependence Of Etch Depth On Experimental Conditions*, J. Polym. Sci. Pol. Chem., 22 (1984) 2601-2609.
16. J.E. Andrew, P.E. Dyer, D. Forster, and P.H. Key, *Direct Etching Of Polymeric Materials Using A Xecl Laser*, Appl. Phys. Lett., 43 (1983) 717-719.
17. R.K. Singh, *Transient plasma shielding effects during pulsed laser ablation of materials*, J. Electron. Mater., 25 (1996) 125-129.
18. R.P. Richner, *Entwicklung neuartig gebundener Kohlenstoffmaterialien für elektrische Doppelschichtkondensatorelektroden,* Diss. ETH (2001)
19. X.N. Wen, D.E. Hare, and D.D. Dlott, *Laser Polymer Ablation Threshold Lowered By Nanometer Hot-Spots*, Appl. Phys. Lett., 64 (1994) 184-186.
20. L. Urech, M. Hauer, T. Lippert, C.R. Phipps, E. Schmid, A. Wokaun, and I. Wysong, *Designed polymers for laser-based microthrusters - correlation of thrust with material, plasma, and shockwave properties*, Proc. SPIE, 5448 (2004) 52-64.
21. F. Weisbuch, V.N. Tokarev, S. Lazare, C. Belin, and J.L. Bruneel, *Millimeter-long nanofibers of PMMA spun at super-high speed by ablation with a single pulse of a KrF excimer laser*, Appl. Phys. A-Mater. Sci. Process., 75 (2002) 677-680.
22. F. Weisbuch, V.N. Tokarev, S. Lazare, C. Belin, and J.L. Bruneel, *Millimeter long PMMA nanofibers - a new form of material removal in laser ablation*, Thin Solid Films, 453-54 (2004) 394-398.
23. J. Luque and D.R. Crosley, *LIFBASE: Database and Spectral Simulation Program (version 1.6)*. 1999, SRI International Report MP 99-099.
24. H.R. Griem, Principles of Plasma Spectroscopy, Cambridge University Press, Cambridge, 1997.
25. M.A. Gigosos and V. Cardenoso, *New plasma diagnosis tables of hydrogen Stark broadening including ion dynamics*, Journal of Physics B-Atomic Molecular and Optical Physics, 29 (1996) 4795-4838.
26. G. Herzberg, Spectra of Diatomic Molecules, D. Van Nostran Company, INC., New York, 1950.
27. M.H. Fisch and R. Bacaloglu, *Kinetics and mechanism of the thermal degradation of poly(vinyl chloride)*, Journal of Vinyl & Additive Technology, 1 (1995) 233-240.

28. R. Bacaloglu and M.H. Fisch, *Reaction mechanism of poly(vinyl chloride) degradation. Molecular orbital calculations*, Journal of Vinyl & Additive Technology, 1 (1995) 241-249.

29. I.C. McNeill, L. Memetea, and W.J. Cole, *A Study of the Products of PVC Thermal-Degradation*, Polym. Degrad. Stabil., 49 (1995) 181-191.

30. M. Hesse, H. Meieer, and B. Zeeh, Spektroskopische Methoden in der organischen Chemie, Georg Thieme Verlag, Stuttgard, 1995.

31. Y. Haas, Y. Ben-Eliahu, and S. Welner, *Pulsed laser induced decomposition of energetic polymers: Comparison of ultraviolet (355 nm) and infrared (9.3 μm) initiation*, Propellants Explosives Pyrotechnics, 21 (1996) 258-265.

32. C.J. Tang, Y.J. Lee, and T.A. Litzinger, *Simultaneous temperature and species measurements of the Glycidyl Azide Polymer (GAP) propellant during laser-induced decomposition*, Combust. Flame, 117 (1999) 244-256.

33. O.P. Korobeinichev, L.V. Kuibida, E.N. Volkov, and A.G. Shmakov, *Mass spectrometric study of combustion and thermal decomposition of GAP*, Combust. Flame, 129 (2002) 136-150.

34. J.J. Shin, D.R. Ermer, S.C. Langford, and J.T. Dickinson, *The role of photoelectronic processes in the formation of a fluorescent plume by 248-nm laser irradiation of single crystal $NaNO_3$*, Appl. Phys. A-Mater. Sci. Process., 64 (1997) 7-17.

35. C. Phipps and J. Luke, *Diode laser-driven microthrusters: A new departure for micropropulsion*, AIAA J., 40 (2002) 310-318.

36. L. Urech, T. Lippert, C. Phipps, and A. Wokaun, *Polymers as fuel for Laser Plasma Thrusters - A correlation of thrust with matreial and plasma properties by mass specrometry*, Proc. of SPIE, Vol. 6261 (2006).

37. C. Phipps, J. Luke, D. Funk, D. Moore, J. Glownia, and T. Lippert, *Laser impulse coupling at 130 fs*, Appl. Surf. Sci., 252 (2006) 4838-4844.

38. C.R. Phipps, G. Albrecht, H. Friedman, D. Gavel, E.V. George, J. Murray, C. Ho, W. Priedhorsky, M.M. Michaelis, and J.P. Reilly, *ORION: Clearing near-Earth space debris using a 20-kW, 530-nm, Earth-based, repetitively pulsed laser*, Laser Part. Beams, 14 (1996) 1-44.

39. C.R. Phipps, T.P. Turner, R.F. Harrison, G.W. York, W.Z. Osborne, G.K. Anderson, X.F. Corlis, L.C. Haynes, H.S. Steele, K.C. Spicochi, and T.R. King, *Impulse Coupling To Targets In Vacuum By KrF, HF, And CO_2 Single-Pulse Lasers*, J. Appl. Phys., 64 (1988) 1083-1096.

40. H.S. Carslaw and J.C. Jaeger, Conduction of Heat in Solids, Clarendon Press, Oxford, 1959.
41. C. Phipps and R.W. Dreyfus, in *Laser Ionization Mass Analysis*, A. Vertes, R. Gijbels, and F. Adamas, Editors. 1993, Wiley: New York. p. 369-441.
42. J. Ihlemann, F. Beinhorn, H. Schmidt, K. Luther, and J. Troe, *Plasma and plume effects on UV laser ablation of polymers*, Proc. SPIE, 5448 (2004) 572.
43. K. Sasaki, T. Wakasaki, and K. Kadota, *Observation of continuum optical emission from laser-ablation carbon plumes*, Appl. Surf. Sci., 197 (2002) 197-201.
44. U. Frenzel, U. Hammer, H. Westje, and D. Kreisle, *Radiative cooling of free metal clusters*, Z. Phys. D-Atoms Mol. Clusters, 40 (1997) 108-110.
45. O. Albert, S. Roger, Y. Glinec, J.C. Loulergue, J. Etchepare, C. Boulmer-Leborgne, J. Perriere, and E. Millon, *Time-resolved spectroscopy measurements of a titanium plasma induced by nanosecond and femtosecond lasers*, Appl. Phys. A-Mater. Sci. Process., 76 (2003) 319-323.
46. S. Amoruso, R. Bruzzese, N. Spinelli, R. Velotta, M. Vitiello, X. Wang, G. Ausanio, V. Iannotti, and L. Lanotte, *Generation of silicon nanoparticles via femtosecond laser ablation in vacuum*, Appl. Phys. Lett., 84 (2004) 4502-4504.
47. W.W.B. Pearse and A.G. Gaydon, The Identification of Molecular Spectra, Wiley, New York, 1976.
48. D. Ashkenasi, A. Rosenfeld, H. Varel, M. Wahmer, and E.E.B. Campbell, *Laser processing of sapphire with picosecond and sub-picosecond pulses*, Appl. Surf. Sci., 120 (1997) 65-80.
49. R. Stoian, A. Rosenfeld, D. Ashkenasi, I.V. Hertel, N.M. Bulgakova, and E.E.B. Campbell, *Surface charging and impulsive ion ejection during ultrashort pulsed laser ablation*, Phys. Rev. Lett., 88 (2002).